8-2014

Dynamics of Polyelectrolyte Adsorption on Surfaces: Applications in the Detection of Iron in Water

Madhira N. Gammana

DYNAMICS OF POLYELECTROLYTE ADSORPTION ON SURFACES: APPLICATIONS IN THE DETECTION OF IRON IN WATER

By

Madhira N. Gammana

B.S. University of Kalaniya, Sri Lanka, 2003

B.S. Open University of Sri Lanka, 2004

A DISSERTATION

Submitted in Partial Fulfillment of the

Requirements for the Degree of

Doctor of Philosophy

(in Chemistry)

The Graduate School

The University of Maine

August 2014

Advisory Committee:

Carl P. Tripp, Professor of Chemistry and LASST, Advisor

Mark L. Wells, Professor of Marine Science

Mitchell Bruce, Associate Professor of Chemistry

Raymond C. Fort, Jr. Professor of Chemistry

David J. Neivandt, Associate Professor of Chemical & Biological Engineering

DISSERTATION ACCEPTANCE STATEMENT

On behalf of the Graduate Committee for Madhira N. Gammana, I affirm that this manuscript is the final and accepted dissertation. Signatures of all committee members are on file with the Graduate School at the University of Maine, 42 Stodder Hall, Orono Maine.

Carl Tripp, Professor of Chemistry Date

LIBRARY RIGHT STATEMENT

In presenting this dissertation in partial fulfillment of the requirements for an advanced degree at The University of Maine, I agree that the Library shall make it freely available for inspection. I further agree that permission for "fair use" copying of this dissertation for scholarly purposes may be granted by the Librarian. It is understood that any copying or publication of this dissertation for financial gain shall not be allowed without my written permission.

Signature: _____

Date:

DYNAMICS OF POLYELECTROLYTE ADSORPTION ON SURFACES: APPLICATIONS IN THE DETECTION OF IRON IN WATER

By Madhira N. Gammana

Dissertation Advisor: Dr. Carl Tripp

An Abstract of the Dissertation Presented
in Partial Fulfillment of the Requirements for the
Degree of Doctor of Philosophy
(in Chemistry)
August 2014

Layer by layer (LbL) self assembly is a simple multilayer thin (nanometer scale) film fabricating technique. The mechanism of film growth remains a topic of much controversy. For example, several models have been proposed to explain the origin of linear and exponential film growth that are attributed to differences in the dynamic processes that occur at the molecular level during film formation. The problem is that there are no methods that directly measure the dynamics of polymer formation during LbL film formation. In this thesis, I describe the essential elements of an ATR-IR spectroscopic method that was developed to enable measurement of the dynamics of the mass adsorbed and polyelectrolyte conformation during the formation of PEM's. In particular, I followed the sequential adsorption of Sodium polyacrylate (NaPA) and Poly (diallyldimethylammonium) chloride (PDADMAC) from deionized (DI) water and as a function of ionic strength to show that polymer diffusion occurs between layers when adsorbed from DI water. In contrast, a denser layer occurs with no polymer interdiffusion for deposition from 0.02M ionic strength solutions of NaPA and PDADMAC. While the

mass deposited increased with ionic strength, linear multilayer growth in films were observed in all cases. This finding disputes a common viewpoint that interdiffusion of polymer layers is a key feature of exponential film growth**.**

The theme of polymer layer adsorption was used in the detection of Fe^{3+} in seawater. A new approach, developed previously in Tripp's group, utilized "vertical amplification" in which a block copolymer assembled on membranes provided multiple anchoring points extending from the surface for attaching a siderophore, desferrioxamine B (DFB). The Fe^{3+} chelates with the siderophore producing a red color that can be quantified by visible spectroscopy. However, the rate of Fe^{3+} uptake was found to be dependent on flow rate. The origin of this flow rate dependence was identified by the work presented in this thesis. It was found that the amount and rate of Fe^{3+} uptake was dependent on the relative size of each block in the polymer and the degree of reaction of DFB with the adsorbed layer. In particular, higher amounts and higher rates were obtained when the density of DFB was lowered. This shows that the DFB was sterically hindered from forming a hexacoordinate complex with Fe^{3+} by the presence of neighboring DFB molecules. This is a key factor that needs to be considered in developing Fe^{3+} detection systems based on siderophores anchored to surfaces.

ACKNOWLEDGEMENTS

The author wishes to express her most sincere appreciation to her advisor for this project, Dr. Carl Tripp for providing such a stimulating and free environment for advanced research and for training the author in trouble shooting, English speaking, writing and presenting. The author also expresses her sincere thanks to the thesis committee member, Dr. Mark Wells for his guidance and financial support for the project. The author would also like to thank her thesis committee members Dr. Mitchell Bruce, Dr. Raymond Fort Jr., and Dr. David Neivandt for the time that was devoted to help lead direction in this project, reading and commenting on this thesis.

The author would like to thank Dr. Whitney King and his research group at Colby Collage, Waterville, Maine for their support for this thesis project. The author wishes to express her appreciation to the fellow students of her research group. The author expresses her thank to all faculty, staff, and graduate students in the Department of Chemistry and Laboratory for Surface Science and Technology (LASST) who have given her help during her study at University of Maine.

Finally, this dissertation is dedicated to my loving husband, Asela and my precious son, Kavera who provided the foundation of this work with their continuous support, encouragement, and love. The author also expresses her gratitude to her parents who gave her the life and provided her a decent childhood full of love and freedom, laying the foundation of her value and personal development and her brother, Amila for his continuous love and encouragement.

TABLE OF CONTENTS

LIST OF TABLES

LIST OF FIGURES

LIST OF SCHEMES

CHAPTER 1: INTRODUCTION

1.1 Thesis outline

This thesis contains two main research areas; Layer-by-Layer (LbL) deposition of thin films via a flow-through technique by using oppositely charged polyelectrolytes, and the use of an adsorbed polyelectrolyte film in the detection of iron in aqueous solutions. Chapter 1 provides a background and current literature overview of the research areas focused on this dissertation. Chapters 2 and 3 present the findings of LbL deposition of thin films *via* a flow based technique together with ATR-FTIR spectroscopy by using sodium polyacrylate (NaPA) and poly(diallyldimethylammonium) chloride (PDADMAC) as the oppositely charged polyelectrolyte components. Chapter 4 presents the findings of iron detection in aqueous solutions by using desferrioxamine B (DFB) tethered to a block copolymer that in turn, was adsorbed on an infrared transparent membrane.

1.2 Background and introduction to LbL assembly

Modern materials are typically composites in which the synergistic interactions of several materials produce a single component with properties that are superior to the properties of the individual materials in the composite. While large scale manufacturing methods such as lamination and metal alloying are still in use, more focus on molecular level assemblies has occurred in recent years where thin films are fabricated from micro- or nano- scale structural units.[1] Among many other methods, atomic layer deposition and liquid phase LbL deposition methods are popular in producing multilayer thin films.[2]

Typically, atomic layer deposition requires volatile precursors and is a more complicated and expensive method[2,3] compared to liquid phase LbL based method.

The first reporting of LbL was the self-assembly of oppositely charged particles by Iler in 1966.[1] In this early work, Iler demonstrated a technique where separate suspensions containing positively charged boehmite fibrils (alumina) and negatively charged silica particles were deposited sequentially onto a smooth glass surface. A cross section of the assembled architecture is shown schematically in Figure 1.1.

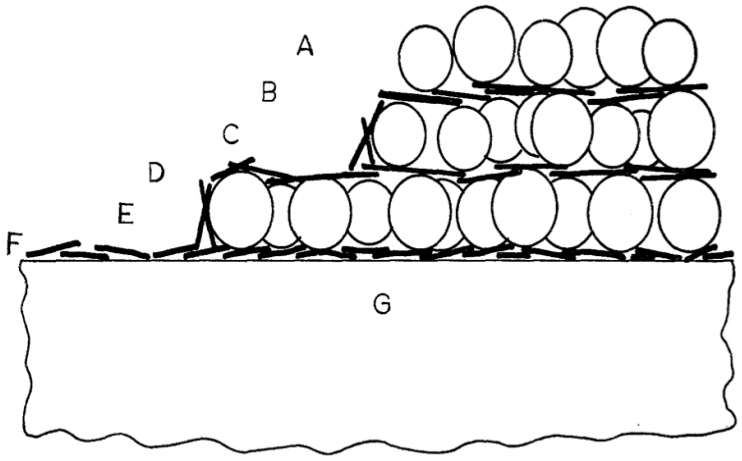

Figure 1.1 Schematic cross section of a multilayer film; A, C, and E represent layers of 100 μm silica at pH 3; B, D, and F, layers of colloidal boehmite fibrils; G, the glass substrate. Figure reproduced from Iler *et al;*[1]

This pioneering work by Iler demonstrated the core steps of LbL deposition and the simple elegance of the method. In brief, a glass slide, which is negatively charged and hydrophilic in nature, was first dipped into an aqueous suspension containing positively charged boehmite fibrils. The fibrils adsorb on the surface through electrostatic

interactions and produce a glass slide whose outer surface is now positively charged. The glass slide was rinsed to remove excess material and then air-dried. Next, the glass slide was dipped into a negatively charged colloidal silica suspension at pH 3 followed by a rinse step to remove excess silica and then air-dried. The silica adsorb on the positively charged fibril layer leading to a new outer surface layer consisting of the negatively charged silica particles. Repeating these steps of dipping in the alumina then silica suspensions led to uniform films that appears homogenous and smooth with increasing thickness.[1]

It was not until later in the 1990's when scientist Zhang *et al;*[4] Decher *et al*;[5-9] and Hammond *et al;*[10] demonstrated the use of LbL self-assembled multilayers to applications such as refractive or anti-refractive surfaces,[11] superhydrophilic surfaces,[12,13] superhydrophobic surfaces (self-cleaning surfaces),[14,15] drug delivery systems,[16,17] and sensors[18] that LbL based methods attracted widespread interest in the science community. A variety of materials including polyelectrolytes,[19] colloid and nanoparticles,[20-22] dyes,[23,24] dendrimers,[25,26] clay minerals,[27] carbon materials,[28,29] enzymes and proteins,[30-32] DNA,[33,34] , viruses[35] and combinations thereof have been used as building blocks to assemble multilayer films by using LbL approach. Many scientists have demonstrated that electrostatic interactions,[7] hydrogen bonding,[36] charge transfer interactions,[37,38] molecular recognition,[30,39-42] and coordination interactions[43] can be used as driving forces for multilayer assembly by LbL deposition. The following sections from 1.2.1 to 1.2.5 provide a brief summary of the different types of interactions.

1.2.1 LbL assembly *via* electrostatic interaction

This is the most common approach for producing LbL based films. Typically, in this method, polyelectrolytes or particles with opposite charges are used to construct multilayer films. The original Iler work depicted in Figure 1.1 falls in to this category. The layers are bound together *via* electrostatic forces of opposite charged molecules or particles. Various anionic polyelectrolytes such as polystyrenesulfonate sodium salt (PSS),[44,45] polyvinylsulfate potassium salt,[5] polyacrylate sodium salt (PAA), hyaluronic acid[46] and cationic polyelectrolytes such as poly-4-vinylbenzyl-(*N,N*-diethyl-*N*-methyl)-ammonium iodide, polyallylamine hydrochloride,[5] sodium-9-anthracenpropionate, and poly(diallyldimethylammonium chloride)[47] have been used as building blocks for LbL assembly.

LbL assembly is not limited to single component systems as there are examples where charged and neutral species are first combined to form inter-polyelectrolyte complexes.[47-51] For example, the cationic polyelectrolyte poly(diallyldimethylammonium chloride) (PDDA) was combined with the anionic dye of sodium 9-anthracenepropionate (SANP) in solution to form an inter-polyelectrolyte complex. An inter-polyelectrolyte complex occurs when oppositely charge components spontaneously form complexes in water. A LbL multilayered film was produced by alternate deposition of PDDA-SANP complex with a second suspension containing the negatively charged polyelectrolyte (4-styrenesulfonate) (PSS).[47]

The use of adsorbed polyelectrolytes to control the properties of colloidal systems is a well-established method and it is this aspect that underlies the basic mechanism of the LbL approach. The general picture of polyelectrolyte adsorption on an oppositely charged surface is that a fraction of the segments will electrostatically bind to surface charged sites and the additional charged sites located in the loops and tails extended further from the surface lead to an overall charge reversal of the system.[52] The adsorption is self-limiting due to this charge reversal as an adsorbed polymer layer repels incoming polymer chains.[53] While the kinetic aspects and thermodynamics for adsorption of a single layer of polyelectrolytes on surfaces has been thoroughly studied, there is little known about the details of the adsorption process occurring with multilayer adsorption of one polymer layer on top of an existing layer. Gaining a better understanding of the adsorption process occurring during LbL deposition of oppositely charged polyelectrolytes is one of the primary motivations of the research conducted in this thesis and this topic will be discussed further in section 1.2.13.

The structure/properties of LbL generated films depend on factors such as choice of polyelectrolytes, pH, ionic strength of the media and nature of the substrate. In many cases, subtle changes in the deposition conditions can lead to vastly different film architectures. One notable case is the appearance of linear or exponential growth in film thickness. The mechanism of exponential and linear growth is a topic of much discussion and controversy. It was widely accepted that exponential growth is due to inter-diffusion of polymer layers[53,54] but more recent work suggest that inter-diffusion is not required.[45,55] The work in Chapter 2 describes a method that provides a measurement of

the dynamic conformational changes and directly addressees the topic of exponential and linear growth. Here, we provide a brief overview of the role of solution pH and ionic strength in LbL film growth and properties.

1.2.1.1 pH of the polyelectrolyte solutions

The effect of solution pH is highly dependent on the use of strong or weak polyelectolytes in the LbL process. LbL deposition using strong polyelectrolytes such as the anionic polymer polystyrenesulfonate (PSS) and cationic poly(diallyldimethylammonium chloride) (PDADMAC) are fully charged over a large pH range and therefore show little dependence in film structure with pH. On the other hand, LbL deposition using strong/weak or weak/weak polyelectrolyte combinations are often highly dependent on solution pH. This is because of the pH sensitivity to the degree of dissociation.[56] For example, the thickness per layer for the weak/weak polyelectrolyte system of poly (acrylic acid) (PAA) and poly (allylamine hydrochloride) (PAH) deposited on a silicon wafer varied from 5 A^0 at pH 4.5 to 80 A^0 at pH 6. The PAH chains are fully ionized and the PAA chains are close to fully ionized over this pH range. This dramatic increase in thickness with pH occurs when the surface charge density of PAA increases from pH 4.5.[57] It was explained that the enthalpy gain from adsorption of polyelectrolyte chain on to the surface is not sufficient to overcome the entropy loss for a polyelectrolyte chain to adopt a flat conformation on the surface. Instead, the polymer chains extend out from the surface and form a thicker layer with high segmental population of loops and tails.

When increasing pH beyond 6, the thickness of the polyelectrolyte layers decreased because both polyelectrolytes in that region are fully ionized and the surface charge density is high. In this case, the entropy loss by the adsorbing polyelectrolyte chain is offset by the larger enthalpy gain from adsorption of the fully charged polyelectrolyte. The polyelectrolytes lay flat on the surface and thickness of the layer is thinner.[57]

1.2.1.2 Ionic strength of the polyelectrolyte solutions

The ionic strength of the polyelectrolyte solutions have the strongest effect on fine tuning the layer by layer deposited thin films in A^0 precision.[58,59] In DI water, electrostatic repulsions between the charged segments of a polyelectrolyte molecule result in a swelling of the coiled blob.[60] By increasing the ionic strength, the charges along the polyelectrolyte chain are screened due to the presence of counterions in solution and counterion adsorption on the polyelectrolyte chain. This leads to a decrease in size of the polymer in solution and also results in a larger thickness of the adsorbed layer.[59] For example, Figure 1.2 shows a linear increase in film thickness as a function of ionic strength for silicon wafers coated with ten layer pairs of polystyrenesulfonate (PSS) and poly (diallyldimethylammonium chloride) (PDADMAC).[58]

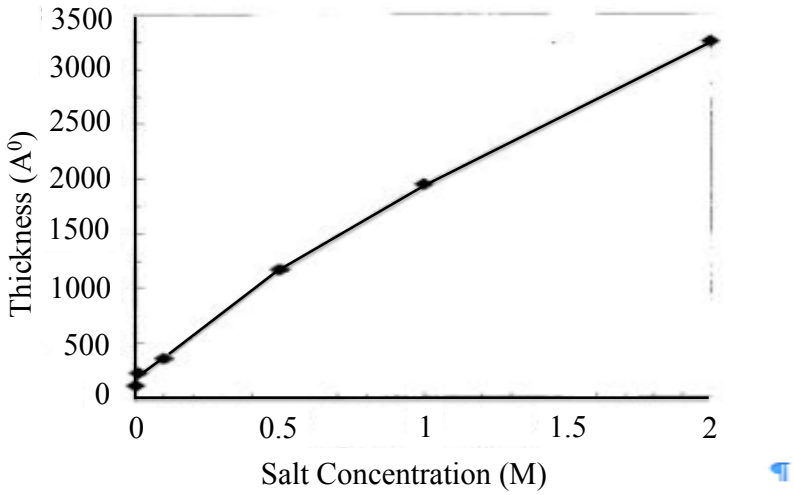

Figure 1.2 Film thickness *vs.* NaCl concentration in the polymer solutions. Figure reproduced from Von *et al;*[59]

1.2.2 LbL assembly *via* Hydrogen bonding

LbL assembly, in which the driving force is hydrogen bonding between two components of the bi-layer, have been used despite the fact that this is a weak force compared to LbL films formed via electrostatic interactions. However, preparing films based on hydrogen bonding have attractive properties as first demonstrated by Zhang *et al*;[36] Rubner *et at*;[61] simultaneously in 1997 and later by Wang *et al;*[62] Fu *et al*;[63] and Zhang *et at;*[25,64,65] using various building blocks to prepare composites. A schematic illustration of an application of LbL films via the hydrogen bonding is shown in Figure 1.3. In this example, poly(acrylic acid) (PAA) is the hydrogen bond donor and poly(4-vinylpyridine) (PVP) is the hydrogen bond acceptor. In short, an amine-functionalized substrate is immersed in particular solvents containing hydrogen bonding donor (Step I in Figure 1.3) and acceptor molecules (Step II in Figure 1.3) alternatively.

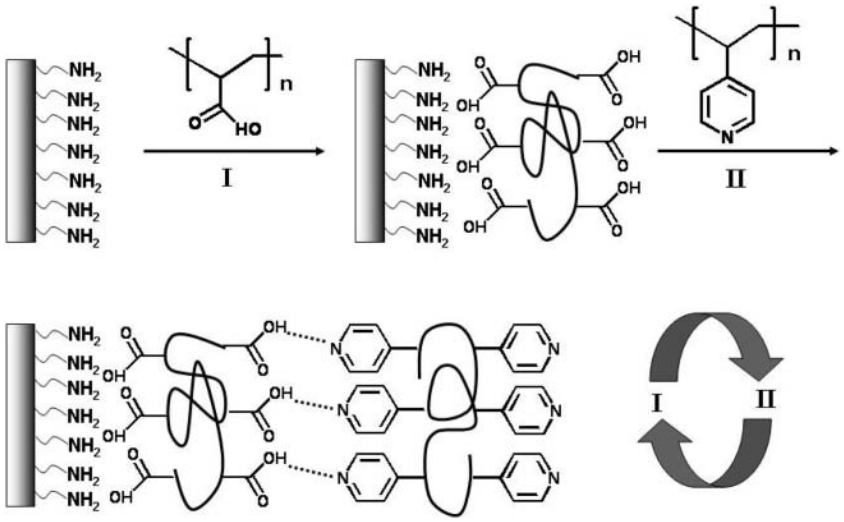

Figure 1.3 Fabrication of LbL self-assembled multilayer films *via* hydrogen bonding between carboxylic acid groups and pyridine groups. Figure reproduced from Zhang *et al;*[65]

Some small organic molecules (non polymeric) are soluble in water and hydrogen bonds have stronger interaction in nonpolar solvents so organic solvents are occasionally used for LbL deposition of hydrogen bonded thin film fabrication.[66,67] One attribute of LbL films based on hydrogen bonding is that the nature of the hydrogen bonding is sensitive to parameters such as pH,[68] ionic strength of the solution,[69] and temperature.[69,70] In one example, it was shown that the LbL films prepared by using PAA and PVP *via* hydrogen bonding interactions are stable up to pH 6.9, and that the PAA component dissolves when pH is raised beyond this point. PAA was removed from the PAA/PVP composite by immersing the LbL film in pH 13 NaOH solution. It was shown that the remaining PVP underwent a gradual reconformation yielding a structure with different surface roughness, porosity, and surface coverage.[65]

1.2.3 LbL assembly *via* charge transfer interactions

In this LbL method, films are constructed with two types of nonionic polymer chains; one polymer with an electron accepting (*e.g.* 3,5-dinitrobenzoyl) and one polymer with an electron donating (*e.g.* carbazolyl) groups attached to the ends of their side chains. This approach was first introduced by Yamamoto and co-workers in 1997.[37] The driving force of the interaction is the charge transfer (CT) interaction between donor and acceptor polymers. Films constructed using this approach have alternating layers of CT complexes as shown in Figure 1.4. Furthermore, layered films can be constructed in organic non-aqueous solvent, which makes it possible to introduce hydrophobic moieties to the composite films.[38]

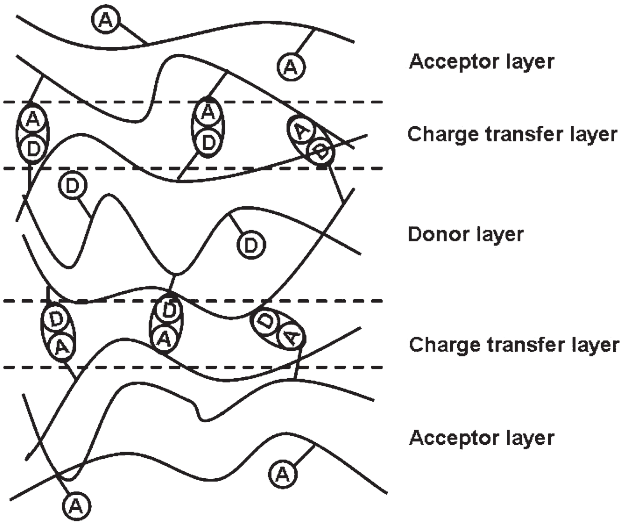

Figure 1.4 An illustration of multilayer film constructed *via* CT interactions. For simplicity the carbazolyl groups and 3,5-dinitrobenzoyl groups are represented as D and A, respectively. Regions of CT complexes formed are circled. Figure reproduced from Zhang *et al;*[65]

In one example, a film with improved electrical conductivity was synthesized by depositing poly(dithiafulvene) and poly(hexanyl viologen) in DMSO solutions as the electron donating and electron accepting groups, respectively.[71] It was also reported that deposition of poly [2-(9- carbazolyl)ethyl methacrylate] (PCzEMA having an electron donating carbazole group) and poly [2-[(3,5-dinitrobenzoyl)oxy]ethyl methacrylate] (PDNBMA having an electron accepting 3,5-dinitrobenzoyl group) in dichloroethane, produced films with second harmonic generation (SHG). First, a non-linear optical (NLO) dye PCzEMA-DR1 was synthesized by random copolymerization of CzEMA and 4′-[[2-(methacryloyloxy)ethyl]-ethylamino]-4-nitroa-zobenzene (DR1MA). Then, LbL films were prepared by the sequential deposition of PCzEMA-DR1 (electron donor NLO dye) and PDNBMA. The SHG was produced in which incident photons interacting with NLO dye PCzEMA-DR1 formed new photons at twice the frequency.[72]

1.2.4 LbL assembly *via* molecular recognition and bio-recognition

In this approach, specific interactions between host - guest system are used as a means of constructing LbL assemblies. The idea of molecular recognition combines hydrogen bonding, hydrophobic force, and van der Waals force that are usually formed between two selected molecules, host and guest.[73] Cyclodextrins (CD) are an example of a host molecule used in LbL assembly.[74,75] LbL films prepared with CDs exhibit reversible swelling and shrinking mediated by the change of pH and ionic strength of the medium, a property that can be used for controlled loading and release of a particular substance.

In one example, Gao *et al;* has demonstrated that the molecular recognition between *β*- cyclodextrin (*β*-CD) and ferrocene can be used as a driving force to construct multilayers.[73] In this study, the two molecules *β*-CD and ferrocene are grafted separately to the polyelectrolyte poly(allylamine hydrochloride) (PAH) backbone. Using the same polymer backbone avoided electrostatic interaction between polyelectrolytes during the LbL deposition. The PAH-g-β-CD and the PAH- g-ferrocene microcapsule is made by layer-by-layer deposition of the above molecules on spherical $CaCO_3$ particles and then the $CaCO_3$ particle is removed by using disodium ethylene diamine tetraacetate dihydrate (EDTA). The microcapsule is sensitive to pH and ionic strength of the medium. With low pH and low ionic strength, the capsules swell in size and with high pH and high ionic strength the capsules shrink in size. A schematic illustration shown in Figure 1.5 depicts *β*-CD encapsulates ferrocene through host - guest interaction during LbL assembly onto Calcium carbonate particles. It was shown that microcapsules of LbL films exhibited sensitivity to pH and ionic strength and that the sacrificial carbonate microparticle core is dissolved by exposure to solutions containing disodium ethylene diamine tetraacetate dehydrate (EDTA). The microcapsules can function as reservoirs for drugs, DNA, enzymes, or other molecules.

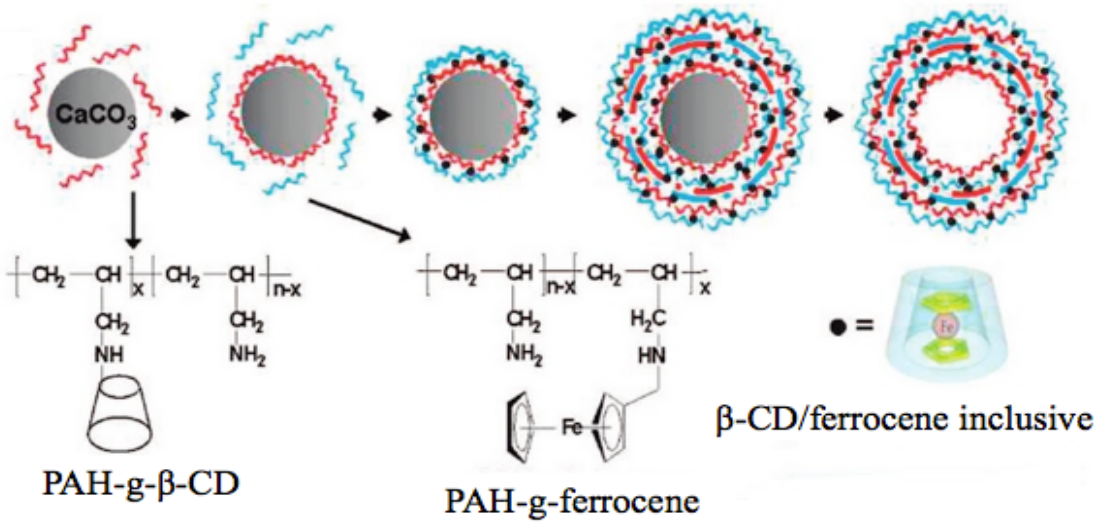

Figure 1.5 LbL assembly of the same polyelectrolyte on Calcium carbonate particles to obtain hollow microcapsules using host-guest interaction. The chemical structure of PAH-g- β -CD, PAH-g-ferrocene, and β -CD/ferrocene inclusive are shown in the second row. Figure reproduced from Gao *et al;*[73]

The use of bio-recognition as a driving force to prepare LbL films is another type of host and guest system. Specific types and combinations of molecules, for example, streptavidin/concanavalin,[65] streptavidin/biotinylated polylysin, sugar/lectin,[41,76] and avidin/biotin[42] are used to construct LbL multilayers. Schematic illustration of streptavidin/consanvalin A multilayers is shown in Figure 1.6. These assemblies extend the scope of LbL in constructing functional thin films since nonionic polymers and polymeric materials with the same polarity can be built into the same assemblies through biological interaction.

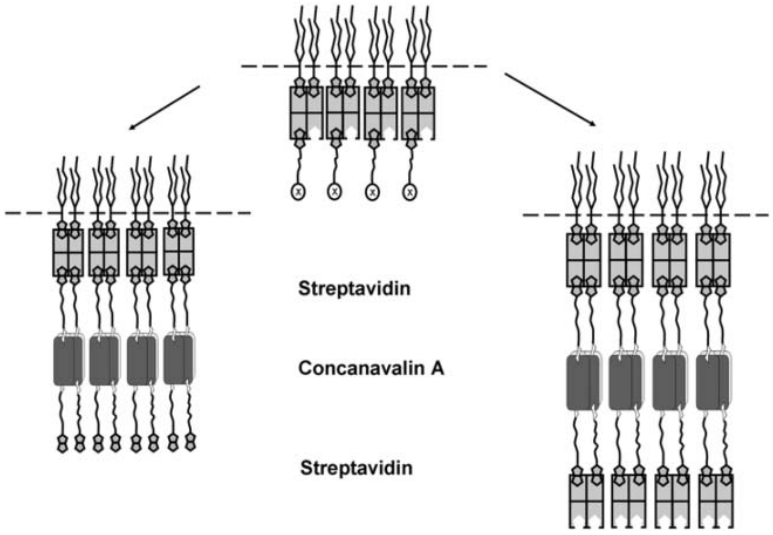

Figure 1.6 LbL self-assembly of streptavidin and concanavalin A through bio-recognition at the air/water interface. Figure reproduced from Zhang *et al;*[65]

Interactions between antigen/glucose oxidase conjugated antibody have been used by Bourdillon *et al;*[40] to construct LbL multilayers of glucose oxidase on glassy carbon as a high performance bio sensor to detect glucose. Another example, as demonstrated by Hong *et al;*[30] is the use of bio recognition interaction between streptavidin and biotinylated polylysine at the air/water interface to construct LbL multilayer depositions at solid/liquid interface with potential applications in the field of biosensors and biocatalysts since streptavidin will bind any biotinylated material and thus allow for the immobilization of a multitude of functional molecules.[30,39]

1.2.5 LbL assembly *via* coordination interaction

Coordination interaction is another type of driving force that scientists have been using to construct LbL multilayer films. The basic concept is to use reactive

polyelectrolytes to form covalent coordination interaction between the layers. One example, as shown in Figure 1.7, employed poly(cadmium 4-styrene sulfonate) ($PSS/Cd_{1/2}$) and poly(vinyl pyridine) (PVP) to prepare LbL assembly.[43] It is anticipated that the method will provide a powerful strategy to prepare robust films of organic/inorganic composites via coordination attachments to produce semiconductor nanoparticles.

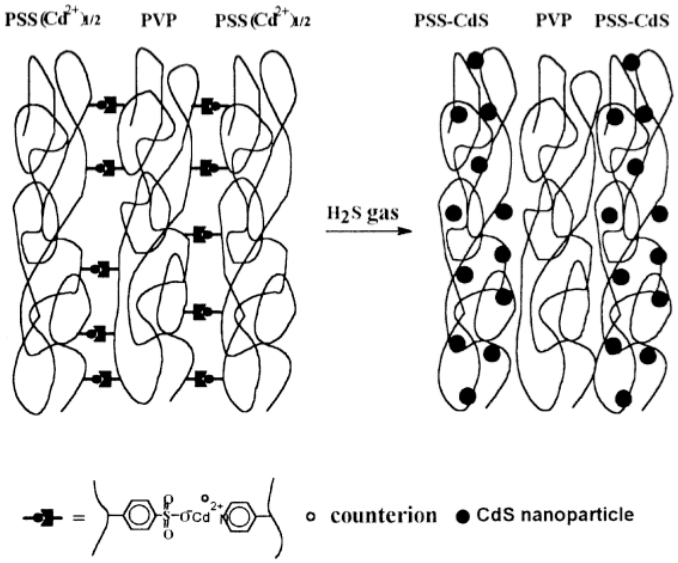

Figure 1.7 Schematic illustrations of the alternating $PSS(Cd)_{1/2}$/PVP multilayers and PSS-CdS nanoparticles/PVP heterostructure. Figure reproduced from Xiong *et al;*[43]

In brief, sodium ions of PSS exchange with the transition divalent Cd^{2+} in solution. The CdS is a direct band gap semiconductor and the Cd^{2+} ion binds with two sulfonate groups in a 2:1 reaction. Then a quartz, CaF_2, or silicon wafer was immersed into a poly(ethyleneimine) (PEI) solution. The PEI functionalized substrate was immersed into a solution containing the cadmium neutralized PSS, followed by a rinse

step. The substrate was then immersed into a second solution of PVP to complete the deposition process and multiple layers achieved by repeating the alternate deposition process. Post treatment of the layered film with H_2S resulted in PSS-CdS nanoparticle/PVP composite films of uniform thickness.[43]

1.2.6 Deposition techniques for LbL assembly

The essential element of the LbL technique is the application of deposition of alternating layers of molecules or particles. It is noted that the number of LbL systems reported has exploded in the last decade and has been extended to well beyond two component systems or single mode of interaction as films produced with mixtures of many different molecules and particles and combinations thereof have been reported. In general, several deposition methods including dip coating, spin coating, spray coating, spin-spray coating, and flow-based deposition are widely used in LbL assembly to form multi-layer composite films. The following sections from 1.2.7 to 1.2.11 summarize primary techniques used in LbL assembly. For simplicity, in describing the deposition methods I will use a two-component multilayer using a cationic and anionic polyelectrolyte.

1.2.7 Dip coating technique

In this method, a positively charged substrate is first immersed into a beaker containing a solution of negatively charged polyelectrolyte. After a defined contact time to allow adsorption of the polyelectrolyte, the substrate is then removed, rinsed and then immersed in a second solution or suspension containing oppositely charged

polyelectrolyte. This is followed by a washing step and completes a cycle in which a layer of each polyelectrolyte is adsorbed onto the charged substrate. Typical substrates used are glass,[7] TiO_2 coated glass,[77] Indium tin oxide (ITO),[78] or Si wafer.[79,80] A simplified schematic representation of the first cycle of LbL deposition *via* electrostatic interaction is shown in Figure 1.8. This cycle is repeated until a desired number of layers (or thicknesses) are achieved. The anions and cations could be polymeric,[7] colloids[29,81,82] or nanoparticles[22,43] and, as mentioned above, does not necessarily have to be restricted to a two component system.[83] As one can imagine, the self-regulatory nature of a monolayer film is controlled by the repulsion of like charged components.

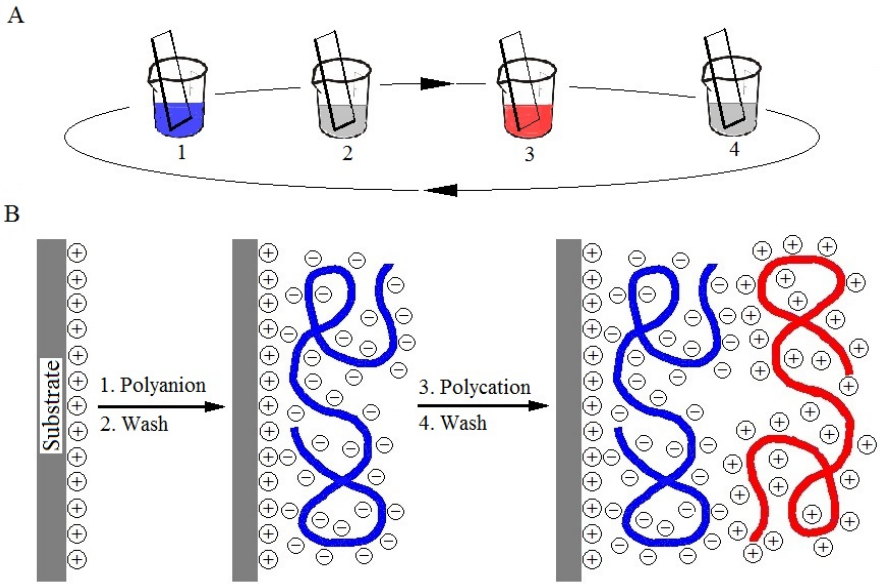

Figure 1.8 (A) Schematic of the film deposition process using slide and beakers. Steps 1 and 3 represent the adsorption of polyanion and polycation, respectively and steps 2 and 4 indicate the washing steps. (B) The four-step sequence represents a complete cycle. Figure reproduced from Decher *et al;*[7]

One or more washing steps is necessary after each adsorption step as it helps to stabilize weakly adsorbed polymer layers.[84] Washing steps also avoid contamination of the next adsorption solution by loosely bound previous solution components, particularly important when using the dip coating technique. If necessary, a drying step can be incorporated after the washing step.[85] It was reported that the time for a single layer deposition ranges from minutes, in the cases of polyelectrolytes,[84,86] to hours, in the case of gold colloids.[87,88]

1.2.8 Spin coating technique

In the spin coating technique, first, a positively charged substrate is mounted on a spin coater and spun at a fixed rate. A few drops of polyanion solution are then added onto the spinning substrate followed by a wash step, by which removes the loosely bound polyanion from the substrate. A consecutive addition of polycation onto the spinning substrate, followed by a wash step, completes a full cycle. (Figure 1.9). This cycle can be repeated until desired numbers of layers or intended properties are achieved.

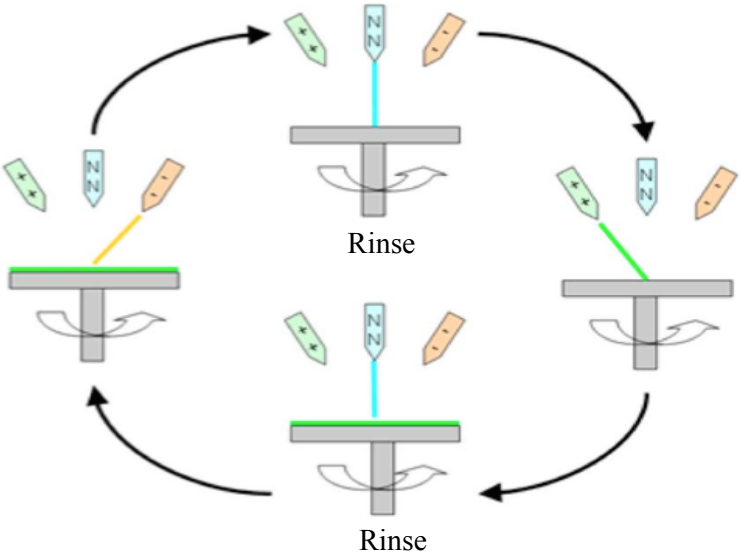

Figure 1.9 Schematic representation of spin assisted LbL assembly alternate adsorption of (+) positively charged and (–) negatively charged polyelectrolyte solution on to a surface with (N) rinsing steps in between. Figure reproduced from Vozar *et al;*[89]

The spin coating technique has a few advantages over the dip coating technique. For example, the adsorption occurs in seconds.[89] The fast adsorption is mainly due to rapid coverage of the entire surface provided by the centrifugal forces acting on the liquid layer. In addition, the molar concentration of polyelectrolytes are significantly increased due to the rapid removal of water from the liquid phase by high rotation speeds and this typically produces thin films compared to dip coating.[90]

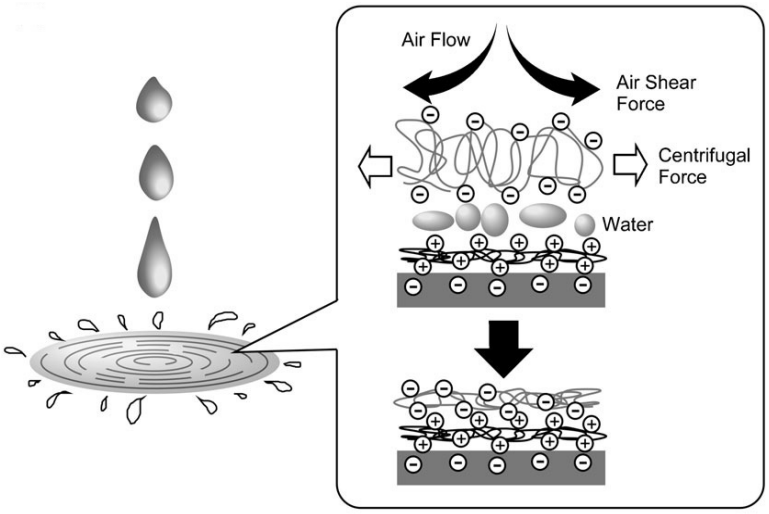

Figure 1.10 Air shear force and centrifugal force acting on liquid phase in spin assisted LbL assembly. Figure reproduced from Ariga *et al;*[90]

It was reported that the films created by the spin coating method yield highly ordered internal structures far superior to the films obtained by the conventional dip coating method. This is primarily due to a mechanical effect upon the air shear force caused by the spinning process which causes the molecules to align in the direction of the centrifugal force (see Figure 1.10).[90,91] The spin coating method creates highly mechanically robust and stratified LbL films.[92-94]

1.2.9 Spray coating technique

In this method, polyanions and polycations are sprayed alternatively or simultaneously on to charged substrates mounted in a vertical position. A schematic representation of the technique is shown in Figure 1.11. Many scientists including Decher *et al;*[95-97], Ferry *et al*;[98] Hammond *et al;*[99] and Farhat *et al;*[100] have successfully employed the spray coating technique in LbL to produce multilayers films.

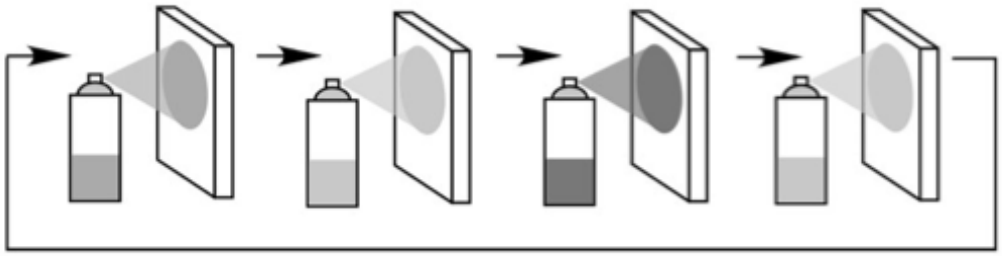

Figure 1.11 Spray coating technique to produce LbL assembled multilayers. Figure reproduced from Ariga *et al;*[90]

One of the advantages of this technique is that the time required to assemble layers is less than conventional dip-coating method. Since the liquid continuously drips along the vertical surface, the rinse step may be eliminated, leading to even less time to assemble the multilayers. Using this technique, films with high uniformity and low surface roughness, as measured by AFM and X-ray reflectometry, can be prepared.[90] In general, the thickness of the multilayers increased linearly with the number of spray-coated layers.

1.2.10 Spin-spray coating technique

This is a hybrid of the spin and spray coating techniques discussed above and was first demonstrated by Merrill and Sun in 2009.[101] In this technique, polyelectrolytes are sequentially sprayed onto a rotating substrate. The technique has more controllability over film thickness and results in less material waste. Gittleson and co-workers[85] have improved the technique, as shown in Figure 1.12, by employing sub-second spray times and active drying of the substrate. The improvements led the cycle time of a deposition from 25 to 13 seconds, significantly reducing the time by 50 %, By controlling

parameters such as solution concentration, spray time, substrate spin rate, drying time, drying air flow and temperature, nanolevel control over layer deposition can be achieved. For example, film thicknesses were obtained that were four times lower than possible with conventional dip LbL assembly methods.

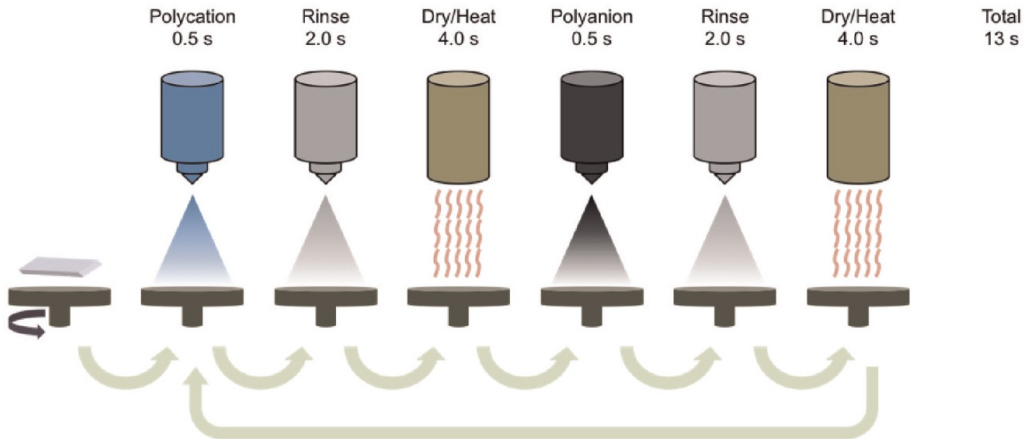

Figure 1.12 Schematic of spin-spray layer-by-layer assembly technique. Figure reproduced from Gittleson *et al;*[85]

It was demonstrated that composite films of poly(styrene sulfonate) + single-walled carbon nanotubes / poly(vinyl alcohol) (PSS + SWNT / PVA), poly(styrene sulfonate) + multiwalled carbon nanotubes / poly(vinyl alcohol) (PSS + MWNT / PVA), Nafion + single-walled carbon nanotubes / polyethyleneimine (Nafion + SWNT / PEI), and poly(styrene sulfonate) + single-walled carbon nanotubes / polyaniline (PSS + SWNT / PANI) can be successfully prepared on glass slides or silicon wafers using this spin spray layer-by-layer method.[85] Packing density of these components in LbL film is higher than the packing density of these materials in dip coated LbL film, leading to high

volumetric density of the film. These composites can potentially be used as electrodes in lithium ion rechargeable batteries.[85]

1.2.11 Flow-based deposition technique

This technique can be classified as a dynamic method of LbL assembly where polyanions and polycations flow through a cavity equipped with a charged substrate. Deposition takes place when molecules in the liquid come in to contact with the substrate. A typical sketch of the flow cell is shown in Figure 1.13, where substrate could be in a horizontal[79] or vertical position.[77,82]

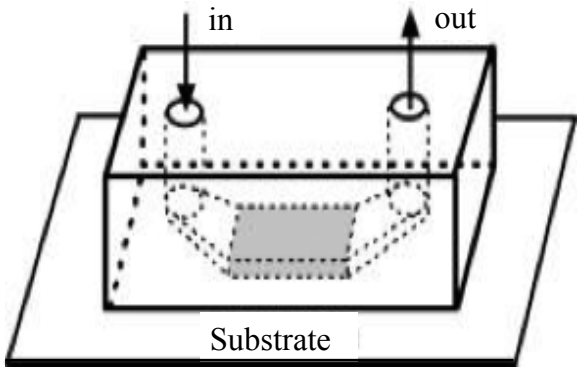

Figure 1.13 Fluidic device used to deposit polyelectrolytes on substrates. The open section (the shaded area) at the bottom of the device has a dimension of 20 x 10 x 2 (length x width x height) mm^3. Figure reproduced from Kim *et al;*[79]

In one example, a multilayer consisting of poly(diallyldimethylammonium chloride) (PDDA) and poly(1-4-(3-carboxy-4-hydroxy-pheylazo)benzene sulfoamido)-1,2-ethandiyil, sodium salt) (PAZO) was prepared using a flow based technique. It was reported that the resulting film qualities, such as surface roughness and porosity, are comparable to the films deposited by conventional LbL techniques.[79]

1.2.12 LbL film characterization methods and techniques

In general, film thickness, mass deposited, pore size, surface uniformity and roughness, are some of the important parameters, that are measured and used to gain a better understanding of the structure-property relationship of the multilayer films. As analysis techniques, Ultraviolet-Visible (UV-VIS), Fourier transform infrared (FTIR) spectroscopy, quartz crystal microbalance (QCM), Atomic force microscopy (AFM), Scanning electron microscopy (SEM), Transmission electron microscope (TEM) and X-ray diffraction are commonly used to follow the deposition process.

In the cases of UV-VIS active materials, the amount deposited is followed by the increase in absorbance of specific bands of the UV spectra. For example, the deposition of Au nanoparticles (Au-NP) and nitrodiazoresin (NDA) layered assembly was followed by UV-VIS spectroscopy.[98] Specifically, the UV-VIS absorbance bands at 379 nm due to $\pi - \pi^*$ transition of N_2^+ in NDA and 577 nm due to Au-NP were used to identify the amounts deposited in each cycle. It was shown that there was a linear increase in thickness with each cycle.[98] Information of the conformation of molecules in films has also been obtained from the use of UV-VIS spectroscopy. In this case, polarized UV-VIS spectra were used to study the orientation of the molecules in multilayered films.[24]

Infrared spectroscopy is also frequently used to identify the nature of the interactions between layers. Functional groups such as carboxylic, amines, nitro groups, hydroxyl groups, and sulfonic groups are common in most of polyelectrolytes used in LbL deposition. Thus, changes in vibrational modes of these functional groups can be

easily monitored by IR spectroscopy. For example, FTIR was used to understand the interaction between poly(4-vinylpyridine) (PVP) and *p*-(hexaflouro-2-hydroxylisopropyl)-α-methylstyrene (PSOH) layers assembled *via* LbL method. In particular, it was shown that H-bonding between the HO^- groups in PSOH and pyridine rings in PVP occurred as indicated by a shift to lower frequency of the HO^- stretching mode.[62]

Quartz crystal microbalance (QCM) is another frequently used technique to monitor the mass deposited. A change in frequency of the quartz crystal resonator is a function of the mass deposited on the surface during the layer deposition. The device can be used in liquid environments, which is a particular advantage as most LbL assemblies take place in aqueous or nonaqueous liquid systems. The technique can be used to monitor average mass deposited in each layer as shown by Chen *et al;*.[102] QCM can detect the adsorption of material on to a quartz electrode, and the precision of the measurement is in the ng range. For example, in one study, QMC was used to determine the average mass deposited onto a quartz electrode per layer during the deposition of porphyrin and phthalocyanine layers. The average mass change per layer deposition was reported as 112 ng for porphyrin and 101 ng for phthalocynanine.[24]

1.2.13 Flow based LbL deposition and *in situ* analysis by FTIR – ATR

Often, it is the kinetic aspects of polymer adsorption and not the equilibrium properties of the polymer layers that define the properties of the adsorbed polymer layer.[103] Experimental studies of the dynamics of polymer adsorption in LbL deposition

has only been reported recently. Guzman *et al.*[104,105] measured the change in adsorbed amount as a function of time using X-ray reflectivity, dissipative quartz crystal microbalance and ellipsometry. They showed that inter-diffusion can exist in linear growth polyelectrolyte multilayers (PEMs) and thus polymer diffusion is not exclusive to exponential growth. Clearly, further insight into the mechanism of film growth in LbL processes would benefit from a method that can measure both the dynamic change in adsorbed amount as well as dynamic changes in the polymer conformation during LbL deposition. This provided the motivation for developing the methods described in this thesis.

An infrared spectroscopic based technique was developed previously in our research lab that enabled the kinetic measurement of polymer adsorption on silica particles[106] and later, this was extended to ATR infrared measurements with TiO_2 films.[77] Both the adsorbed amount and segment/surface interactions are measured as a function of time and from this the dynamic of the polymer conformation can be followed for single layer.

Specifically, Li and Tripp,[77] used a flow based technique with TiO_2 functionalized ZnSe ATR crystal as the substrate to deposit sodium polyacrylate (NaPA) from an aqueous solution. Changes in intensity of IR adsorption bands due to COO^-, COOH and CH_2 groups were used to determine the amount and conformation of NaPA adsorbed on a positively charged TiO_2 surface.[77]

The normalized intensities of COO^- and COOH with CH_2 band for NaPA polymer

are different for the polymer in solution and adsorbed on TiO_2 layer. This difference occurs due to COO^- binding with positively charged sites in TiO_2 surface and hence provides a method to measure the dynamic bound fraction. It was also shown that the bound fraction of cationic surfactants to the NaPA layer could be determined from the changes occurring in the COO^- and COOH bands. Thus, it is a natural extension of this work to examine the dynamic conformation and amount during deposition of LbL deposited thin films.

The research presented in Chapters 2 and 3 describe the use of the ATR approach to obtain molecular details of the dynamic processes occurring during sequential adsorption of cationic and anionic polyelectrolytes on surfaces and as a function of ionic strength. Chapter 4 is a study of Fe^{3+} uptake by a self-assembled block copolymer on a membrane. The introduction section of Chapter 4 provides the background and rationale for these measurements.

CHAPTER 2: DYNAMICS OF THE LAYER BY LAYER DEPOSITION OF POLYELECTROLYTES STUDIED IN SITU BY USING ATTENUATED TOTAL REFLECTANCE INFRARED SPECTROSCOPY

2.1 Introduction

Layer-by-Layer (LbL) deposition is a multistep thin film fabricating technique that has experienced a rapid increase in the number of applications in the last decade.[4,79] The most common approach in generating LbL films involves the sequential adsorption of anionic and cationic polymers onto a substrate.[56,79,96] Much of our understanding of the structure-property relationships of polyelectrolyte LbL films is derived from measurement of the thickness,[95,107,108] mass, and surface texture[14,109] recorded after deposition of each layer. While the nature of the molecular structure of a single layer of a polyelectrolyte onto an oppositely charged substrate is often dictated by kinetic factors,[110] much less is known regarding the dynamics that occur during sequential adsorption of alternating layers of cationic and anionic polyelectrolytes.

In this chapter, I present my work of developing a method for monitoring the dynamics during the sequential adsorption of polyelectrolytes on TiO_2. The work is an extension of an infrared spectroscopic method developed for dynamically measuring both the mass adsorbed and changes in the number of segment/surface interactions (i.e., bound fraction) for a single polymer layer on TiO_2.[77]

For adsorption of a single polyelectrolyte layer onto charged surfaces and interfaces, there has been extensive theoretical and experimental activity conducted over

the last four decades aimed at gaining an understanding of the equilibrium behavior of adsorbed polymers on surfaces.[7,111,112] It is generally accepted that the polyelectrolyte attaches to the surface by multiple segment/surface charge points leading to the formation of loops and tails that extend out into solution away from the substrate[52,113] (see Figure 2.1). While charge neutralization occurs at the segment/surface charged points,[114] it is the charged sites contained in the loops and trains of the polymer that electrostatically repel incoming polymer molecules for adsorbing on the surface, and hence, self-limits the amount adsorbed, as well as an overall reversal, of the surface charge.[53] The primary interest is the extended region because it produces the repulsive force that is the essential element in important industrial processes such as the steric stabilization of colloidal systems.

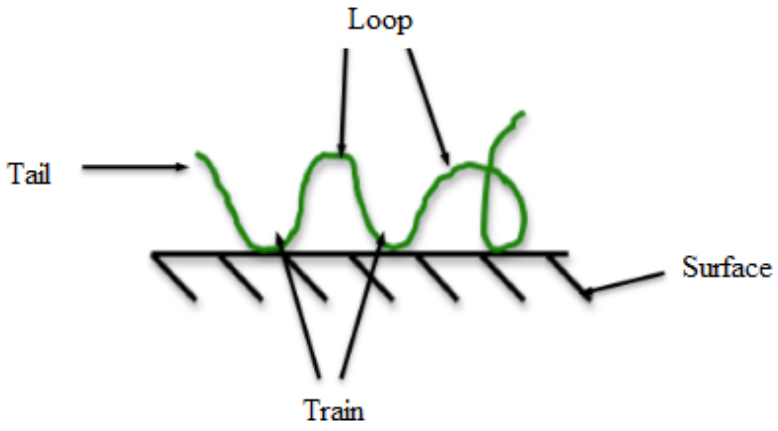

Figure 2.1 Polymer adsorbed on a surface.

As a result, theoretical work was focused on deriving expressions for predicting the surface density and thickness and the concentration profile of the extended polymer layer. Experimental methodology was designed to measure the surface density or the

extended length of adsorbed polymers for verification and comparison to theoretical predictions. It is the self limiting nature of the polyelectrolyte adsorption leading to charge reversal of the surface and repulsion of further adsorption of the same charged polyelectrolyte, that is the central concept underlying LbL generation of thin films of well–controlled morphology and thickness.[115]

Often, it is the kinetic aspects of polymer adsorption and not the equilibrium properties of the polymer layers that define the properties of the adsorbed polymer layer.[103] Typically, large kinetic barriers exist because of changing the polymer conformation involves breaking and reforming of bonds between polymer segments of adsorbed polymer chains. It is generally found that simple alteration of sample history or experimental procedures can result in polymer trapped in a different metastable non-equilibrium conformation. Thus, kinetic factors often dominate the adsorption process and, in the end, either impede the equilibrium process or make it prohibitively slow to attain for practical applications.

The kinetic factors should also dominate the LbL adsorption process, given the variety of deposition methods and the emphasis placed on reducing the time of each adsorption step. There are four main types of LbL deposition methods dip coating method,[7] spin coating method,[89] spray coating method[99] and flow-based method. In all these methods, the incubation time with the polymer fluid is on the order of seconds to minutes, therefore, equilibrium conformation of the polymer layer is unlikely to occur under these short times since the time needed to reach equilibrium is typically longer.

There are cases where the dynamics of the polymer adsorption are used to explain the different structural properties of the linear and exponential multilayer growth regimes. For example, it has been widely accepted that exponential growth is due to the diffusion of polymers within the film and is generally known as the "in/out" diffusion model.[53] According to this model, polyanions from solution may diffuse into the growing film to form a reservoir of "free" polymers, and these "free" polymers subsequently diffuse out of the film to contribute to complexation of the next layer of incoming polycations. Evidence to support this diffusion model mainly comes from Confocal Laser Scanning Microscopy (CLSM), in which a fluorescently tagged polymer layer was found to diffuse throughout the entire structure[116]. Salomaki *et al*.[117] also proposed that all LbL systems follow exponential buildup but become linear when diffusion is slower than deposition time. Recently, other models involving island and dendritic growth have also been proposed to explain exponential growth in films[118].

The importance of the dynamics of polymer adsorption in LbL deposition has only been reported recently. Guzman *et al*.[104,105] measured the change in adsorbed amount as a function of time using X-ray reflectivity, dissipative quartz crystal microbalance and ellipsometry. They showed that inter-diffusion can exist in linear growth polyelectrolyte multilayers (PEMs) and thus polymer diffusion is not exclusive to exponential growth. Further insight into the mechanism of film growth in LbL processes would benefit from a method that can measure both the dynamic change in adsorbed amounts as well as dynamic changes in the polymer conformation during LbL deposition.

An infrared spectroscopy based technique was developed in my lab which enabled the kinetic measurement of polymer adsorption on silica particles[106] and later extended this to ATR infrared measurements with TiO_2 films.[77] Both the adsorbed amount and segment/surface interactions are measured as a function of time for single polymer layer. From this, the dynamic of the polymer conformation can be followed. In this chapter, I examine the potential of extending the IR measurements to study the dynamics of multilayer buildup. In particular, I use IR-ATR to study the sequential adsorption of sodium Polyacrylate (NaPA) and Poly (diallyldimethylammonium) chloride (PDADMAC) on a TiO_2 film. I selected the anionic NaPA and the cationic PDADMAC because these polymers are often used in LbL work. Furthermore, our ATR methods used to measure the bound fraction were developed using NaPA adsorption on TiO_2, and therefore, the adsorption of this polymer on TiO_2 is a natural choice for extending the IR methods to LbL multilayers. I show that rearrangement and polymer diffusion are observed for NaPA, whereas, PDADMAC pancakes onto the underlying layer during the multilayer formation. I obtain a linear film growth, and therefore, in agreement with Guzman *et al.*[104], I find that rearrangement and diffusion do not necessarily correlate to exponential growth.

2.2 Experimental

2.2.1 Materials and methods

A flow-through ATR cell was purchased from Harrick and used a 45° ZnSe internal reflection element (IRE) of dimensions 50 × 10 × 2 mm^3. A description of the flow-through ATR cell and its use to measure polymer adsorption on TiO_2 coated IRE is described elsewhere.[77] All spectra were recorded on an ABB-Bomem FTLA 2000 spectrometer at 8 cm^{-1} resolution. Typically 100 scans requiring about 2 minutes used to collect each spectrum.

Fumed TiO_2 powder (P25) was purchased from Degussa, and had a (BET) N_2 surface area of about 50 m^2/g. The measured isoelectric point of the P25 powder was pH 6.6 and was determine by using electrophoretic mobility.[82] Sodium polyacrylate (NaPA) has an average molecular weight (Mw) of 30,000, and polydispersity index (Mw/Mn) of 1.4 and poly (diallyldimethylammonium) chloride (PDADMAC) has an average molecular weight (Mw) of 100,000-150,000 and polydispersity index (Mw/Mn) of 1.6 were purchased from Sigma Aldrich and used as received. A 20 ppm solution of NaPA and 30 ppm solution of PDADMAC were prepared by adding a known quantity of polymer to distilled water. Then pH of these solutions and water were adjusted using either dilute HCl or NaOH solutions.

2.2.2 TiO_2 coating on ZnSe crystal

The ZnSe IRE was coated with a layer of TiO_2 using an established procedure.[77,82] Specifically, the TiO_2 powder (30 mg) was dispersed in 25 ml of methanol and

ultrasonicated for 30 minutes. A 200 µl aliquot of the suspension was evenly deposited on one side of the ZnSe crystal surface using a pipette. Evaporation of the methanol under ambient conditions resulted in a uniform TiO_2 film on the crystal and the Atomic Force Microscopy (AFM) exhibit the film thickness as about 500 nm and surface roughness about 80 A^{0}.[82]

2.2.3 LBL deposition method

The TiO_2-coated ZnSe crystal was mounted on the flow-through cell and the cell was continuously flushed at a flow rate of 5.8 ml/min with stock deionized water adjusted to pH 3.5 using HCl. A reference spectrum was recorded at the start of flowing water through the cell. The recording of ATR spectra (100 % baseline) at various time intervals during this initial flow period usually showed changes in the amount of water probed by the IRE. This was primarily due to removal of air bubbles from the cell cavity and associated tubing. A procedure of recording a reference spectrum, followed 15 minutes later by a 100 % baseline spectrum, was repeated until no changes in a 100 % baseline spectra was observed. This typically required about 30-45 minutes from the start of flushing the cell with water. It is also noted that no evidence of removal of the TiO_2 layer was observed (decrease in TiO_2 bulk modes near 900 cm^{-1}) during this initial flow of water or in subsequent additions of polymer solutions. Once this initial "break-in" period was established, a reference spectrum was recorded and used for the remainder of the experiment.

A NaPA solution (20-ppm) at pH 3.5 was flowed through the cell at 5.8 ml/min and spectra were recorded as a function of time for approximately 3.5 hours. This deposition cycle is referred to as NaPA-1. (It is noted that at 20 ppm, the bands due to NaPA in the solution phase was not observed) Thus all bands in the spectra are due to adsorption of the NaPA on the TiO_2.[77] The cell was then flushed with pH 3.5 water for 5 minutes to remove excess NaPA from the cell cavity. This flushing step did not lead to any changes in the IR bands of NaPA or TiO_2 showing that the NaPA adsorbed on TiO_2 was not removed from the IRE during this wash cycle with water.

Next, a 30 ppm PDADMAC solution at pH 3.5 was flowed through the cell for 3.5 hours at 5.8 ml/min and spectra were recorded at specified time intervals. This cycle is referred to as PDADMAC-1. The cell was then again flushed with water at pH 3.5 for 5 minutes to remove excess PDADMAC from the tubing and cell cavity. No change in the IR spectrum was observed during this flushing step. The sequential flowing of NaPA, water, PDADMAC, and water was repeated twice using the above procedures and are denoted as NaPA-2, NaPA-3, PDADMAC-2 and PDADMAC-3. IR spectra were collected every 5 minutes during each deposition cycle. All experiments were repeated at least three times.

2.3 Results and Discussion

The structures of NaPA and PDADMAC are shown in Figure 2.2. The PDADMAC is positively charged at all pH values (strong polyelectrolyte), whereas, the NaPA has pH dependence in the number of charged groups (weak polyelectrolyte). The repulsion between segments in negatively charged NaPA molecules is decreased at low pH values leading to higher adsorbed amounts. The isoelectric point (IEP) of TiO_2 is 6.6 so the TiO_2 layer is positively charged at lower pH values. The amount of NaPA adsorbed on TiO_2 passes through a maximum value at pH 3.5 and is the reason we selected this pH for the study[77]. At pH 3.5, the TiO_2 surface is positively charged and 25 % of the NaPA segments are negatively charged as determined from absorbance due to COOH and COO^- modes in IR spectra.[77]

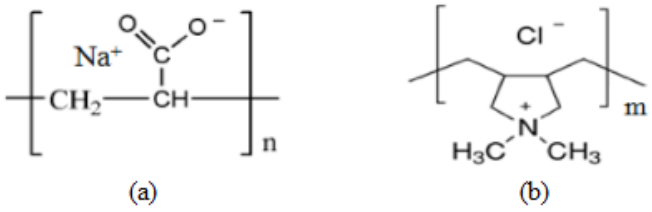

Figure 2.2 Structures of (a) NaPA and (b) PDADMAC.

Typical IR spectra recorded at the end of the first two cycles for the sequential addition of NaPA and PDADMAC are shown in Figure 2.3. Figure 2.3a is the spectrum after addition of NaPA only and the key bands are 1713 cm^{-1} assigned to a C=O stretching mode of the free COOH, 1547 and 1414 cm^{-1} assigned to the asymmetric and symmetric stretching modes of the COO^- mioety and 1455 cm^{-1} due to a CH_2 bending

mode. The inset in Figure 2.3 shows a band at 2930 cm^{-1} which is due to the CH_2 stretching mode. The intensity of the CH_2 band at 1455 cm^{-1} is used to measure the amount of NaPA adsorbed on the TiO_2. The addition of PDADMAC (Figure 2.3b) results in a decrease in intensity of the COOH band at 1713 cm^{-1} and this is accompanied by an increase in the bands due to COO^- at 1547 and 1414 cm^{-1}. The changes in these bands are due to an interaction of the positively charged sites on the PDADMAC with the negatively charged COO^- groups on the adsorbed NaPA layer. The band at 1455 cm^{-1} does not change in intensity, showing that no NaPA is removed upon addition of the PDADMAC. It is the change in intensity of the $COOH/COO^-$ bands that are used to compute the bound fraction which, in turn, provides information of the conformation of the adsorbed polymer layer. The procedure used to calculate values for the bound fraction is given in section 2.3.3. Bands at 2930 and 1455 cm^{-1} in Figures 2.3a, 2.3b, 2.3c and 2.3d are CH modes of the adsorbed NaPA and PDADMAC and these are used to calculate the amount adsorbed.

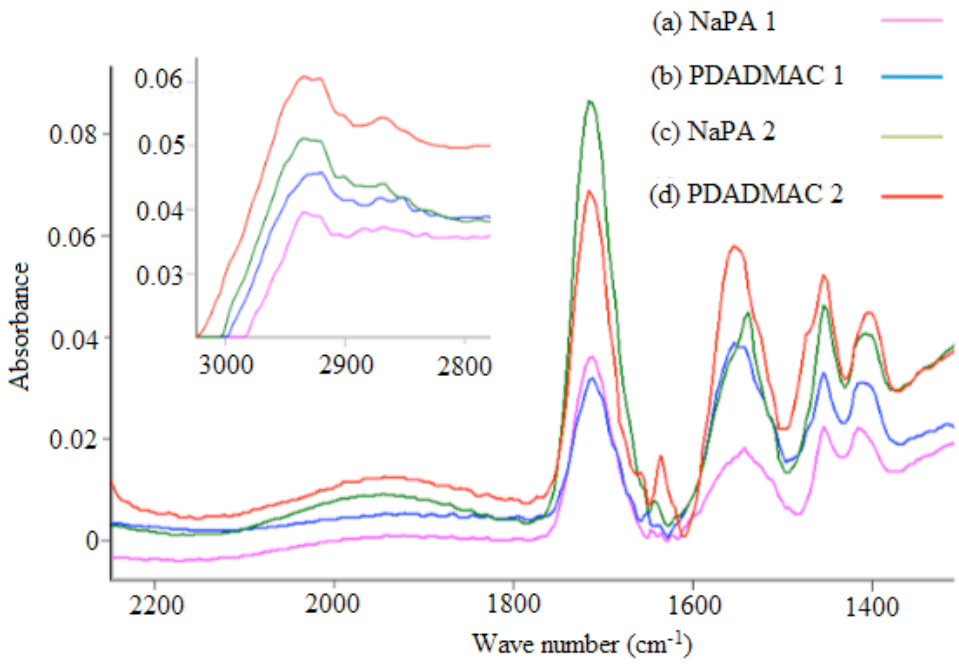

Figure 2.3 IR spectra recorded at the end of the cycle for the (a) first layer of NaPA, (b) first layer of PDADMAC, (c) second layer of NaPA, and (d) second layer of PDADMAC.

2.3.1 Measurement of adsorbed amount of NaPA and PDADMAC

The intensity of a CH_2 stretching mode at 2930 cm^{-1} and the CH_2 bending mode at 1455 cm^{-1} was used to determine the adsorbed amounts of PDADMAC and NaPA respectively. However, the 1455 cm^{-1} band overlaps with the COO^- symmetric stretching mode at 1414 cm^{-1}. To separate these two bands and obtain a value for the intensity of the 1455 cm^{-1} band, I applied a curve-fitting program in GRAMS/AI version 7.00 Thermo Galactic Software using a 75 % Lorentzian lineshape. It is also noted that both NaPA and PDADMAC contribute to the intensity of the CH stretching mode near 2930 cm^{-1}. The contribution to this band from NaPA was determined from the relative intensity of the CH stretching mode at 2930 cm^{-1} to the intensity of the CH bending mode at 1455

cm^{-1} obtained from Figure 2.3a. In practice, a scaled subtraction using the spectrum of adsorbed NaPA (Figure 2.3a) was done manually to zero out the band at 1455 cm^{-1}. The remaining band intensity at 2930 cm^{-1} after this zeroing out procedure was then due to PDADMAC

The next step was to establish a value for the amount of NaPA and PDADMAC adsorbed from the intensity of the IR bands recorded during the ATR experiments. This was accomplished using a series of calibration experiments. In the first calibration experiment, a single deposition cycle was performed (i.e., flow NaPA followed by DI water rinse, flow PDADMAC followed by DI water rinse). The ZnSe crystal was then removed from the flow cell, dried and a transmission spectrum was recorded through the ZnSe crystal. Using the extinction coefficient for the CH bands at 1455 and 2930 cm^{-1} predetermined from Beer's law plots of KBr pellets containing NaPA and PDADMAC, the amount of each compound (mg/m^2 beam area) from the spectrum of the dried ZnSe crystal was calculated. Using this same procedure, the amount of TiO_2 on the IRE was calculated using the intensity of the bulk mode near 900 cm^{-1}. Finally, the value of 50 m^2/g for the surface area of the TiO_2, the mass of polymer per m^2 TiO_2 was calculated. These values were used to calibrate the intensity of the bands measured in the final ATR spectrum recorded at the end of the first cycle.[77]

For the second NaPA layer (NaPA-2) the amount was determined by: (1) obtaining the total integrated absorbance due to CH_2 bending mode at 1455 cm^{-1}; (2) subtracting the final absorbance value of NaPA-1 from this total absorbance and; (3) converting the net absorbance to amount in mg/m^2 using the calibration from above. The

amount of the third NaPA (NaPA-3) was obtained similarly as the second one except that in step (2) the total absorbance of previous NaPA-1 and NaPA-2 were subtracted from that of the total integrated absorbance during NaPA-3 deposition. The amounts of second and third PDADMAC layers were obtained in a similar procedure as those of NaPA-2 and NaPA-3 respectively, but for the CH_2 asymmetric stretching mode at 2930 cm^{-1}.

It is noted that bands due to NaPA or PDADMAC were not observed when LbL deposition cycles were performed on a bare ZnSe IRE. Therefore, the IR spectra are due to the polymers adsorbed only with the 500 nm thick TiO_2 coating. It is also noted that the amount of NaPA adsorbed in this TiO_2 layer (5-10 mg/m^2) is in the typical range for polymers adsorbed on powders.[77,119] Thus the NaPA appears to penetrate into this highly porous TiO_2 layer and does not simply adsorb on the outer layer of the TiO_2 coating. Nevertheless, in calculating the amount of polymer adsorbed, I recognize that the evanescent wave decays exponentially from the IRE surface, and as such, each deposition cycle would be positioned further away from the IRE.

2.3.2 Correction for evanescent wave decay

In ATR the electric field intensity (E) decays exponentially with the vertical distance from the surface (Z) according to the Equation (2.1).

$$E = E_0 e^{-zdp} \qquad - \qquad \text{Equation (2.1)}$$

Where E_0 is the electric field strength at the interface and dp is the depth of penetration, the dp is defined as the distance from the surface of the IRE where the intensity of the electric field is 1/e in value of E_0 and is defined by Equation 2.2.

$$d_p = \lambda / 2 \pi n_1 (\sin^2 \theta - n^2_{21})^{1/2} \quad - \quad \text{Equation (2.2)}$$

In my experiments $n_2 = 2.4$ (ZnSe), the angle of the crystal is $\theta = 45^0$, and when in contact with water (n_1=1.33), the depth of penetration would be $\lambda/6.6$. Under these conditions, the depth of penetration at 3000 cm^{-1} is 0.51μm and at 1700 cm^{-1} 0.9 μm. Since each layer will be deposited further away from the IRE surface, the evanescent wave dependence on the intensity needs to be evaluated. In addition, the adsorption of polyelectrolytes on the TiO_2 could decrease the refractive index of the rarer medium and this would lead to a decrease in the depth of penetration.

At first glance, we do not expect a large nonlinear dependence on intensity due to the evanescent wave with multiple polymer layer deposition as a typical thickness per LbL polymer layers on the order of 10 nm. However, these LbL films are usually dried between coatings that would collapse the polymer layer and the short contact times of seconds to minutes are much shorter than the incubation times (hours to days) required for the polymer to adopt an extended brush configuration. The scaling model for polyelectrolyte in dilute solutions represents polyelectrolytes as chain of electrostatic blobs. The electrostatic blob concept and the separation of different length scales are the assumption based on conformations in dilute solutions. The electrostatic interactions do not perturb the conformations in electrostatic blob.[112,120] The polymer chains that are

tethered one end to the surface and other end stretched away from the surface called as brush configuration. If the distance between adsorbed polyelectrolyte molecules is less than the size of the polyelectrolyte molecule, the polyelectrolyte molecules stretch and reduces the entropy.[121] In our experiments, there is no drying of the coatings between deposition cycles, the incubation times are 3.5 hours, and thicker polymer layers extending out from the surface are anticipated. Furthermore, the TiO_2 layer is 500 nm thick and adsorption of the polymer could occur throughout this layer. Therefore, there is a need to determine the calibration of the amount from layer to layer.

In a series of experiments, the same procedure described above to measure the adsorbed amount of NaPA and PDADMAC in the first layer was performed for coatings in the second, third and fourth cycles. That is, in separate experiments at the end of the second, third and fourth cycles the ZnSe was removed from the cell, dried and a transmission spectrum recorded. The band at 1455 cm^{-1} was used to calculate the amount of NaPA adsorbed and the band at 2930 cm^{-1} was used to calculate the amount of PDADMAC adsorbed. When calculating the amounts adsorbed on the second and third layers, the intensities of the bands 2930 cm^{-1} and 1455 cm^{-1} for the previous layers were subtracted from the total intensity for that band.

The intensity of the CH_2 band computed for each layer in the transmission spectrum was then divided by the corresponding band intensity for that layer in the ATR spectrum. The data points in Figure 2.4 show that the dependence on the evanescent wave is about 10 % for the first three cycles (bilayers) and increases to more than 25 % in the

fourth cycle. Hence, I limited my study to three cycles and provided the correction from Figure 2.4 to calculating the adsorbed mass of polymer in each layer.

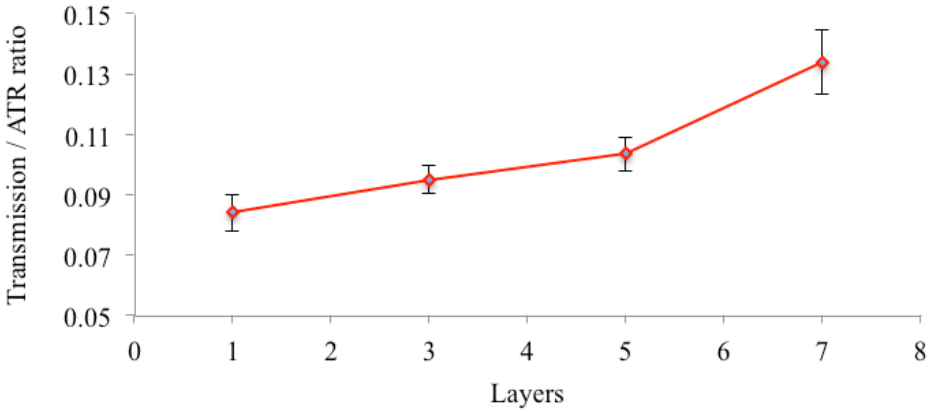

Figure 2.4 Transmission IR/ATR CH_2 intensity ratio for each NaPA layer. Error bars are the 95 % CI for three experiments.

2.3.3 Determination of the bound fraction

The procedure for determining the bound fraction for adsorption of NaPA on TiO_2 has been reported.[77] The adsorption of the NaPA occurs through an interaction of the COO^- groups and the positively charged sites on the TiO_2 surface. Thus, a percentage of the COO^- groups will be bound to the surface (bound % COO^-). There will be a percentage of the segments in the loops and tails containing COO^- groups (free % COO^-) and COOH groups (free % COOH) that are not bound to the surface. The band intensity of the C=O stretching mode for COOH group at 1713 cm^{-1}, ratioed to the intensity of CH_2 bending mode at 1455 cm^{-1} ($COOH/CH_2$), was used to calculate the % COOH. In the spectrum of the NaPA in solution at pH 2, there are no bands due to COO^- and the COOH band at 1713 cm^{-1} is at a maximum intensity. Therefore, the value obtained for

the $COOH/CH_2$ ratio in the spectrum of NaPA in solution at pH 2 equals 100 %. From the spectrum of NaPA in solution at pH 3.5 the % COOH is equal to 75 %. Once the % COOH was established. The total % COO^- was simply calculated by Equation 2.3. Therefore, at pH 3.5, 25 % of the segments of the NaPA in solution are negatively charged.

$$\text{Total \% } COO^- = 100\ \% - \%\ COOH \quad \text{- Equation (2.3)}$$

Now when NaPA is adsorbed on TiO_2 at pH 3.5, the % COOH drops to 40 % and the total COO^- groups increases to 60 %. This is because the adsorption of COO^- groups on the $TiOH_2^+$ surface sites results in a shift in the number of COOH groups according to the Le Chatelier's principle (see Scheme 2.1). The drop in the % COOH is because these COOH groups located in the loops and trains of the adsorbed polymer layer are at the solution equilibrium concentration with the free % COO^-. Now the total % COO^- has two contributions as shown in Equation 2.4.

$$\text{Total \% } COO^- = \text{Bound \% } COO^- + \text{Free \% } COO^- \quad \text{- Equation (2.4)}$$

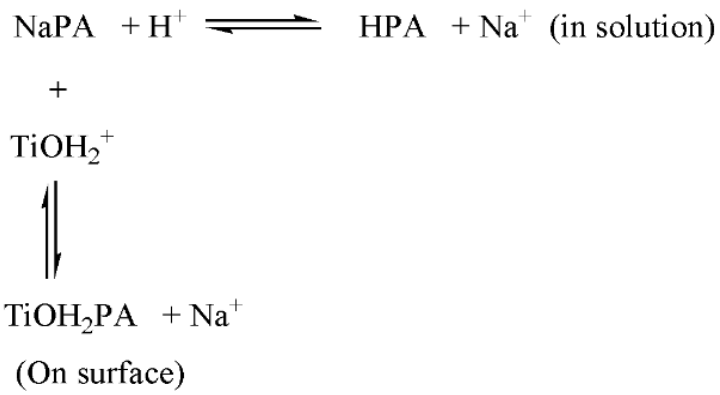

Scheme 2.1 The competing equilibrium process for NaPA adsorption on TiO_2 surfaces. Figure reproduced from Li *et al;*[77]

Since the ratio of COOH groups to COO^- groups for NaPA in solution at pH 3.5 is about 3:1 (75 % COOH/25 % COO^-), there would be approximately 13 % free % COO^- for the 40 % COOH in the loops and trains. The remaining 47 % are COO^- groups that would be bound to positively charged sites with TiO_2 and is a measure of the bound fraction of segments to the surface. Thus, by recording spectra as a function of contact time, both the adsorbed amount and bound fraction are measured dynamically.

This same approach was extended to determine the bound fraction of each polymer layer. In Figure 2.3b, the addition of PDADMAC leads to a decrease in the intensity of the C=O band at 1713 cm^{-1}. There is no loss of NaPA (the CH_2 band at 1455 cm^{-1} remains constant) and thus, the decrease in the C=O band arises from adsorption of the positive sites on PDADMAC with the free COO^- located in the loops and trains of the adsorbed NaPA layer. Furthermore, rearrangement of the polymer molecules in NaPA-1 that occur with PDADMAC deposition could lead to a change in the bound fraction of NaPA to the underlying TiO_2 substrate. The combination of the two effects lead to a

decrease in the total number of COOH groups because an overall change in the ratio of $COOH/COO^-$ groups in the loops and tails occurs to reestablish their solution equilibrium values. Thus, from the decrease in the value for the $COOH/CH_2$ ratio upon addition of PDADMAC, it is possible to measure dynamically the bound fraction of PDADMAC to sites on NaPA. The central assumption in calculating the bound fraction for each layer is that the number of COO^- groups bound to the underlying TiO_2 does not change with the adsorption of PDADMAC. The validity of this assumption will be discussed in section 2.3.4.2. Given a 1:1 interaction between charged segments on PDADMAC with the COO^- groups and a value for the amount of PDADMAC adsorbed, the bound fraction for PDADMAC is then determined. This same procedure was then repeated to calculate the bound fraction in subsequent layers.

2.3.4 Sequential adsorption of NaPA and PDADMAC

Figure 2.5 contains the curves of the amount of NaPA and PDADMAC adsorbed as a function of time for each cycle. Figure 2.6 is the corresponding plot of the change in % COO^- bound. While Figure 2.5 plots the results for one experiment, there are several general trends in the time profiles that are observed common to all experimental runs (see Figures 2.7 and 2.8). The average values for all three experiments for the bound % COO^-, free % COO^-, free % COOH and amount adsorbed at the end of each cycle is presented in Table 2.1.

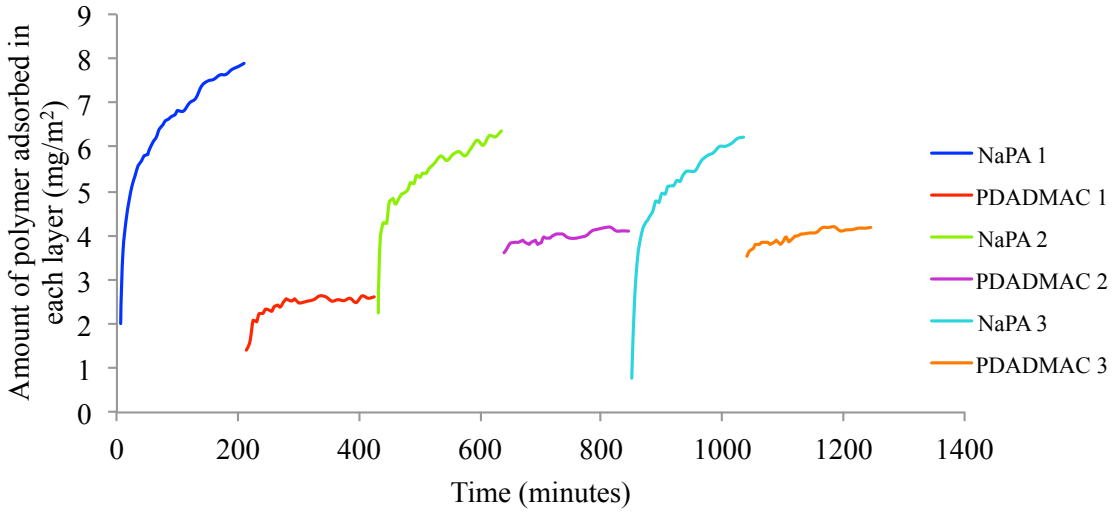

Figure 2.5 The amount of polymer (NaPA and PDADMAC) adsorbed (mg/m^2) as a function of time for the first experimental run.

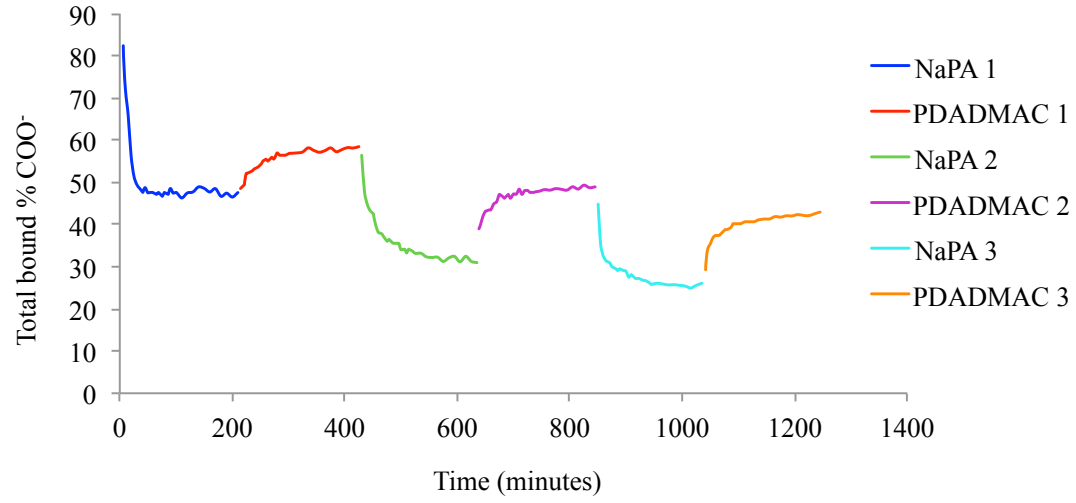

Figure 2.6 The total bound % COO^- as a function of time.

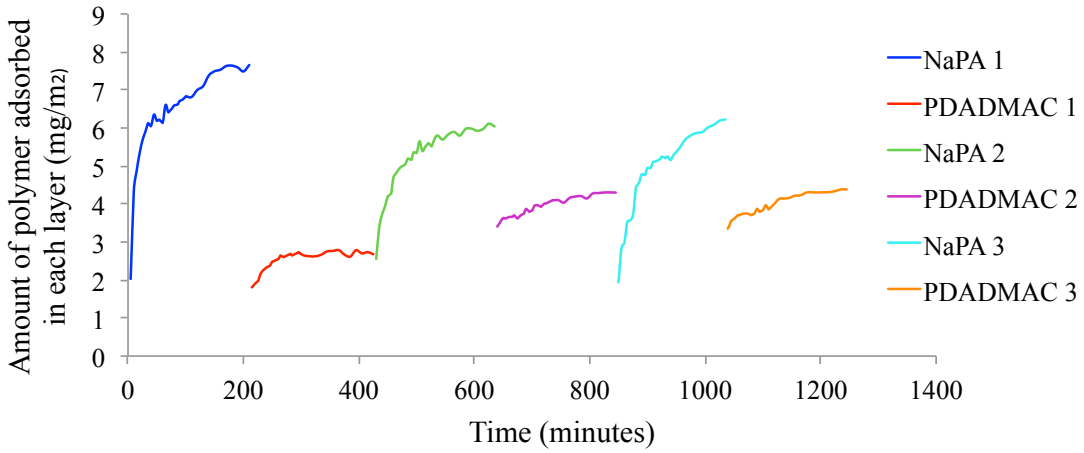

Figure 2.7 The amount of polymer (NaPA and PDADMAC) adsorbed (mg/m^2) as a function of time for the second experimental run.

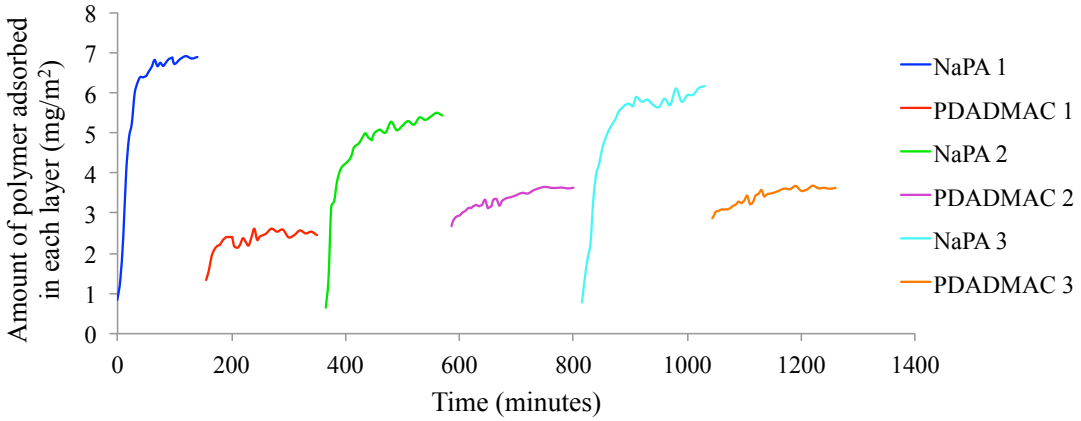

Figure 2.8 The amount of polymer (NaPA and PDADMAC) adsorbed (mg/m^2) as a function of time for the third experimental run.

Table 2.1 Calculated amount adsorbed, total bound % COO^-, total free % COO^- and total free % COOH for each NaPA and PDADMAC polymer layers.

Cycle	*Polymer bound*	*Mass of polymer deposited on each layer (mg/m^2)*	*Total free % COOH*	*Total free % COO^-*	*Total bound % COO^-*
1	NaPA	7.5 ± 0.4	40 ± 0.3	12 ± 0.5	48 ± 0.7
	PDADMAC	2.6 ± 0.3	32 ± 0.9	10 ± 0.5	58 ± 1.2
2	NaPA	6.4 ± 0.5	51 ± 2.2	15 ± 1.6	34 ± 3.7
	PDADMAC	4 ± 0.4	39 ± 0.3	12 ± 1.5	49 ± 0.7
3	NaPA	6.7 ± 0.6	57 ± 1.2	18 ± 1.3	25 ± 2
	PDADMAC	4.2 ± 0.5	43 ± 1.4	14 ± 1.2	43 ± 1.5

There are clear differences in the amounts obtained for the first layer compared to the second and third layers. The total amount adsorbed for NaPA-1 is about 20 % higher compared to NaPA-2 and NaPA-3. On the other hand, the adsorbed amount of PDADMAC-1 is 40 % lower than the succeeding PDADMAC layers. Clearly, the adsorption of NaPA-1 and PDADMAC-1 represent a transition layer. This transition is well known to occur in LbL based depositions but typically the transition occurs over 3-4 layers.[122-125] In our experiment, the transition occurs in the first cycle and this shorter transition is likely due to the long incubation times (3.5 hours). Typically, the longest incubation times in LbL depositions are on the order of 10 to 30 minutes per layer.[124,126]

Figure 2.9 shows the cumulative amount of adsorbed polymer at the end of each deposition and is the most common way of plotting LbL growth of PEM films.[123,126-128] The plot (Figure 2.9) follows a typical saw-tooth pattern[127,129] and the LbL shows a linear growth regime with a calculated R-squared value of 0.98.

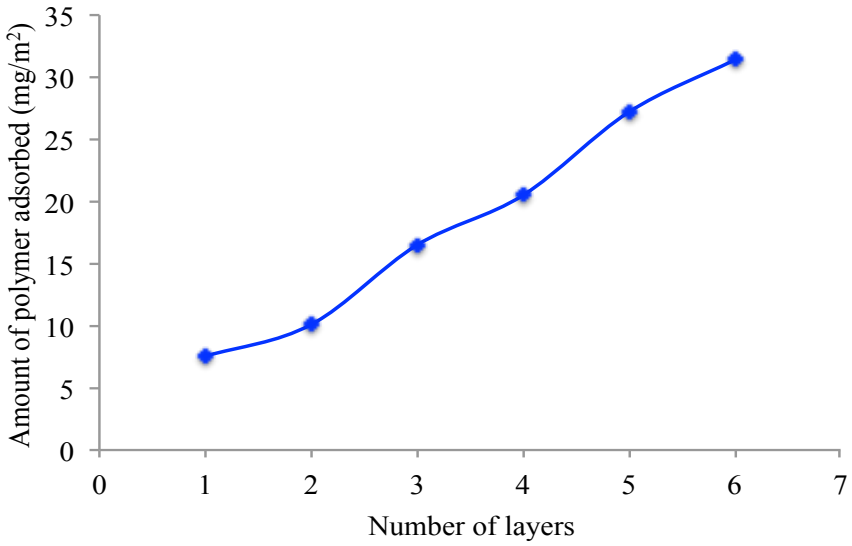

Figure 2.9 Cumulative amount of polymer deposited for each layer.

Figures 2.5, 2.7 and 2.8 shows that the dynamics for NaPA and PDADMAC adsorption follow different profiles. For NaPA, the curves have a sharp initial rise followed by a slow increase in amount that tends towards a plateau value. In contrast, the PDADMAC curves rise rapidly to a plateau value within 20 minutes. To better understand these differences in dynamics of the adsorbed amount, I examine the dynamics of the bound fraction.

Figure 2.6 is a plot of the total bound % COO^- recorded as a function of time during the deposition of each layer in the LbL process. The NaPA-1 layer forms on TiO_2 with an initial bound fraction greater than 80 % that drops to a plateau value of 48 % at 40 minutes. This is because the initial NaPA in solution arriving at a bare TiO_2 pancakes (lay flat) on to the surface and subsequently rearranges to a conformation with lower bound fraction containing more loops and tails to accommodate more polymer adsorption on TiO_2[77].

The curves obtained for dynamic amount adsorbed in NaPA-2 and NaPA-3 (Figure 2.5, 2.7 and 2.8) are similar in shape to NaPA-1. This could be evidence that there is a slow rearrangement of the NaPA on top of the PDADMAC layer with little, if any, diffusion of the NaPA into the PDADMAC layer. However, there are differences in the trend in total bound fraction for NaPA-1 and other deposition cycles (Figure 2.5). The value for the bound fraction reaches a constant value of 48 % within 40 minutes for NaPA-1 whereas; in all other NaPA cycles, the bound fraction continues to vary, albeit slowly at the end of the 3.5 hours incubation. Therefore, NaPA diffuses into the underlying PDADMAC layer.

The total bound fraction at the end of NaPA-2 and NaPA-3 are lower in value (about 34 % and 25 % respectively) than the value obtained at the end of NaPA-1 (48 %). This shows that the number of bonds between PDADMAC and NaPA is lower than that of NaPA with TiO_2. Furthermore, there is a stronger interaction between the COO^- groups on NaPA and the positively charged sites on TiO_2 than with the positively charged sites on PDADMAC. The difference in wavenumbers ($\Delta\nu = \nu_{as} - \nu_s$) between the

asymmetric (ν_{as}) and symmetric (ν_s) stretching frequencies of COO^- bands for NaPA-1 was $\Delta\nu$= 132 cm^{-1} whereas for NaPA-2 and NaPA-3 we obtain $\Delta\nu$ of 134 cm^{-1} and 142 cm^{-1}, respectively (see Table 2.2). A smaller $\Delta\nu$ implies a stronger interaction with the COO^- functionalities[130]. Thus, the combination of a higher bound fraction and stronger interaction shows that NaPA-1 is more strongly bound to TiO_2 than to the PDADMAC layers.

Table 2.2 The IR peak positions for the symmetric and asymmetric stretching modes of COO^- in solution and for each adsorbed layer.

Cycle	*Polymer layer*	$\nu_s\ COO^-\ (cm^{-1})$	$\nu_{as}\ COO^-\ (cm^{-1})$	$\Delta\nu\ (cm^{-1})$
	In solution	1404	1554	150
1	NaPA	1415±1.5	1544±1.8	132
	PDADMAC	1409±1	1551±1.3	142
2	NaPA	1412±1.5	1546±1	134
	PDADMAC	1406±1	1554±1.5	148
3	NaPA	1407±1.5	1550±1.5	143
	PDADMAC	1404±1	1555±1.3	151

2.3.4.1 Bound Fraction of Individual Layers

Deposition of PDADMAC onto the underlying NaPA layer always increases the bound fraction of NaPA (Figure 2.5). From the knowledge of the amount of PDADMAC adsorbed and assuming a 1:1 interaction between the positively charged sites on PDADMAC and the negatively charged sites on NaPA, an estimate of the bound fraction of PDADMAC was determined. Specifically, the bound fraction of PDADMAC-1 to NaPA-1 layer was obtained using Equation 5, where *n* is the amount (mg/m^2) of the respective polyelectrolyte (NaPA or PDADMAC) and *N* is the mass of a monomeric unit of NaPA or PDADMAC.

$$\text{Bound Fraction [PDADMAC]} = \frac{(n_{NaPA}/N_{NaPA})}{(n_{PDADMAC}/N_{PDADMAC})} * \text{Bound Fraction [NaPA]} \quad - \text{Equation (2.5)}$$

The bound fractions of PDADMAC-2 and PDADMAC-3 were obtained similarly as that for PDADMAC-1 using Equation 5 and also the amount of polymer (*n*) was adjusted to match the number of deposition cycle.

Figure 2.10 displays the bound fraction for each layer. Here, the bound fraction of PDADMAC refers to the fraction of NR_4^+ moieties binding to COO^- groups of NaPA. In generating these values, it was assumed that the number of groups already bound to the underlying layer do not change in value. In other words, adsorption of PDADMAC-1 onto NaPA-1 does not result in any change in bound fraction of NaPA-1 to the

underlying TiO_2. This is a reasonable assumption for PDADMAC-1 given the strong interaction between COO^- groups and the charged sites on TiO_2.

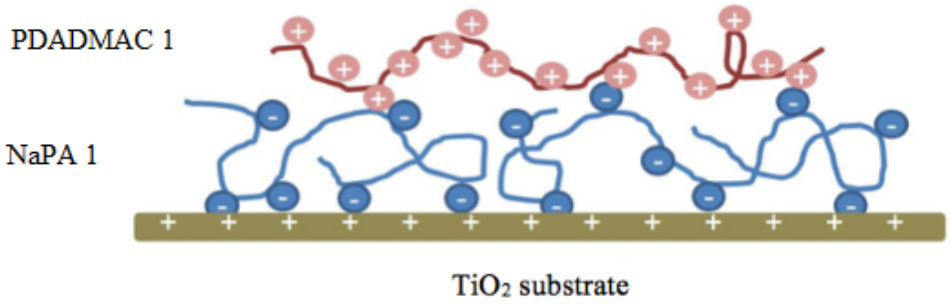

Scheme 2.2 Molecular picture of NaPA-1 and PDADMAC-1 adsorbed on TiO_2.

From Figure 2.5, addition of PDADMAC-1 leads to 12 % increase in COO^- bound fraction and, using the mass of adsorbed PDADMAC, I calculate that the 12 % of the COO^- groups bind with 68 % of the charged sites on the PDADMAC. A value of 68 % bound fraction could indicate a high level of interpenetration of PDADMAC into the underlying NaPA-1 layer. However, this is unlikely, given the rapid plateau observed for the dynamic amount for PDADMAC-1 in Figure 2.5 and the rapid plateau in the dynamic bound fraction shown in Figure 2.6. Thus, a value of 68 % bound fraction indicates that PDADMAC pancakes on top of the NaPA layer (Scheme 2.2). Decher[7] described that self-regulation of LbL is achieved because, when charge reversal occurs, the incoming equally charged molecules are repelled from the growing film surface. Therefore, since each segment of PDADMAC carries a charge, the incoming molecules will be repelled upon approaching the initial pancaked PDADMAC molecules in the layer. As a result,

the pancaked PDADMAC does not rearrange to accommodate the adsorption of more PDADMAC.

Figure 2.5 shows that PDADMAC-2 and PDADMAC-3 have similar profiles in that both show a rapid plateau in adsorbed amount. Guzman *et al*.,[105] reported that for poly(allylamine hydrochloride)/poly(sodium 4-styrenesulfonate) (PAH/PSS) and PDADMAC/PSS multilayers, inter-diffusion of the polymer layer occurs at high ionic strength and not at low ionic strength. It was concluded that the charge on the polymer layer dictated the level of diffusion into the underlying layer. This is consistent with the work reported here. Thus, it is concluded that diffusion of PDADMAC into the underlying NaPA layer does not occur to any significant extent.

In contrast to PDADMAC-1, there is rearrangement of the initial pancaked layer of NaPA on the TiO_2. In this case, there will be minimal repulsion of incoming NaPA molecules because 25 % of the segments are charged, much lower than the 100 % charged segments on PDADMAC. Hence, there is rearrangement of the adsorbed NaPA to accommodate more NaPA, which is evidenced by the slow increase of adsorption towards a plateau during NaPA-1 deposition (Figure 2.5, 2.7 and 2.8) and the drop in value for the bound fraction with time.

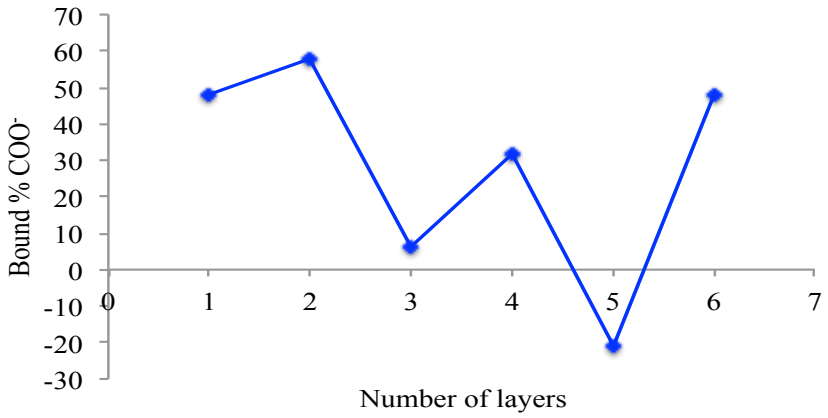

Figure 2.10 Bound fraction of individual layers to the respective underlying layer. Data points refer to the fraction of COO^- in NaPA or NR_4^+ in PDADMAC from spectra at the end of deposition of each layer.

Figure 2.6 and 2.10 shows there is a general trend of a decrease in bound fraction for each NaPA layer and in fact, the bound fraction for NaPA-3 is negative in value. While a decrease in bound fraction may imply an increase in coil-like conformation of adsorbed layer[77], a negative bound fraction could indicate loss of PDADMAC from the underlying layer to the solution phase. However, the IR spectra show no loss of PDADMAC during any of the NaPA cycles. Furthermore, the mass adsorbed for NaPA-3 was 6.3 mg/m^2 (Table 2.1) and this layer must have some positive value for the bound fraction to the underlying PDADMAC layer. Thus, a negative bound fraction means that the assumption that the bound fraction of the underlying layer does not change is invalid for cycle -2 and higher. This shows that adsorption of PDADMAC leads to a reduction of charged sites on NaPA bound to the underlying PDADMAC layer. Hence, the adsorption of the next PDADMAC layer leads to a rearrangement of the entire underlying NaPA layer. This is also consistent with the slow change in bound fraction for NaPA-2 and

NaPA-3, which was attributed to inter-diffusion of NaPA into the underlying layer. Moreover, the dynamic amount of NaPA-2 and NaPA-3 keeps increasing (Figure 2.5), suggesting there is slow diffusion of NaPA. Since there is linear growth in the adsorbed amount and polymer diffusion in the multilayer, polymer diffusion in PEM films does not necessarily indicate exponential growth. Therefore, my work is in agreement with that of Guzman *et al;* which shows exponential growth is dictated more by adsorption dynamics and the charge density of the polymer.[45,55]

2.4 Conclusion

We demonstrate, for the first time, a method that simultaneously determines the dynamics of the mass adsorbed and polymer conformation during the LbL process. This work provides evidence that linear growth can occur in systems in which polymer diffusion occurs. For the NaPA/PDADMAC system, I observe linear growth despite the slow adsorption and inter-diffusion of NaPA into the underlying PDADMAC layer. In contrast, the PDADMAC adsorbs rapidly and pancakes on the underlying NaPA layer showing no evidence of diffusion. However, the underlying NaPA layer responds to the PDADMAC by rearranging and reducing the number of bonds to the underlying PDADMAC layer. In addition to rearrangement, there is diffusion into the underlying film by NaPA but not PDADMAC. Polymer diffusion therefore, does not correlate to exponential growth.

CHAPTER 3: LAYER BY LAYER (LBL) DEPOSITION OF SODIUM POLYACRYLATE (NaPA) AND POLY (DIALLYL DIMETHYL AMMONIUM) CHLORIDE (PADAMAC) AS A FUNCTION OF IONIC STRENGTH

3.1 Introduction

The experimental conditions that have a major influence in the structure of polyelectrolyte based LbL include ionic strength, solvent quality, pH and temperature.[131] In regards to ionic strength, the presence of ionic salts alters the conformation of the adsorbing polyelectrolyte by shielding the charge on the repeating polyelectrolyte units and by neutralizing some of the charged sites along the polymer backbone by adsorption of counterions. The multilayer film growth depends on the electrostatic charge, as this controls the amount of polyelectrolyte adsorbed in a multilayer film, diffusion into the underlying layer[132], as well as layer mixing and complexation of the polyelectrolytes.[133] As the ionic strength increases, the conformation of the polymer alters from a rod-like structure to an expanded three-dimensional random coil. It is the adsorption of these expanded random coils that leads to a layer thickness that is proportional to the square of the ionic strength.[134,135]

The effective charge on a polyelectrolyte backbone as a function of ionic strength that has been measured by electrophoretic and dielectric methods is lower than the electrical charge determined by elemental analysis and titration curves.[136] The reduction in the effective charge has been attributed to adsorption of counterions and is often

referred to as the Manning counterion or extrinsic condensation. This originates from the Manning-Oosawa theory[137,138] , which was the first model for describing counterion condensation on the backbone of a polymer molecule. According to this theory, the polyelectrolyte molecule is treated as an infinitely long rigid rod that contains monomer units with point charges. The counterions localizing along the polymer backbone are dictated by a balance between (1) the electrostatic interaction of counterions with the polyelectrolyte backbone and (2) the loss of translational entropy due to counterion localization on the polyelectrolyte chains. The effect can be large, as the charge on strong electrolytes, such as polyvinyl pyridinium and polystyrene sulfonate, have been measured at 40 % lower than their fully ionized value.[139] Muthukumar[136] extended this model for counterion condensation to flexible polyelectrolytes and showed that the degree of ionization of the polymer chains decreases with an increase in salt concentration, monomer concentration and chain flexibility. It was also shown that the degree of ionization decreases continuously with $1/\epsilon T$ where ϵ and T are the dielectric constant and temperature of the solvent.

In Chapter 2, we showed that adsorption of COO^- groups of NaPA to oppositely charged centers on the underlying surface result in a change in intensity of the COOH band at 1713 cm^{-1}. This provided a way of measuring the bound fraction. Guzman *et al.*[131] referred to this type of charge neutralization as intrinsic charge compensation. The intrinsic compensation mechanism implies a 1:1 monomer ratio in the deposition of each layer and, as shown in Chapter 2, was measured directly by my ATR method. Moreover, direct evidence of the level of the adsorption of counterions on NaPA should also lead to

changes in the intensity of the COOH band. Thus, I may be able to obtain evidence with my ATR method of both intrinsic and extrinsic charge compensation during the LbL process. Furthermore, measuring the dynamic change in adsorbed amount and bound fraction with ionic strength should provide molecular detail of the adsorption processes occurring during LbL deposition as a function of ionic strength. Thus, a natural extension of my ATR method is a study of the effect of ionic strength on polyelectrolyte structure in solution and on multilayer formation in LbL based processes.

3.2 Experimental

3.2.1 Materials and methods

Sodium chloride powder, NaPA, average molecular weight (Mw) of 30,000, and polydispersity index (Mw/Mn) of 1.4, PDADMAC average molecular weight (Mw) of 100,000 – 150,000, polydispersity index (Mw/Mn) of 1.6, sodium hydroxide, and hydrochloric acid were purchased from Fisher Scientific. TiO_2 powder (P25) was obtained from Degussa. The horizontal flow-through ATR cell and a 45° ZnSe internal reflection element (IRE) of dimensions 50 × 10 × 2 mm^3 were obtained from Harrick. An ABB-Bomem FTLA 2000 spectrometer was used to record IR spectra. Typically, 100 scans at 8 cm^{-1} resolution were used to record each spectrum. The description of the flow-through ATR cell and its use to measure polymer adsorption on TiO_2 coated IRE is described elsewhere.[82]

3.2.2 Ionic strength dependency of adsorption of Na^+ on NaPA in solution

IR spectra of NaPA in solution as a function of ionic strength were recorded in order to determine the bound fraction of Na^+ to COO^- groups. To separate 100 ml volumetric flasks containing 100,000 ppm NaPA solutions in DI water, NaCl was added to prepare 100,000 ppm NaPA with ionic strength of 0.05M, 0.1M, 0.15M, 0.2M and 0.25M. A 100,000 ppm NaPA solution was required to obtain IR bands for NaPA in solution phase. The pH of these polymer solutions, as well as a sample of DI water, was adjusted to 3.5 using HCl. Solutions containing higher ionic strength than 0.25M resulted in precipitation of the NaPA and, therefore, were not used in this study. Ikeda *et al,*[140]

showed that with increasing ionic strength, the radius of gyration and the hydrodynamic radius of a polyelectrolyte decreases, eventually leading to precipitation of the polyelectrolyte from solution.

A reference spectrum was obtained by flowing DI water pH 3.5 at a rate of 5.8 ml/min through the ATR cell. IR spectra were then recorded by passing each 100,000 ppm NaPA solution at different ionic strength through the flow cell. The ATR cell was rinsed with DI water before introducing the next concentration of NaPA/NaCl solution.

3.2.3 Exposure of NaPA adsorbed TiO_2 to solutions of different ionic strength

A 20 ppm solution of NaPA at pH 3.5 was prepared by adding 5 mg of NaPA to 100 ml of DI water. The pH of this solution was adjusted using HCl. Solutions of 0.01M and 0.02M NaCl solutions prepared using DI water were adjusted to pH 3.5 using HCl. The change in ionic strength, due to the addition of the HCl to DI water, was approximately 0.0004M which was insignificant compared to the ionic strength (0.01 and 0.02M) used for LbL deposition. The ionic strength of the solution (0.01, 0.02M) and concentration of NaPA (20 ppm) were much lower than used for measurement of spectra of NaPA in solution (100,000 ppm and 0.05-0.25M ionic strength, see section 3.2.2). A high concentration of NaPA was needed in order to observe IR bands due to NaPA in the solution phase. At 20 ppm NaPA, the polymer precipitated when the solution ionic strength was raised above 0.02M, which was lower than the 0.25M threshold for precipitation from the 100,000 ppm NaPA solution.

The same procedures described in Chapter 2 were used to prepare a TiO_2 coated internal refractive element (IRE), mounting the IRE in the flow-through cell and in recording a reference spectrum. The 20 ppm NaPA solution in DI water at pH 3.5 was flowed through the cell at 5.8 ml/min. IR spectra were recorded at regular intervals over approximately 3.5 hours. At 20 ppm, detection of bands due to NaPA in the solution phase were not observed. Thus, all bands in the spectra are due to adsorption of the NaPA on the TiO_2.[77] The flow-through cell was then flushed with water at pH 3.5 for 5 minutes to remove excess NaPA. This flushing step did not lead to any changes in the IR bands of NaPA or TiO_2, showing that the NaPA adsorbed on TiO_2 was not removed from the IRE during this wash cycle.

Next, a 0.01M NaCl solution at pH 3.5 was flowed through the cell at 5.8 ml/min. Spectra were recorded as a function of time until no further change in the spectra were observed. The cell was again flushed with DI water at pH 3.5 to remove NaCl from the system. The DI water was flowed until no further change in the spectra was observed. Then, a 0.02M NaCl solution at pH 3.5 was flowed through the cell at 5.8 ml/min while recording spectra as a function of time. The cell was then flushed with DI water at pH 3.5.

3.2.4 Adsorption of NaPA on TiO_2 at ionic strength of 0.01M and 0.02M

The procedures below are described only for adsorption of NaPA from 0.01M NaCl. The same experiments were also performed for NaPA adsorption from 0.02M NaCl using these same procedures. Aqueous solutions of 0.01M NaCl were prepared by

adding NaCl powder to DI water. Then separate solutions of 20 ppm NaPA in 0.01M NaCl were prepared by the addition of polymers to the 0.01M NaCl solution. The pH of the solutions were adjusted to pH 3.5 using HCl.

A TiO_2 suspension was evenly deposited onto a ZnSe crystal as described in Chapter 2. The coated ZnSe crystal was mounted in the flow-through cell. The cell was flushed with 0.01M NaCl solution at pH 3.5 at a flow rate of 5.8 ml/min until a repeatable 100 % baseline was obtained. A reference spectrum was then recorded and used for the remainder of the experiment. The TiO_2 bulk modes near 900 cm^{-1} did not change during this initial flow of 0.01M NaCl solutions or with the addition of NaPA solution, showing that there is no loss of TiO_2 during the entire experiment.

A solution of 20 ppm NaPA in 0.01M NaCl solution at pH 3.5 was then flowed through the cell at a flow rate of 5.8 ml/min for 3.5 hours. Spectra were recorded at 5 minute intervals for the first 100 minutes and then at 10 minute intervals. Next, a 0.01M NaCl aqueous solution at pH 3.5 was flowed through the cell for 5 minutes to remove excess NaPA.

3.2.5 LbL deposition of NaPA and PDADMAC at ionic strength of 0.02M

Aqueous solutions of 0.02M NaCl were prepared by adding NaCl powder to DI water. Then separate solutions of 20 ppm NaPA in 0.02M NaCl and 30 ppm PDADMAC in 0.02M NaCl were prepared by addition of the polymers to the 0.02M NaCl solution. The pH of the solutions were adjusted to pH 3.5 using HCl.

A TiO_2 suspension was evenly deposited onto a ZnSe crystal as described in Chapter 2. The coated ZnSe crystal was mounted in the flow-through cell. The cell was flushed with 0.02M NaCl solution at pH 3.5 at a flow rate of 5.8 ml/min until a repeatable 100 % baseline was obtained. A reference spectrum was then recorded and used for the remainder of the experiment. The TiO_2 bulk modes near 900 cm^{-1} did not change during this initial flow of 0.02M NaCl solutions or the addition of NaPA or PDADMAC solutions showing that there was no loss of TiO_2 during the entire experiment.

A 20 ppm NaPA in 0.02M NaCl solution at pH 3.5 was then flowed through the cell at a flow rate of 5.8 ml/min for 3.5 hours. Spectra were recorded at 5 minute intervals for the first 100 minutes and then at 10 minute intervals. Next, a 0.02M NaCl aqueous solution at pH 3.5 was flowed through the cell for 5 minutes to remove excess NaPA. Then a 30 ppm PDADMAC in 0.02M NaCl polymer solution at pH 3.5 was flowed through the cell at a flow rate of 5.8 ml/min for 3.5 hours. Spectra were recorded in 5 minutes intervals for the first 100 minutes and then at 10 minutes intervals. The cell was flushed again with the 0.02M NaCl at pH 3.5 for 5 minutes to remove excess PDADMAC. The sequential addition of 20 ppm NaPA in 0.02M NaCl, rinse with 0.02M NaCl, followed by 30 ppm PDADMAC in 0.02M NaCl, rinse with 0.02M NaCl, was repeated three times. All experiments in this chapter were performed a minimum of three times.

3.3 Results and discussion

3.3.1 Ionic strength dependence of Na^+ adsorbed on NaPA in solution

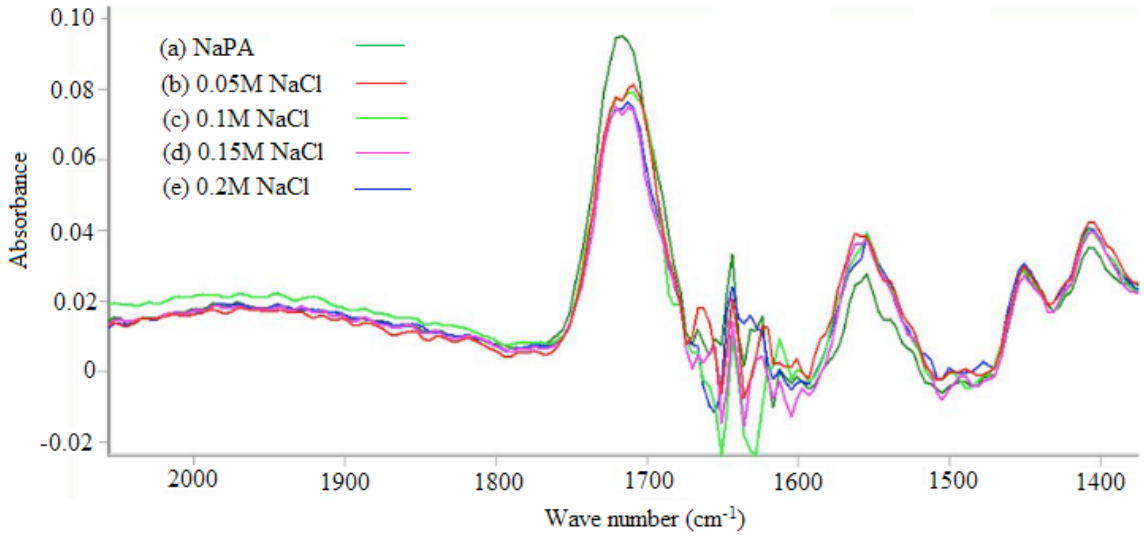

Figure 3.1 IR spectra of 100,000 ppm NaPA at pH 3.5 in (a) DI water and at ionic strength (NaCl) of (b) 0.05M, (c) 0.1M, (d) 0.15M and (e) 0.2M.

The spectrum obtained for NaPA in DI water at pH 3.5 is shown in Figure 3.1(a). The other spectra in Figure 3.1 are NaPA solutions of (b) 0.05M, (c) 0.1M, (d) 0.15M and (e) 0.2M NaCl. The key bands are; 1713 cm^{-1} due to the C=O stretching mode of COOH groups; 1554 cm^{-1} and 1404 cm^{-1} due to the COO^- asymmetric and symmetric stretching mode, respectively; and 1455 cm^{-1} due to a CH_2 bending mode. The 1713/1455 intensity ratio decreased in value in 0.05M NaCl (Figure 3.1b) compared to the spectrum recorded in DI water (Figure 3.1a). The decrease in the 1713/1455 intensity ratio tended towards a constant value at higher ionic strength.

In Chapter 2, I showed that the 1713/1455 intensity ratio gave a value for the % COOH groups on the polymer backbone and that a decrease in this ratio occurred when the NaPA adsorbed on TiO_2. This ratio was used to calculate the bound fraction of COO^- sites on the NaPA with positively charged sites on the TiO_2. Here, there is no TiO_2 and hence, the decrease in the 1713/1455 intensity ratio is due to the bound fraction of COO^- with Na^+ ions, thus providing a direct measurement of the Manning or extrinsic counterion condensation.

Now, the total % COO^- groups are given by the following equation:

$$\text{Total \% } COO^- = 100 - \text{\% COOH} \qquad \text{- Equation (3.1)}$$

The total % COO^- have two contributions; charged COO^- groups (free % COO^-) and COO^- groups neutralized by Na^+ ions. At pH 3.5, the values for free % COO^- and % COOH measured for NaPA in DI water were 25 % and 75 %, respectively. Thus, 25 % of the monomer units are ionized in DI water and this value will decrease with increasing ionic strength due to adsorption of Na^+ ions with the COO^- groups. This reduction in number of COO^- groups, due to adsorption of Na^+ ions, leads to a decrease in the number of COOH groups in order to maintain the 25 % COO^- : 75 % COOH equilibrium ratio. Hence, the reason for the reduction in the 1713/1455 intensity ratio, with increasing ionic strength in the spectra in Figure 3.1. So, from the measured value for the % COOH, the free % COO^- is calculated from the equilibrium ratio. The remaining COO^- groups are bound to Na^+ (% COO^-Na^+) according to the equation:

$$\text{\% } COO^-Na^+ = 100 - (\text{\% COOH} + \text{Free \% } COO^-) \qquad \text{- Equation (3.2)}$$

Figure 3.2 is a plot of the % COO^-Na^+ for NaPA in solution as a function of ionic strength. The curve has an initial sharp rise that plateaus above an ionic strength of 0.15M. Muthukumar[136] theoretically predicted an exponential decrease in the degree of ionization of a polyelectrolyte as a function of ionic strength. The degree of ionization was defined as $f = 1 - (M/N)$, where N is the number of monomers and M is the number of counterions adsorbed on the polyelectrolyte. The degree of ionization (f) in my case is simply the free % COO^-. Figure 3.3 is a plot of the degree of ionization measured in my experiments. An exponential decrease is observed with increasing ionic strength and is in agreement with calculations performed by Muthukumar and Ghosh[141]. At 0.1M NaCl and pH 3.5, approximately 8 % of the total groups of NaPA are bound to Na^+ (COO^-Na^+), 69 % are COOH and 23 % are COO^- groups. Thus, the NaPA changed from about 25 % ionized groups in DI water at pH 3.5 (ionic strength of about 0.0004) to 23 % ionized groups at 0.1M NaCl.

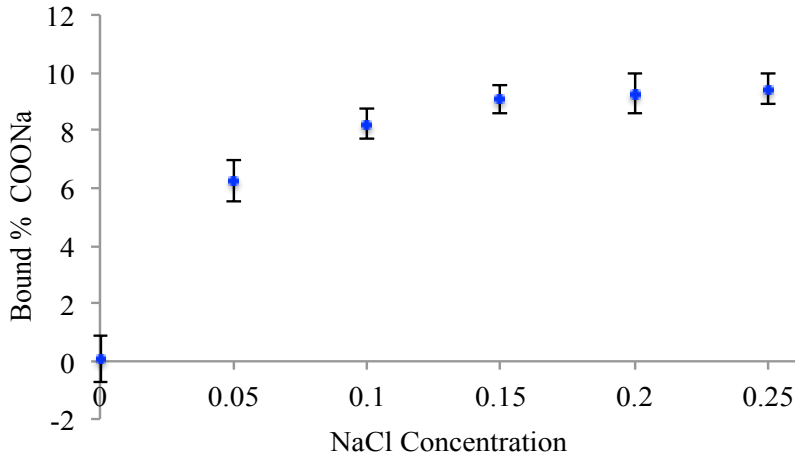

Figure 3.2 The % COO^-Na^+ for NaPA in solution as a function of ionic strength. Error bars are the 95 % CI for three measurements.

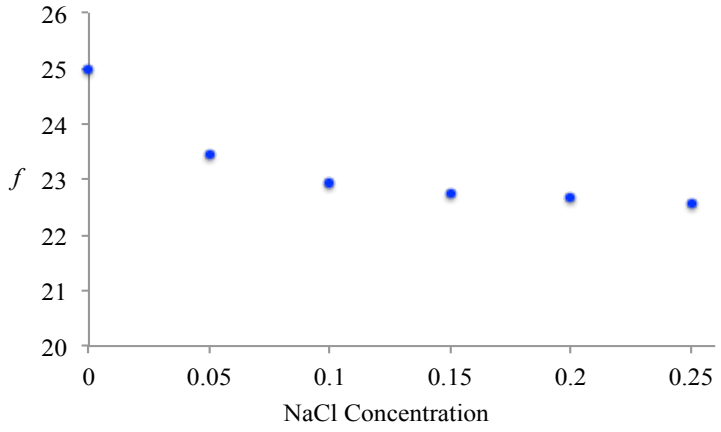

Figure 3.3 Degree of ionization of the polyelectrolyte (*f*) (free % COO^-) in NaPA in solution phase as a function of ionic strength.

The data in Figures 3.2 and 3.3 demonstrate that the degree of ionization as a function of ionic strength for NaPA in solution can be measured directly by recording IR spectra of the solution. A second reason for measuring the equilibrium values for % COOH, free % COO^- and % COO^-Na^+ in solution as a function of ionic strength is that these values would be used in computing the bound fraction of COO^- groups for NaPA adsorbed on TiO_2. Here, I would follow the same procedure as outlined in Chapter 2 and assume that the % COOH, free % COO^- and % COO^-Na^+ in the loops and tails of an adsorbed NaPA layer would be at the same ratio as in solution. The problem is that the NaPA concentration for the solution studies was 5000 times higher in magnitude than used in the LbL adsorption studies on TiO_2 in this chapter. It is noted that at 100,000 ppm, the NaPA precipitated from solution above an ionic strength of 0.25M whereas, at 20 ppm, the NaPA precipitated when the ionic strength was above 0.02M. From Figure 3.2, the % COO^-Na^+ varies little above 0.15M ionic strength and thus, at first glance, we could estimate that near the precipitation limits the % COO^-Na^+ is about

9.7 %. This value would then be the same as the precipitation limit (0.02M ionic strength) for the 20 ppm NaPA solution. However, there are many factors that contribute to precipitation of a polymer from solution including polymer concentration.[142] Furthermore, the degree of ionization of a polyelectrolyte decreases with ionic strength.[136] Hence, an alternative method for estimating the % COO^-Na^+ for NaPA adsorbed on TiO_2 was needed. This was investigated in the next section.

3.3.2 Adsorbed NaPA layer exposed to NaCl solution

In this section, I examine the changes that occur to an adsorbed layer of NaPA deposited from DI water upon subsequent exposure to solutions of different ionic strength. In particular, NaPA was adsorbed on TiO_2 from DI water, then exposed to a flowing solution of 0.01M NaCl, followed by rinsing with DI water, then a 0.02M NaCl solution, followed by a second rinse with DI water.

Figure 3.4 shows that there is no change in the amount of NaPA adsorbed when the adsorbed layer is exposed to the 0.01 and 0.02M NaCl solutions. Post-treatment in salt solutions of polyelectrolyte multilayers (PEM's) can soften, swell and dissolve the PEM because the salt screens the charge interaction with polyelectrolytes.[143] I clearly am not seeing any dissolution. This would not be expected for the first layer of NaPA strongly bound to NaPA nor at the relatively low ionic strength used in this work. Dissolution of PSS/PDADMAC and PAA/PAH multilayers occur only when the salt concentration exceeds 2M.[144]

Figure 3.5 is a plot of the corresponding dynamic change in total bound % COO^- and shows an overall increase in this value when the NaPA layer is exposed to a 0.01M, then a 0.02M NaCl solution. Here, the total bound % COO^- is defined as the COO^- groups adsorbed on positively charged sites on TiO_2 and those with Na^+. From the % COOH, the free % COO^- are calculated at their equilibrium 25 % free COO^-: 75 % COOH ratio. The remaining COO^- groups are either bound to TiO_2 or Na^+ (total bound % COO^-). The equilibrium values measured at the end of each step are given in Table 3.2.

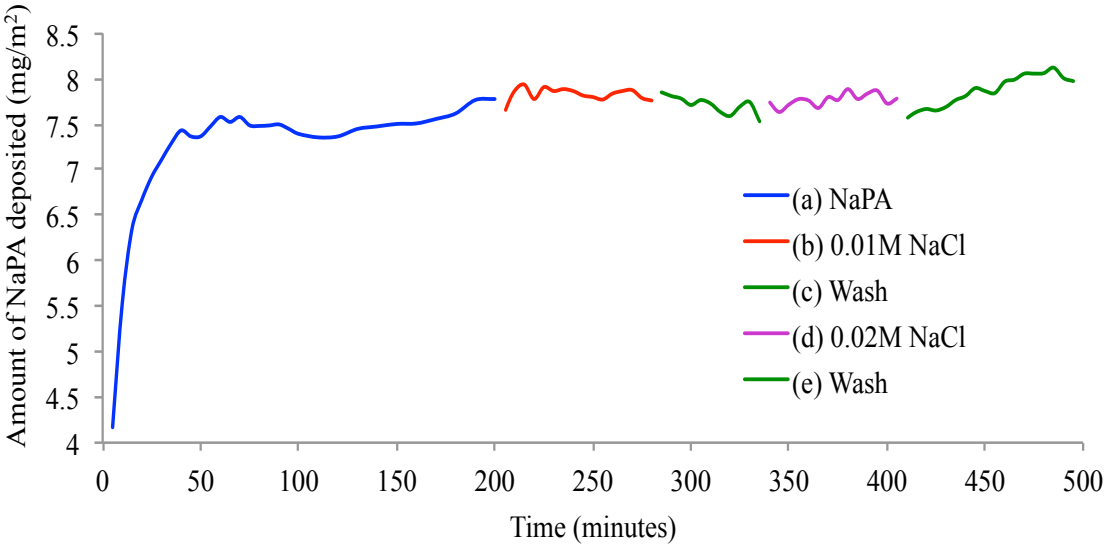

Figure 3.4 The amount of NaPA adsorbed on TiO_2 during sequential flow and rinse cycles.

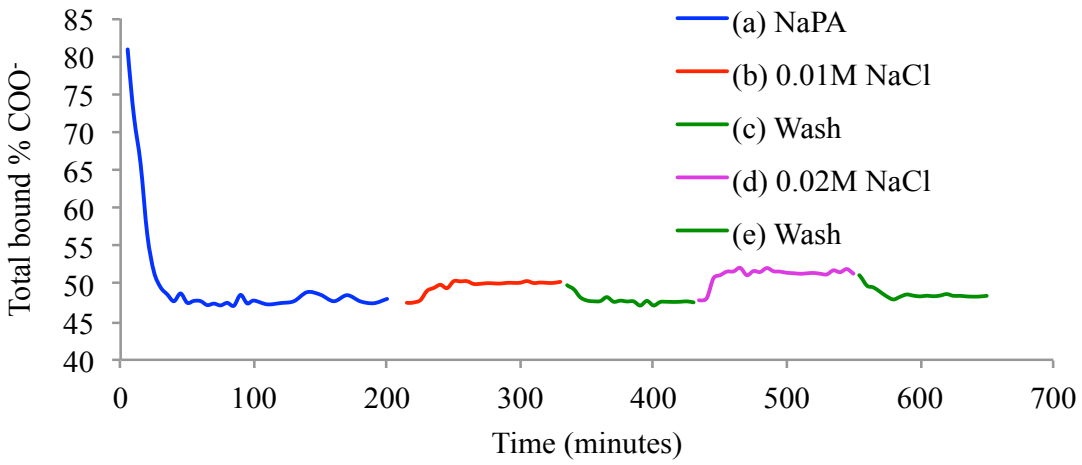

Figure 3.5 The total bound % COO^- as a function of time.

Table 3.1 Calculated mass of polymer deposited, free % COO^-, free % COOH and total bound % COO^- at the end of each cycle for the curves shown in Figures 3.4 and 3.5.

Name of the compound	*Mass of polymer deposited (mg/m^2)*	*% COOH*	*Free % COO^-*	*Total bound % COO^-*
NaPA	7.8 ± 0.4	40 ± 0.3	13 ± 0.4	47 ± 0.7
0.01M NaCl	7.7 ± 0.2	37.7 ± 0.4	12.3 ± 0.3	50 ± 0.5
Wash	7.6 ± 0.5	39 ± 0.3	12.7 ± 0.5	48.3 ± 0.2
0.02M NaCl	7.7 ± 0.3	36.7 ± 0.5	11.9 ± 0.7	51.4 ± 0.4
Wash	7.5 ± 0.5	38 ± 0.5	12.3 ± 0.3	49.7 ± 0.2

As discussed in Chapter 2, the decrease in total bound % COO^-, from a value near 80 % to 47 % occurring during adsorption of NaPA, is due to rearrangement of the polymer layer from a flat to extended conformation on TiO_2. The adsorption of NaPA was from DI water which means the total bound % COO^- is solely due to adsorption of the polymer on TiO_2 sites.

After flowing a 0.01M NaCl solution, the total bound % COO^- increased from 47 % to 50 %. At first glance, this 3 % increase could be attributed solely to adsorption of Na^+ ions with COO^- groups located in the loops and trains of the NaPA layer. The assumption here is that the number of COO^- groups bound to the underlying TiO_2 layer does not change. However, the screening of charged sites by ions in solution, along with the reduced charge arising from adsorption of Na^+ along the polymer loops and tails, could also lead to a rearrangement of the polymer layer to have a higher bound fraction on the surface. It is noted that upon rinsing with DI water, the total bound fraction does not return to the initial value which shows that the removal of the Na^+ ions is not reversible or that the polymer had rearranged adsorbing at a higher bound fraction on the TiO_2. This is also observed when the polymer layer is then exposed to a solution of 0.02M NaCl. When exposed to a 0.02M NaCl solution, the total bound fraction on NaPA layer increased to 51.4 % compared to 50 % with 0.01M NaCl. Upon rinsing, the NaPA layer did not return to its original value.

I also note that the time scale for completion of change in total bound % COO^- with exposure to the solution of 0.01M NaCl is about the same time for completion of change in % COO^- that occurs during the original adsorption and rearrangement of the

NaPA layer. However, this is not strong proof of rearrangement as the time scale for adsorption and removal of Na^+ ions in the adsorbed NaPA layer are about the same. This can simply be due to slow diffusion of the Na^+ into and out of the layer. While there is a constant flow of solution into the cell, the flow is tangential to the coated layer and thus, diffusion of Na^+ into and out of the layer could account for the longer length of time to achieve equilibrium. Nevertheless, a 3 % increase in total bound % COO^- with exposure to 0.01M NaCl would set an upper limit on the value for the % COO^-Na^+.

3.3.3 Adsorption of NaPA on TiO_2 at ionic strength of 0.01 and 0.02M

Figure 3.6 is a plot of the amount of NaPA at ionic strengths of 0.01 and 0.02M NaCl adsorbed on TiO_2 as a function of time. For comparitive purposes, the amount of NaPA adsorbed from DI water is also plotted in this figure. All three curves in Figure 3.6 show an initial rapid increase in adsorbed amount during the first 15 minutes, followed by a gradual increase for the remaining 3.5 hours. More important, the final amount of NaPA adsorbed is 1.6 and 2.5 times higher from 0.01M and 0.02M NaCl compared to DI water.

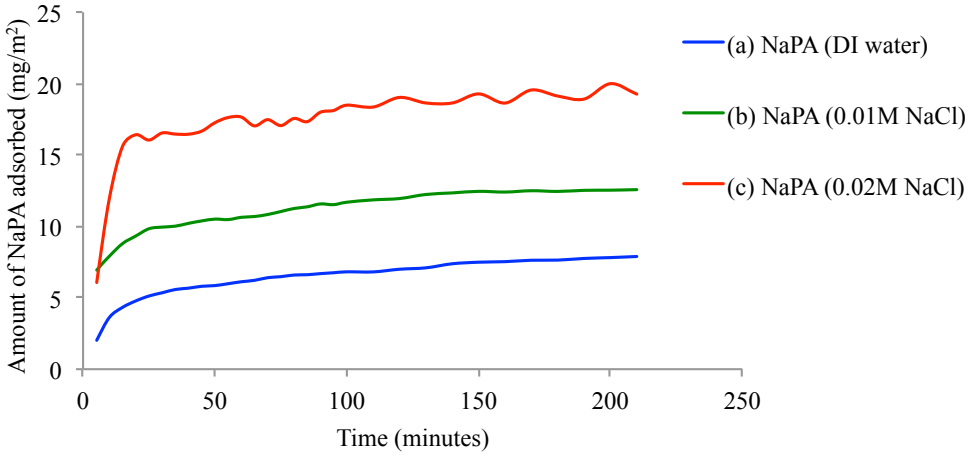

Figure 3.6 The amount of NaPA adsorbed (mg/m^2) on TiO_2 as a function of time at pH 3.5 from (a) DI water (b) 0.01 M NaCl and (c) 0.02 M NaCl solution.

Figure 3.7 is a plot of the dynamic total bound % COO^- groups for adsorption of NaPA at pH 3.5 from DI water, 0.01M and 0.02M NaCl solutions. In Figure 3.5, I showed that there was a 3 % change in total bound fraction when an adsorbed NaPA layer was exposed to 0.02M NaCl. This is mainly due to the binding of Na^+ with COO^- groups. While the number of COO^- groups binding with Na^+ is relatively small (3 % or less), it is not possible to obtain a separate value for these from the bound COO^- groups with TiO_2. Hence, we plot only the total bound % COO^- groups in Figure 3.7.

The dynamic bound fraction in all three cases shows an initial high value that drops to a plateau within 25 minutes. This shows that in all cases the polymer first adopts a flat configuration then rearranges to accommodate additional polymer arriving at the surface. The initial bound fraction for adsorption from DI water was 82 %. This is higher than the values of 77 % and 63 % for adsorption from 0.01M and 0.02M NaCl solutions.

It is noted that the total bound fraction values of 77 % and 63 % do include those sites in the loops and tails neutralized by the adsorption of Na^+ counterions, whereas, the 82 % is the bound fraction to the TiO_2. Therefore, the initial bound fraction to TiO_2 for adsorption from 0.01M and 0.02M NaCl is lower than 77 % and 63 %, respectively. The polymers first arriving to the surface do not lie as flat as those from DI water. As noted earlier, there is a maximum of about 3 % in charge neutralization and it is unlikely that a relatively small change in counterion adsorption along the polymer backbone would lead to a large difference in the initial conformation or in the final adsorbed amount of NaPA on TiO_2.

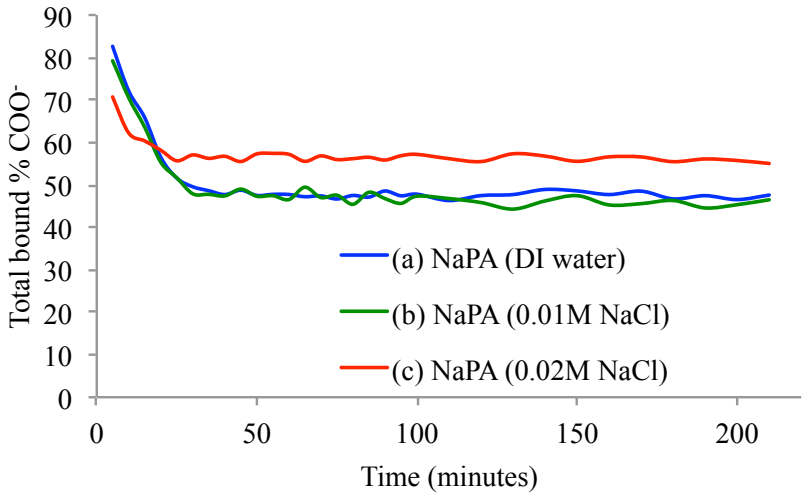

Figure 3.7 Total bound % COO^- for NaPA adsorbed on TiO_2 as a function of time at pH 3.5 from (a) DI water (b) 0.01M NaCl and (c) 0.02M NaCl solution.

The equilibrium values obtained at the end of each cycle are given in Table 3.2. Since the % COO^-Na^+ would be < 3 %, the bound fraction of NaPA to TiO_2 is essentially the same value whether adsorption occurs from DI water, 0.01 or 0.02M NaCl. Now the

adsorbed amount from 0.02M NaCl is 2.5 times higher than obtained from DI water, which means that there are 2.5 times more segments bound to the surface. This produces a more strongly bound and denser layer on the surface. This shows that the electrostatic screening by NaCl solution of the charge interaction between polymers dictates the density of the polymer at the surface.

Table 3.2 Calculated mass of polymer deposited, bound % COO^-, free % COO^-, and free % COOH for adsorption of NaPA in DI water, NaPA in 0.01M NaCl solution and NaPA in 0.02M NaCl solution.

Polymer	*Mass of polymer deposited (mg/m^2)*	*% COOH*	*Free % COO^-*	*Bound % COO^-*
NaPA/DI water	7.5 ± 0.4	40 ± 0.3	13 ± 0.5	47 ± 0.7
NaPA/0.01M NaCl	12.6 ± 0.7	39 ± 0.5	12.8 ± 0.7	48.2 ± 0.4
NaPA/0.02M NaCl	18.1 ± 0.4	37.7 ± 0.4	12.3 ± 0.3	50 ± 0.6

3.3.4 Dynamics of LbL deposition of NaPA/PDADMAC at 0.02M ionic strength

Figure 3.8 shows typical IR spectra recorded at the end of the first two cycles for the sequential addition of NaPA and PDADMAC from solutions at 0.02M NaCl. These spectra, along with the spectra recorded as a function of time, were used to calculate the dynamic adsorbed amount and total bound % COO^-. These curves are shown in Figures 3.9 and 3.10. For comparitive purposes, the curves obtained for the LbL deposition from DI water are provided in Figures 3.9 and 3.10.

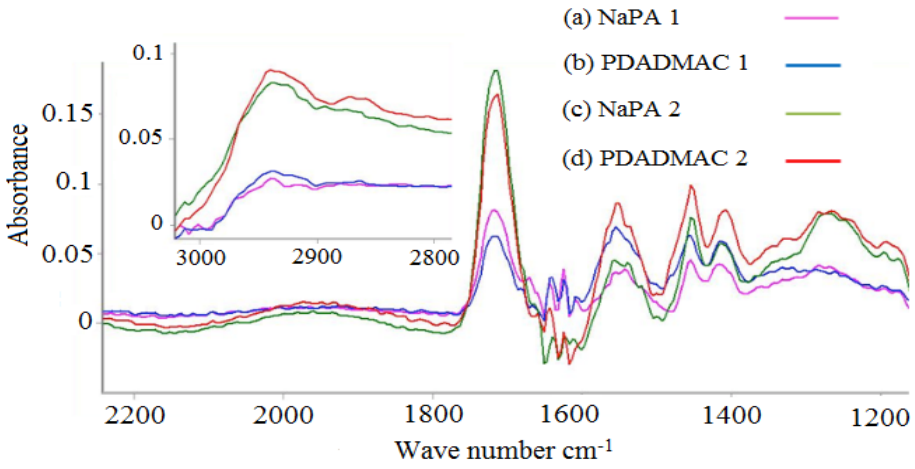

Figure 3.8 Typical IR spectra of (a) first layer of NaPA (b) first layer of PDADMAC (c) second layer of NaPA and (d) second layer of PDADMAC recorded at the end of each cycle. Adsorption was from 0.02M NaCl solutions.

The values obtained at the end of each cycle are given in Table 3.3. The adsorbed mass is for the mass deposited in that specific cycle. The % COOH, free % COO^- and total bound % COO^- are for the combined values for the entire polymer layer. Since rearrangement of underlying layers can occur it is not possible to determine these parameters for individual cycles.

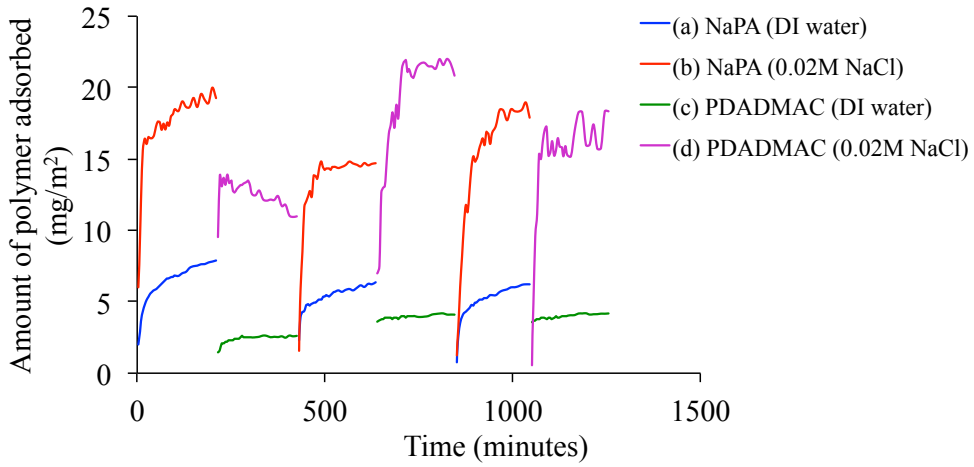

Figure 3.9 The amount of NaPA and PDADMAC adsorbed (mg/m^2) as a function of time from DI water and 0.02M NaCl.

3.3.4.1 Measurement of adsorbed amount of NaPA and PDADMAC

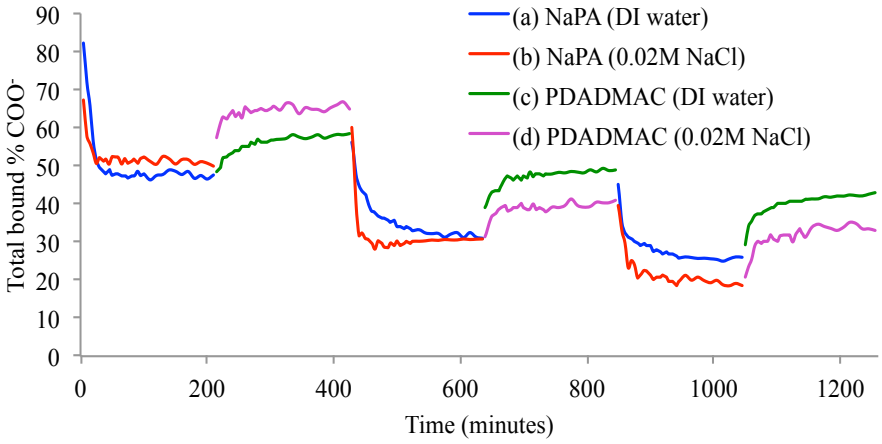

Figure 3.10 The total bound % COO^- as a function of time for the sequential deposition of NaPA and PDADMAC from DI water and 0.02M NaCl solution.

Table 3.3 Calculated mass of polymer deposited in each cycle, and free % COOH, free % COO^- and total bound % COO^- for all layers during sequential adsorption of NaPA and PDADMAC from 0.02M NaCl and DI water.

Cycle	*Polymer adsorbed*	*Mass of polymer deposited (mg/m^2)*	*% COOH*	*Free % COO^-*	*Total bound % COO^-*
1	NaPA/NaCl	19.3 ± 0.3	37.7 ± 0.2	12.3 ± 0.4	50 ± 0.6
	NaPA/ DI water	7.5 ± 0.4	40 ± 0.3	12 ± 0.5	48 ± 0.7
	PDADMAC/ NaCl	11 ± 0.7	26.7 ± 0.9	8.4 ± 0.5	64.9 ± 1.3
	PDADMAC/ DI water	2.6 ± 0.3	32 ± 0.9	10 ± 0.5	58 ± 1.2
2	NaPA/NaCl	14.7 ± 0.7	52.6 ± 1.7	16.6 ± 1.5	30.8 ± 2.8
	NaPA/ DI water	6.4 ± 0.5	51 ± 2.2	15 ± 1.6	34 ± 3.7
	PDADMAC/ NaCl	20.8 ± 0.6	48.9 ± 1.3	14.2 ± 1.6	41 ± 2.4
	PDADMAC/ DI water	4 ± 0.4	39 ± 0.3	12 ± 1.5	49 ± 0.7
3	NaPA/NaCl	16.9 ± 0.8	61.9 ± 1.5	19.5 ± 1.8	18.6 ± 2.7
	NaPA/DI water	6.7 ± 0.6	57 ± 1.2	18 ± 1.3	25 ± 2
	PDADMAC /NaCl	18.3 ± 0.8	50.9 ± 2.3	16.1 ± 2.8	33 ± 3.1
	PDADMAC/ DI water	4.2 ± 0.5	43 ± 1.4	14 ± 1.2	43 ± 1.5

Figure 3.9 and Table 3.3 show that the amount of polymer adsorbed for each layer was at least two times higher for NaPA and about 4-5 times higher for PDADMAC from a 0.02M NaCl solution compared to DI water. In Figure 3.10, the total bound % COO^- for the initial cycle of NaPA adsorption on TiO_2 shows only a 2 % higher value for deposition from 0.02M NaCl compared to DI water. As shown in Section 3.2, the condensation of Na^+ with COO^- groups would account for this 2 % difference in total bound % COO^-, and that a more densely packed NaPA layer accounts for the higher mass of NaPA.

Adsorption of PDADMAC in the first cycle is accompanied by an increase in the total bound % COO^-. The increase in the total bound % COO^- is mainly due to the positively charged segments of PDADMAC electrostatically adsorbing with the COO^- groups of NaPA. However, a value cannot be determined because the adsorbed PDADMAC could displace Na^+ from COO^- groups and could also lead to polymer rearrangement, which in turn, changes the number of COO^- groups interacting with the underlying TiO_2. Displacement of Na^+ would lead to a zero gain in the total bound % COO^- and, as shown in Chapter 2, rearrangement of the polymer layer by adsorption of PDADMAC leads to a decrease in the bound % COO^- to the underlying TiO_2. Thus, the increase in total bound % COO^- during the first addition of PDADMAC would at best, underestimate the bound fraction of PDADMAC with the first layer of NaPA.

Now, the first addition of PDADMAC leads to 4.2 times more adsorbed amount than from DI water. This is accompanied by a higher change in bound fraction (14.9 %) of NaPA charged sites to PDADMAC than the corresponding change (10 %) in DI water.

As mentioned above, the value of 14.9 % is actually lower that the true bound fraction of PDADMAC. Nevertheless, by factoring in the difference in mass of NaPA, there would be about 3.8 times more PDADMAC segments adsorbed to the underlying NaPA layer from 0.02M NaCl. However, given that there is also 4.2 times more mass of PDADMAC adsorbed, the bound fraction of PDADMAC is about the same from 0.02M NaCl or DI water. I note that in Chapter 2, I showed that the first PDADMAC layer does not penetrate into the underlying first NaPA layer. Since the underlying NaPA layer is more densely packed relative to the layer formed from DI water and in both cases, the PDADMAC have similar values for the bound fraction, penetration into NaPA is even less likely. Furthermore, Figure 3.9 shows that the first PDADMAC layer adsorbs rapidly and in fact, the amount decreases with time. There is no loss of NaPA and thus, the loss of PDADMAC would not be due to interpenetration of this polymer in the underlying layer.

For the second and third NaPA/NaCl cycles, the total bound % COO^- for the entire film decreases from cycle to cycles. This shows that the bound fraction between NaPA and PDADMAC are lower than between NaPA and the TiO_2. It is noted that the increase in adsorbed amount is much greater (4-5 times) for each PDADMAC cycle compared to the factor of 2 for NaPA. NaPA is a weak polyelectrolyte and partially charged at pH 3.5, whereas, PDADMAC is a strong electrolyte with each segment possessing a positive charge. Because PDADMAC is a strongly charged polymer, the Cl^- neutralizes and screens a higher percentage of the charged sites on PDADMAC, which leads to a more dramatic increase in the adsorbed amount relative to deposition

from DI water. When the charge density on the polyelectrolyte chain is decreased, the polyelectrolyte chains come closer to each other and hence, the amount of polyelectrolyte adsorbed increases.

Figure 3.11 is a plot of the amount of polymer deposited per cycle and shows that a linear growth occurs for both LbL deposition from DI water and 0.02M NaCl. This is expected as nonlinear growth regimes typically occur when the ionic strength exceeds 1M.[126] Thus, this represents another example of linear growth occurring without polymer diffusion between layers.

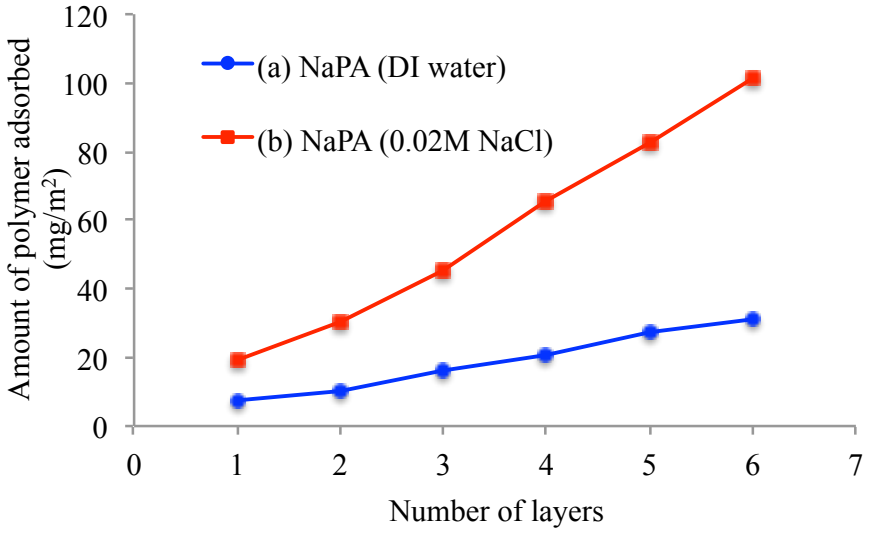

Figure 3.11 Cumulative amount of polymer deposited for each layer (a) NaPA/PDADMAC in 0.02M NaCl solution and (b) NaPA/PDADMAC in DI water.

3.4 Conclusion

The level of extrinsic compensation arising from the adsorption of Na^+ on COO^- groups of NaPA as a function of ionic strength can be determined from recording IR spectra of the NaPA in solution. The main drawback is that highly concentrated solutions are required. Measuring the extrinsic compensation for an adsorbed NaPA layer on TiO_2 shows that the Na^+ absorbs on less than 3 % of the negatively charged COO^- groups at pH 3.5 and ionic strength of 0.02M. The Na^+ can be washed from the polymer layer but the process is not completely reversible as the polymer undergoes a rearrangement on the surface when exposed to solutions of ionic strength of 0.01M and 0.02M.

The IR studies of LbL deposition of alternating layers of NaPA and PDADMAC show a large increase in adsorbed amount of both NaPA and PDADMAC from 0.02M NaCl compared to deposition from DI water. At these low ionic strength systems, we show that the more densely packed layers occur, which prevents interpenetration of polymer between layers. In both DI water and 0.02M NaCl, a linear film growth is obtained without interpenetration of the polymer between layers.

CHAPTER 4: A VISIBLE SPECTROSCOPIC BASED METHOD FOR Fe^{3+} DETECTION IN AQUEOUS SOLUTIONS BY USING DFB TETHERED TO OPTICALLY TRANSPARENT MEMBRANES

4.1 Introduction

Anthropogenic CO_2 is one of the main contributing factors to global warming and this is the impetus behind the critical need to reduce the levels of CO_2 in the atmosphere.[145] The oceans are a potential major avenue for sequestering carbon and currently adsorb about one-third of the CO_2 emitted by human activity.[146] In particular, phytoplankton, which inhabit the upper sunlit layer of oceans and fresh water bodies, removes vast amounts of CO_2 by photosynthesis.[145] Approximately 40 % of the oceans are High Nutrient Low Chlorophyll (HNLC) regions which have a lower level of phytoplankton growth, even though they contain excess major plant nutrients such as PO_4^{-3}, NO_3^{-1}, SiO_3^{-2}.[147] This is because the growth inhibition of phytoplankton in these regions is dictated by the low concentration of dissolved Fe^{3+} in ocean waters. It has been suggested that seeding the oceans with Fe^{3+} could provide an avenue to increase the capacity of the oceans to sequester carbon. This is known as the "Iron Hypothesis" and first put forward and field-tested[134,147-149] by Martine *et al.*in 1993.

Large-scale ocean fertilization of Fe^{3+} could alter the marine ecosystems by increasing the growth of certain types of harmful phytoplankton.[92,147,150] This is one of

many potential problems. What is clearly needed is a much better understanding of the role and fate of Fe^{3+} in seawater before contemplating the use of Fe^{3+} seeding on any large scale. However, a major hurdle is that there is little data available on the amount and fate of Fe^{3+} in seawater. This is because the concentration of Fe^{3+} in seawater is in nanomole range which makes it difficult to measure.[151] Moreover, seawater matrix contains 3 % salt and other elements and interferes with the quantification of Fe^{3+}. As a result, sensitive analytical methods such as flow injection analysis,[94] spectrophotometry,[152,153] cathodic stripping voltammetry[154] and inductively coupled plasma mass spectrometry (ICP-MS)[155] are required for the detection of Fe^{3+} in seawater[94,151]. Water samples analyzed for Fe^{3+} by these traditional detection methods also require careful sampling and transportation techniques.

There are some methods that rely on chemiluminescence, which can be performed onboard ships.[135,156] However, ship time is expensive and ship-based methods still require careful sampling procedures. In the end, ship-based methods will not provide the volume of data needed to map the spatial distribution of Fe^{3+} in the ocean for developing predictive models on the role of Fe^{3+} in global climate change. What is needed to provide this volume of data are sensors mounted on gliders or buoys that could provide autonomous detection of Fe^{3+} levels in seawater. It is this need that has provided the motivation for the work presented in this chapter. Specifically, the work here is targeted to the development of a field deployable technique for autonomous detection of Fe^{3+} in picomolar to sub-nanomolar range on buoy and gliders.[151]

At the heart of our method is the use of the siderophore, desferrioxamine B (DFB). DFB is a Fe^{3+} specific chelating agent produced by the bacteria and fungi (see Figure 4.1a) [157] that has a high affinity and selectivity[149] for Fe^{3+} through formation of a six coordinate chelate (see Figure 4.1b).[151,157]

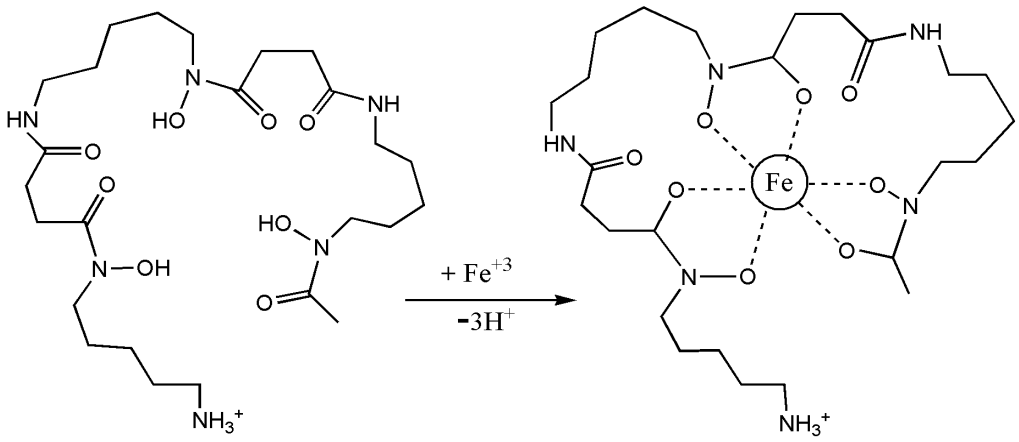

Figure 4.1 Structure of (a) desferrioxamine B (DFB) and (b) ferrioxamine B (Fe-DFB) Figure reproduced from E. Roy *et al.*[151]

The first approach developed involved attachment of the DFB to a solid phase material to extract the Fe^{3+} from solution. Quantification of the Fe^{3+} was then performed by transmission infrared spectroscopy recorded directly through the solid phase material. In brief, a high surface area mesoporous silica film was deposited on a silicon substrate (see Scheme 4.1). The surface of the film was then functionalized with an alkoxysilane containing a carboxylic acid group.

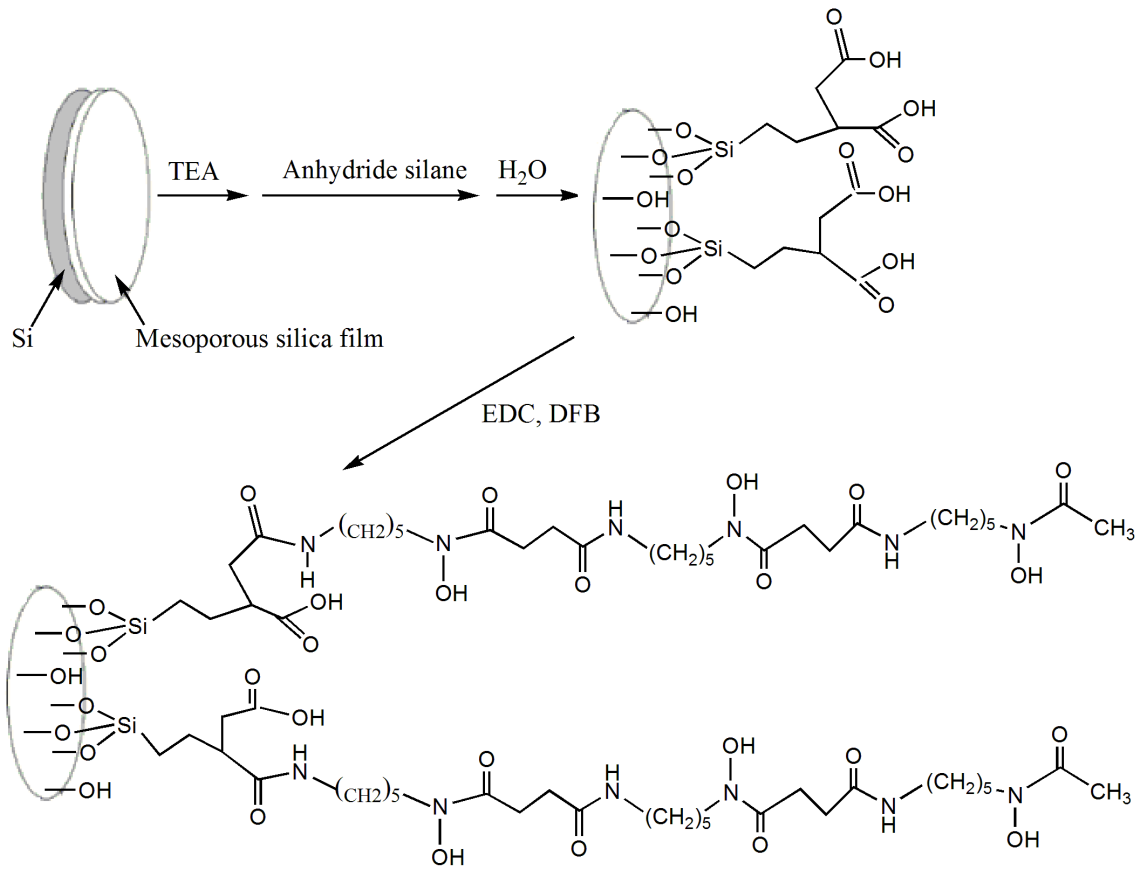

Scheme 4.1 Stepwise reaction for coupling DFB to silane bound mesoporous silica film. *N*-(3-Dimethylaminopropyl)-*N*′-ethylcarbodiimide hydrochloride (EDC) is the catalyst. Figure reproduced from C. Jiang.[158]

Next, the DFB was tethered *via* formation of an amide linkage with the carboxylic acid groups using *N*-(3-Dimethylaminopropyl)-*N*′-ethylcarbodiimide hydrochloride (EDC) as a catalyst. The DFB derivatized Si wafer was then immersed into a 1L beaker containing the sample of seawater. After stirring for 24 hours to ensure complete mass transport of Fe^{3+} to the wafer, the Si wafer was removed, washed and dried and an infrared transmission spectrum recorded. While numerous spectral changes occur when Fe^{3+} complexes with the DFB (see Figure 4.2),[151] analysis was performed by simply

measuring the intensity of the Fe – O band at 560 cm^{-1}. The detection limit of this method was 100 picomole and it could be used in a wide range of pH in seawater.[151]

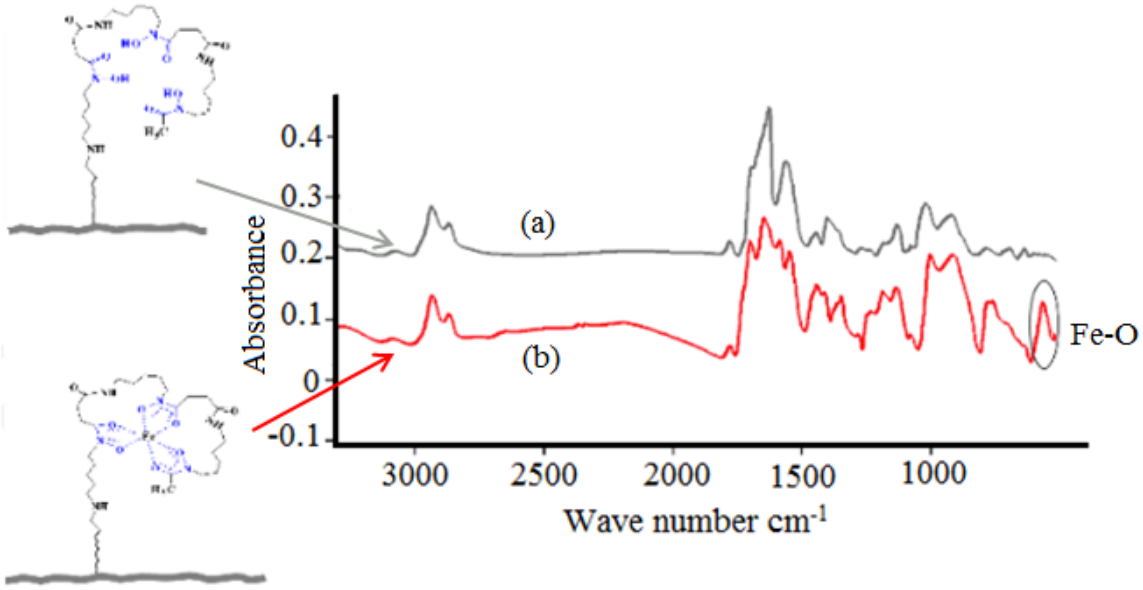

Figure 4.2 IR spectra of (a) DFB modified silica substrate, (b) Fe (III) adsorption. (Spectrum of an unmodified silica coated chip was subtracted for clarity). Figure reproduced from E. Roy *et al*.[151]

While this Solid Phase Extraction / Fourier Transform Infrared spectroscopy (SPE/FTIR) method could be used on ships, there were limitations to adapting it for use on buoys or gliders. The surface area of the mesoporous film was high (1000 -1500 m^2/g) due to the small internal pore size (6 nm in diameter) and ultimately led to a high DFB density.[151,159] The problem is that water could not pass through a film with 6 nm pores. Therefore, the mesoporous films were deposited on a solid silicon wafer for support and placed in contact with an Fe^{3+} containing stirred beaker for 24 hours in order to ensure complete mass transport of the Fe^{3+} to the wafer. Stirring for 24 hours in a beaker is not a

practical option for deployment on buoys and gliders. Another problem is that water is a strong IR absorber, and thus the silicon wafer had to be dried before recording an IR spectrum. Deploying an IR spectrometer and a drying stage on a glider or buoy would not be practical.

In order to address the mass transportation limitation, the SPE system was changed from mesoporous silica film/Si wafer to an optically transparent membrane treated to contain DFB. This work was performed by Zachery Helm and is described in detail in his MS thesis.[160] In this case, water samples were flowed through the DFB tethered on the membrane and this eliminated the need for stirring in the beaker for days. In addition, the membrane was chosen because it has a refractive index close in value to that of water. When the membrane was immersed in water, it became optically transparent in the visible region of the spectrum. When Fe^{3+} complexes to DFB, it produces a red color with a maximum adsorption at 470 nm. Therefore, the analysis changed from FTIR to Visible spectroscopy so that the samples did not need to be dried before analysis.

There was one major drawback in moving to a membrane from a high surface area mesoporous film. The pore size of the membrane was relatively large (0.4 μm) in order to enable flow rates of 1-10 ml/min. However, the larger pore structure was accompanied by a 100 times less surface area compared to the mesoporous films. Therefore, there was a need to develop an approach to increase the DFB density on the membrane in order to obtain sufficient signal intensity for detection of Fe^{3+}. The approach was to self-assembly poly (styrene-acrylic acid) block copolymers on the

membranes. The polyacylic acid formed a brush extending from the membrane surface, which provided vertical amplification, as each monomer unit contained a COOH group. This is depicted in Figure 4.3. This compensates for the 100 times lower surface area compared to the mesoporous silica (1000 - 1500 m^2/g).[161,162]

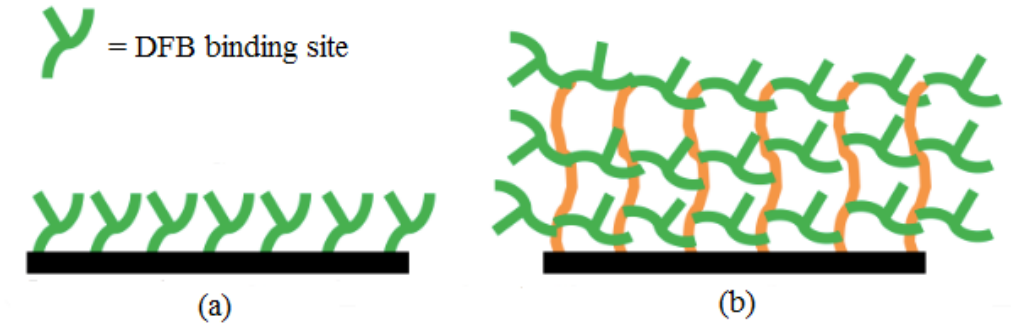

Figure 4.3 Schematic representation of vertical amplification produced by block copolymer bound to the membrane (a) DFB directly bound to a surface (no vertical amplification) and (b) DFB bound to block copolymer that are bound to a surface (vertical amplification). Figure reproduced from Z. Helm.[160]

The DFB was then reacted with the COOH groups using the reaction sequence depicted in Scheme 4.2. The COOH groups were activated by the water soluble catalyst EDC to form an intermediate isourea active ester. Addition of DFB, which contains a primary amine, completed the coupling reaction between COOH of polyacrylate and NH_2 of the DFB, forming an amide linkage.

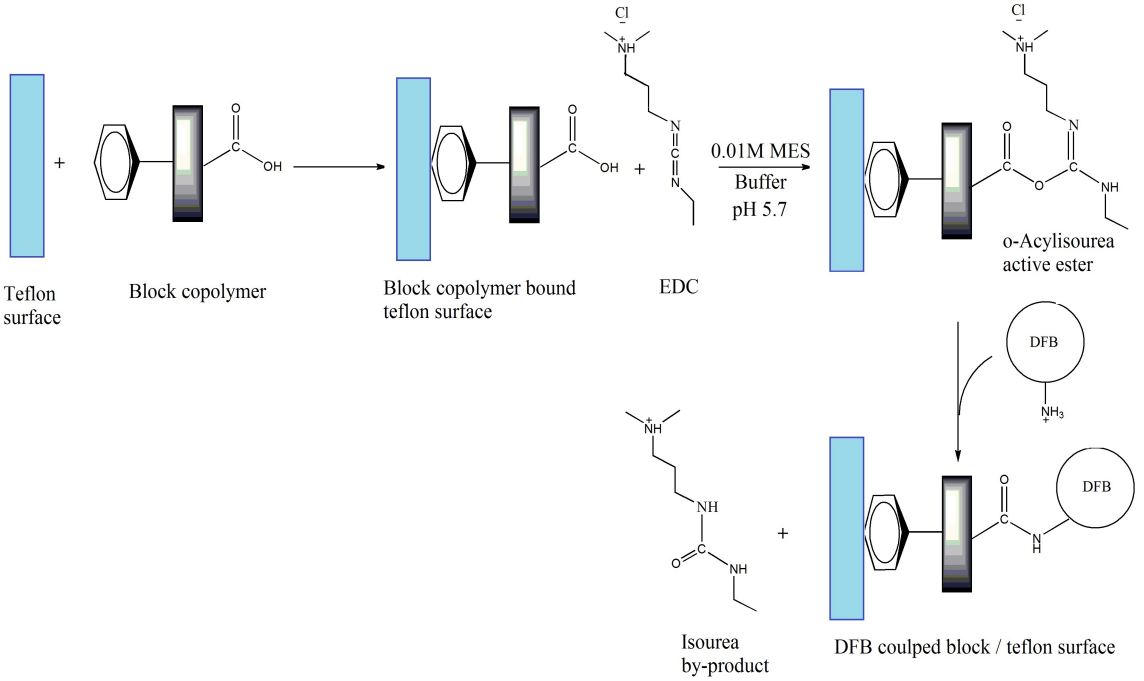

Scheme 4.2 Stepwise reaction for coupling DFB to block copolymer adsorbed on the membrane. *N*-(3-Dimethylaminopropyl)-*N*′-ethylcarbodiimide hydrochloride (EDC) is the catalyst.

The DFB modified membranes were mounted in a flow through cell that allowed the recording of UV-Vis spectra while simultaneously flowing sample solutions through the membrane. One of the main findings was that the percent capture was flow rate dependent. The slower the flow rate the higher the percent capture. In particular, a flow rate of about 0.1 ml/min was required to obtain capture rates of 48 % .[160] At a flow rate of 2 ml/min the percent capture reduced to 3 %.[160]

A second issue was the inherent sensitivity of the UV-Vis based detection using a membrane. From the known extinction coefficient for the DFB-Fe complex (2.5 x 10^6 cm^2/mole),[160] it is calculated that approximately 35 ng of Fe^{3+} captured by DFB

throughput matched to the 7 mm diameter would give an absorbance of 0.004 at 470 nm. This would require one liter of a 35 part per trillion (ppt) Fe^{3+} sample to be passed though a 7 mm diameter membrane at a flow rate of 0.1 ml/min. At this flow rate, a 1L sample would require 10,000 minutes, which clearly is not practical.

The solution to this problem was to decrease the volume required by introducing a pre-concentration step. In brief, a 1L water sample is first passed through a packed column containing DFB derivatized toyopearl beads. The column size was approximately 2 cm long and had a 100 percent capture of the Fe^{3+} at relatively high flow rates of 10 ml/min. The Fe^{3+} was then eluted by applying a reverse pulse of an oxalate/pH 2 solution into a 1 ml volume or less. This volume is then passed through the membrane at pH 7.

The question remained as to why the percent capture on the membranes was flow rate dependent. One possibility is that the contact time of the solution through the 100 μm thick membrane did not allow sufficient time for the DFB to fold around and capture the Fe^{3+} molecules. This would be in contrast to the 100 % capture of the Fe^{3+} obtained on the DFB derivatized toyopearl column at much higher flow rates.[160] It could be argued that the contact time of the Fe^{3+} with the toyopearl beads was much longer because the column is 2 cm long. However, the Fe^{3+} was concentrated at the very front edge of the toyopearl column. This was a key factor that enabled concentration of the Fe^{3+} in a small volume by applying a reverse pulse of oxalate/pH 2 solution. However, it also suggests there is a fundamental difference in the reaction kinetics of the DFB attached to the toyopearl compared to the DFB attached to the block copolymers. One possibility is that the higher DFB density provided by the block copolymer is what sterically inhibits the

mobility of the DFB and in turn, slows the capture rate of the Fe^{3+}.

This possibility provided the motivation described in the first part of this chapter. Specifically, I have measured the capture rate of Fe^{3+} on membranes on three different block copolymers of different relative block sizes assembled on the surface. The packing density of the polyacrylic acid (PAA) on the surface depends on the adsorbed amount and the relative block size and this would lead to a difference in the packing density of the DFB. Furthermore, after assembled on the membrane, each block copolymer was reacted with DFB at 50 and 100 % loadings. The two different loadings would lead to different packing densities of DFB on the membrane.

The second part of this chapter provides preliminary findings on the use of coating transparent beads with block copolymers to capture Fe^{3+}. Essentially, the idea is to mimic the toyopearl column in terms of 100 % capture of Fe^{3+} at relatively high flow rates. The advantage of using transparent beads is to eliminate the need to elute into a small volume, as the UV spectroscopy could be accomplished directly by transmission mode through the beads. Here, I present some initial results in screening materials that are transparent after treatment with block copolymers and DFB.

4.1.1 Block copolymer adsorption on Membranes

In my study, I have used three types of block copolymers consisting of polystyrene and polyacrylate units as the building blocks. An empirical structure of the block copolymer is shown in Figure 4.4 (a, b and c), where X represents styrene and Y represents acrylate monomers, respectively. In all three types of block copolymers, the

number of polystyrene units was constant (X = 50) and the number of polyacrylate units varied with Y = 47, 89, and 180 monomer units. For simplicity, these block copolymers are referred to as block-47, block-89, and block-180.

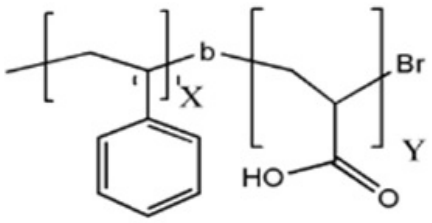

(a) X=50, Y=47

(b) X=50, Y=89

(c) X=50, Y=180

Figure 4.4 Unit structures of (polystyrene)$_x$-b-poly(acrylic acid)$_y$ block copolymer.

The hydrophobic PS block, which is called the anchor block, adsorbs onto the membrane surface.[163,164] The PAA block, known as the buoy block, is highly soluble in water and extends out into the solution. The length of the adsorbed polymer brush depends on the relative size of each block in the copolymer. If $N_{buoy} >> N_{anchor}$ (N being the number of monomer units), the buoy block overlap and extend out from the surface in order to accommodate the adsorption of more PS units on the surface (see Figure 4.5a). This overlap of the buoy blocks in the same spatial area results in an osmotic pressure, which leads to the PAA polymer extending out into the solution phase. If $N_{buoy} << N_{anchor}$, as shown in Figure 4.5c, the anchor blocks are comparatively larger than the buoy blocks. In this case, it is the footprint size of the PS on the surface that limits the adsorbed amount of polymer. The buoy blocks do not overlap; hence, there is no driving force for the PAA block to extend away from the surface. In this case, the PAA block exists as a loosely packed random coil. For other block sizes, which fall in between these two

extremes, as represented by Figure 4.5b, the adsorbed amount is dictated by the size of the PS and the PAA. If the adsorption energy of the PS is greater than the entropy loss from stretching of the buoy block, then the surface adsorption is anchor-dominated. [163-165] Thus, the packing density of the PAA and hence, the packing density of the DFB is expected to be dependent on the relative block size.

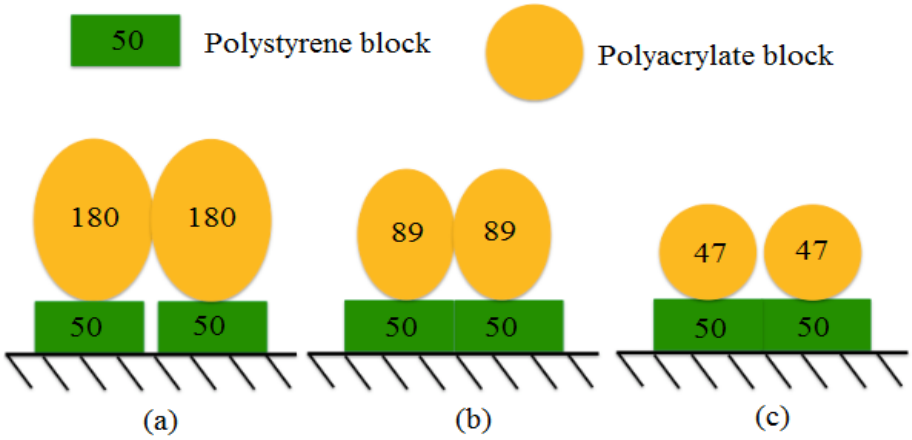

Figure 4.5 Schematic diagram of block copolymer asymmetry and the resulting structures. (a) buoy-dominated regime, (b) almost symmetric regime and (c) anchor-dominated regime.

4.2 Experimental

4.2.1 Materials and methods

Poly(tetrafluoroethylene) powder (35 μm particle size), methanol, *N*-(3-Dimethylaminopropyl)-*N*′-ethylcarbodiimide hydrochloride (EDC), Desferrioxamine mesylate (DFB), 2-(N-morpholino)ethanesulfonic acid (MES) buffer, sodium oxalate, and iron (III) chloride ($FeCl_3$) were purchased from Sigma Aldrich. Sodium hydroxide, trace metal grade hydrochloric acid, glacial acetic acid and trace metal grade ammonium hydroxide were purchased from Fisher Scientific. Polystyrene-b-Poly (acrylic acid) block copolymers of (PSt_{50}-b-PAA_{43}), (PSt_{50}-b-PAA_{89}), and (PSt_{50}-b-PAA_{180}) were purchased from ATRP Solutions. Polyacrylamide hydrogel (water gel crystals) was purchased from Educational Innovations Inc. Deionized water was used throughout the experiments. The optically transparent membranes were obtained from Orono Spectral Solutions Inc. These membranes were 13 mm in diameter and had a pore diameter of 0.4 um. Metal grids and swinnex o-rings were purchased from Millipore - Biomanufacturing and Life Science Research. Teflon tubes (PFA tubing 1/16 OD) were purchased from Upchurch Scientific. All the chemicals were used as received, unless otherwise noted.

IR spectra were recorded on an ABB-Bomem FTLA 2000 spectrometer at 8 cm^{-1} resolution. Typically, 100 scans requiring about 2 minutes was used for each spectrum. For UV-vis measurements, an in-house designed cell was used and details are provided elsewhere.[160] The solutions were flowed through using a 10 ml syringe containing a

Cavro® XLP 6000 Modular Syringe Pump (Tecan® pump) with Waterville analytical software. Uv-visible spectra were recorded on an OceanOptics-USB2000+ Fiber Optic Spectrometer with SpectraSuite software.

4.2.2 Section I: Fe^{3+} adsorption on membranes and detection of Fe^{3+} by visible spectroscopic methods

4.2.2.1 Adsorption of block copolymer on the membranes

A solution of block copolymer was made by adding 0.025 g of block-89 to 100 ml of DI water and pH adjusted to 4.5 by adding dilute HCl. The temperature of the solution was adjusted to 50 ^{0}C and was stirred for 4 hours to ensure all polymer dissolved into solution. The membrane was attached to a flow through cell and the block copolymer solution was passed through the membrane using the Tecan® pump at 0.1ml/min flow rate for 7 hours. Then the membrane was washed for 5 minutes by passing DI water at 0.1 ml/min using the Tecan® pump. By blowing a dry nitrogen stream for about 30 minutes, the membrane was dried and an IR spectrum of the membrane was recorded. The same procedure was repeated to adsorb block-180 and block-47 on the membranes.

4.2.2.2 Coupling DFB to the block copolymer/membrane

A solution of 0.01M MES buffer containing DFB was made by dissolving 0.12 g of MES powder and 0.17 g of DFB in a volumetric flask and adjusting the volume to 100 ml with DI water. The pH of the solution was adjusted to 5.5 by adding dilute NaOH. In a separate beaker, 0.055 g of EDC was added to 100 ml of a 0.01M MES buffer solution.

We have found that it was important to always use freshly prepared solutions as the EDC activity decreased with time in the presence of DFB. This is why I made two separate solutions, one containing the DFB and the second containing the EDC. The two solutions were mixed in the syringe of the Tecan® pump and then immediately passed through the membrane. The mixing procedure involved sequentially filling the syringe with 1 ml from each beaker for a total of 10 ml. This solution was then passed through the block derivatized membrane at a 0.1 ml/min flow rate. This procedure was under software control and the mixing in the syringe, followed by passing the solution through the membrane was repeated several times. Two levels (50 % and 100 %) of DFB coverage on the membranes were prepared. The percent coverage was defined by the relative decrease in the COOH band in the infrared spectrum after reaction with the DFB. A 100 % DFB coverage was prepared by passing the DFB/EDC solution for 4h through the membrane. IR spectra were recorded every 30 minutes to measure the extent of reaction of DFB with the membrane.

A 50 % DFB coverage was prepared by passing the DFB/EDC solution through the membrane for approximately 30 minutes. IR spectra were recorded every 10 minutes to determine when 50 % coverage on the membrane was obtained. When taking an IR spectrum, it was important to dry the membrane with a nitrogen gas stream for about 30 minutes. When the desired level of reaction was obtained, the membrane was washed for 5 minutes by passing DI water at 1 ml/min. An IR spectrum of the dried membrane was recorded.

4.2.2.3 Visible spectroscopic measurements with DFB bound membranes

The DFB derivatized membrane was mounted in the flow through cell. The cell was fitted with fiber optic that enabled recording of UV-Vis spectra in transmission mode directly through the membrane while flowing aqueous solutions. A USB2000 Ocean Optics UV-Vis spectrometer (wavelength range: 175-885 nm) controlled by SpectraSuite software (Ocean Optics, Inc.) was used to collect spectra. Details of the flow through cell design are reported elsewhere.[160] Deionized water was then passed through the flow cell at 1ml/min using a Tecan® pump controlled by Waterville analytical software. A dark current spectrum was recorded by turning off the light source. Blocking the light source to take a dark current spectrum was not possible as the fiber optic couplings were attached directly to the flow cell. A reference spectrum was then recorded through the cell while flowing water. This reference spectrum was used during collection of all subsequent absorbance spectra. Typical spectrometer settings were: 1 second integration time, 10 scans averaged and boxcar width of 20.

A solution of 10 ppm $FeCl_3$ was prepared by using DI water and pH was adjusted to 2.7 by adding dilute HCl. This pH was used because the the solubility of Fe^{+3} is high below pH 3.[160] This solution was then passed through the membrane at three different flow rates (2 ml/min, 1 ml/min and 0.1 ml/min) using the Tecan® pump. A band appeared at 429-470 nm, due to the Fe^{3+}/DFB complex, and the UV-Vis spectral intensity at 375 nm, 429 nm, 470 nm, 600 nm and 650 nm were monitored with time using the strip chart function in the software. The solution was flowed until the spectral intensity at the

measured wavelengths reached a plateau in value. Spectra were also recorded and saved at each point in time.

Next, an oxalate rinse step was used to remove the bound Fe^{3+} from the membrane. In particular, a 0.1M oxalate solution at pH 1.5 was passed through the membrane at a flow rate of 1 ml/min for 30 minutes, followed by a DI water rinsing step at 1 ml/min for 10 minutes. The lamp was turned off during the oxalate and DI water rinsing steps to avoid photochemical degradation of the DFB-block copolymer complex on the membrane.[160] The ability to remove Fe^{3+} with the oxalate rinse step meant that the DFB coupled block/membrane could be reused without preparing a new membrane for each experiment. Each experiment consisted of at least three Fe^{3+} addition/oxalate rinse cycles.

4.2.3 Section II: Modification of transparent beads (DFB coupled block copolymer/Teflon® beads)

4.2.3.1 Preparation of block copolymer bound Teflon® beads

In a 100 ml beaker, 0.025g of block-180 was mixed with a suspension containing 0.3g of Teflon® beads with particle size of 35μm. The total volume was adjusted to 80 ml with DI water. The Teflon® beads floated on top of the surface of the water but, after 2-3 hours of vigorous stirring, the beads began to sink. Vigorous stirring was repeated for an additional 4 days until all the beads were coated and sank to the bottom of the beaker. The solution was then centrifuged at 4800 rpm for 10 minutes and the supernatant was discarded. The Teflon® beads were washed three times with DI water. To record an IR spectrum of the block copolymer coated beads, a reference was recorded through a

membrane. The block-180/Teflon® beads were dispersed in about 5 ml of DI water and the solution was then flowed through the membrane. The membrane with the block-180/Teflon® beads was dried in air for about 24 hours and an IR transmission spectrum was recorded.

4.2.3.2 Preparation of DFB coupled block copolymer/Teflon® beads

To a 100 ml sample of freshly prepared 0.01M MES buffer solution, 0.27g of the block copolymer treated Teflon® beads prepared in section 4.2.3.1, 0.17g of DFB and 0.055g of EDC (catalyst) were added. The amount of DFB added was based on 1:1 DFB per COOH binding site on the block copolymer. The pH of the solution was adjusted to 5.5 with NaOH. Next, 5 ml of methanol was added to the suspension, which was stirred for 4 hours at 50 ^{0}C. The suspension was then centrifuged at 4800 rpm for 10 minutes and the supernatant was decanted. The beads were washed three times with DI water and air dried for about 24 hours. An IR spectrum of the dried DFB coupled block copolymer/Teflon® beads was recorded.

4.2.3.3 Fe^{3+} reaction with treated beads

The DFB derivatized Teflon® beads, as prepared in section 4.2.3.2 and suspended in 20 ml of water, were packed into a glass pasture pipette. A small piece of glass wool was used to plug in the end of the pasture pipette, which was then vertically clamped in a ring stand. The suspension containing the DFB derivatized Teflon® bead was slowly poured into the open end of the pasture pipette, followed by passing DI water through the column to tightly pack the beads. The column remained wet and was not allowed to dry.

A solution of 100 ppm $FeCl_3$ at pH 2.7 (adjusted with dil. HCl) was then flowed through the column. A 100 ml volume typically required 30 to 60 minutes to elute completely.

4.2.4 DFB coupled block copolymer/hydrogel

4.2.4.1 Preparation of block copolymer bound hydrogel

A suspension of polyacrylamide hydrogel was prepared by adding 15 mg of hydrogel to 100 ml of DI water. The hydrogel particles were allowed to soak in water for 12 hours to swell. The swollen, transparent hydrogel were broken into 2-4 mm diameter particles using a spatula. A 3 mg sample of the hydrogel was transferred onto a ZnSe crystal and allowed to dry for about 48 hours. An IR spectrum of polyacrylamide hydrogel was recorded.

A mixture of block copolymer and hydrogel was made by adding 0.025g of block-180 to 2g of soaked polyacrylamide hydrogel in a 100 ml beaker. 80 ml of DI water was added to the beaker and the suspension was stirred for 4 days, then centrifuged at 4800 rpm. The supernatant was discarded and the particles were washed three times with DI water. In order to record an IR spectrum, a small amount of hydrogel particles were transferred on to a ZnSe window and dried for 48 hours in an atmospheric air. An IR spectrum of the hydrogel particles coated with block copolymer was recorded.

4.2.4.2 Preparation of DFB coupled block copolymer/hydrogel

A solution of 0.01M MES buffer was prepared by dissolving 0.195g of MES powder in a volumetric flask and adjusted to 100 ml with DI water. Next, 0.5g of the

block-180/hydrogel produced in section 4.2.3.2, 0.17g of DFB and 0.055g of EDC were added to the MES buffer solution. The amount of DFB added to the flask was calculated so that there would be 1:1 DFB per COOH binding site on the block copolymer. The pH of the sample was adjusted to 5.5 with dilute sodium hydroxide. Five milliliters of methanol was added to the sample and the suspension was stirred for 4 hours. Then the suspension was centrifuged at 4800 rpm for 10 minutes and the supernatant was discarded. The DFB coupled block-180/hydrogel sample was washed three times with DI water and dried for 48 hours. An IR spectrum was then recorded by placing the sample on a ZnSe window.

4.3 Results and Discussion

4.3.1 Section I: Fe^{3+} adsorption on membranes and detection of Fe^{3+} by UV-Vis spectroscopic method

4.3.1.1 Preparation of DFB derivatized membranes and reaction with DFB

An IR spectrum of the block-180 adsorbed on the optically transparent membrane is shown in Figure 4.6a. For clarity, the spectrum of the membrane has been subtracted from the spectra shown in order to remove the strong C-F modes. The band at 1720 cm^{-1} is due to the C=O stretching mode of the COOH groups from the block-180 adsorbed on the membrane and the decrease in the intensity of this band is used to measure the percent of the COOH groups reacted with DFB. The band at 700 cm^{-1} (see Figure 4.6a inset) is due to the C-H bending mode of styrene and is used to calculate the amount of adsorbed block copolymer.

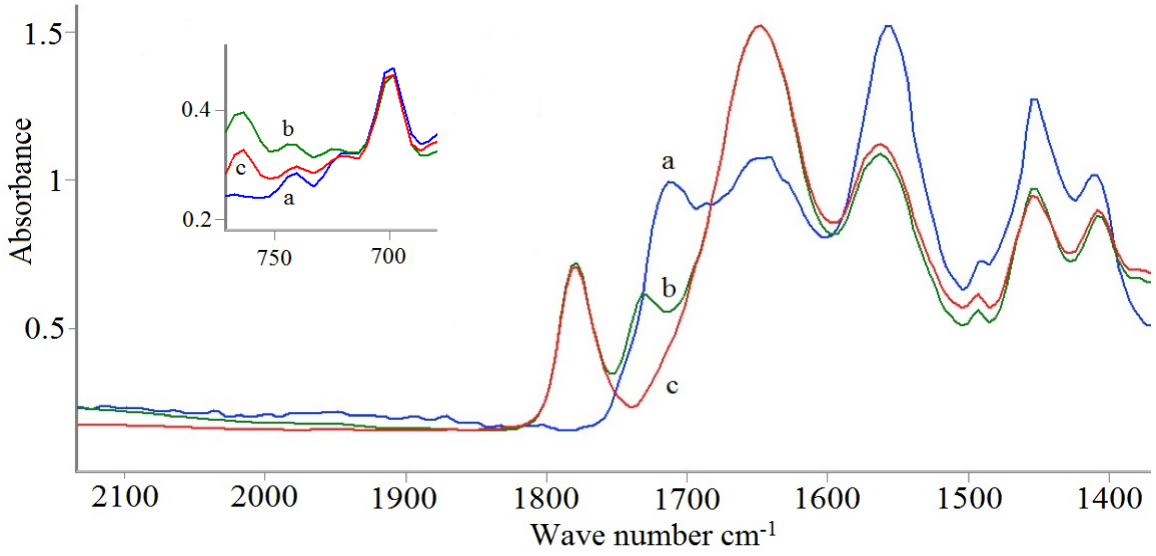

Figure 4.6 IR spectra of (a) block-180 adsorbed on the membrane, (b) DFB 50 % and (c) DFB 100 % reacted with the block-180. Inset: spectral region between 900 and 700 cm^{-1}.

A Beer's Law plot was obtained using transmission IR spectra of known amounts of block-180 dispersed in KBr pellets. The adsorption coefficient of the band at 700 cm^{-1} was calculated to be 0.2035 cm^2/mg from the data of a Beer's Law plot. Using this value, the amount of block-180 copolymer adsorbed on the membrane was 0.77 mg/cm^2. When mounted in the flow cell, the Fe^{3+} based solutions pass though a 7 mm diameter area of the membrane. In the case of the block-180, this translates to the Fe^{3+} solutions passing through 0.3 mg of block copolymer. The same approach was used to determine the amount of block-47 and block-89 adsorbed and the values obtained were 0.38 and 0.37 mg/cm^2, respectively.

The percent reaction of DFB with the block copolymer was controlled by the total time while passing the DFB/EDC solution through the block/membrane. An IR spectrum of 100 % DFB/block-180/membrane is shown in Figure 4.6c. The ratio of carboxylic band at 1720 cm^{-1} to the band at 700 cm^{-1} is reduced to a weak shoulder, indicating that the reaction between DFB and COOH of block-180 is almost complete. The slight shoulder at 1720 cm^{-1} due to unreacted COOH groups is less than 1 % of its original 1720 cm^{-1}/700 cm^{-1} value. Longer reaction times did not eliminate this band and I attribute this to a small fraction of COOH groups that are sterically hindered to react with DFB. The two bands that appear at 1635 cm^{-1} and 1554 cm^{-1} are the amide I (C=O stretching) and amide II (N-H bending) modes.

An IR spectrum for 50 % DFB/block-180/membrane is shown in Figure 4.6b, which was recorded after 30 minutes contact time with the DFB/EDC solution. In Figure 4.6b, the value for the 1720/700 cm^{-1} ratio was reduced to about half of the initial value,

indicating that half of the COOH groups of the adsorbed block copolymer reacted with DFB. We have repeated this procedure for all three block copolymers on the membrane at 50 % and 100 % DFB and the spectra are shown in Figure 4.7.

The 700 cm^{-1} band (Figure 4.6 and 4.7 for block-180 and block-89) decreases by 13 % and 12 % respectively after reaction with DFB. A small portion (0.09 mg, 0.012 mg, respectively) of block copolymers was removed from membranes as a result of reaction with the DFB. This could be due to a weakly bound fraction of block-180 that becomes more soluble with attachment of the DFB. The block-47 did not show any loss of polymer after reaction with DFB. In this case, derivatization of the relatively shorter PAA segments with DFB would not dislodge the underlying PS units and lead to removal of the block.

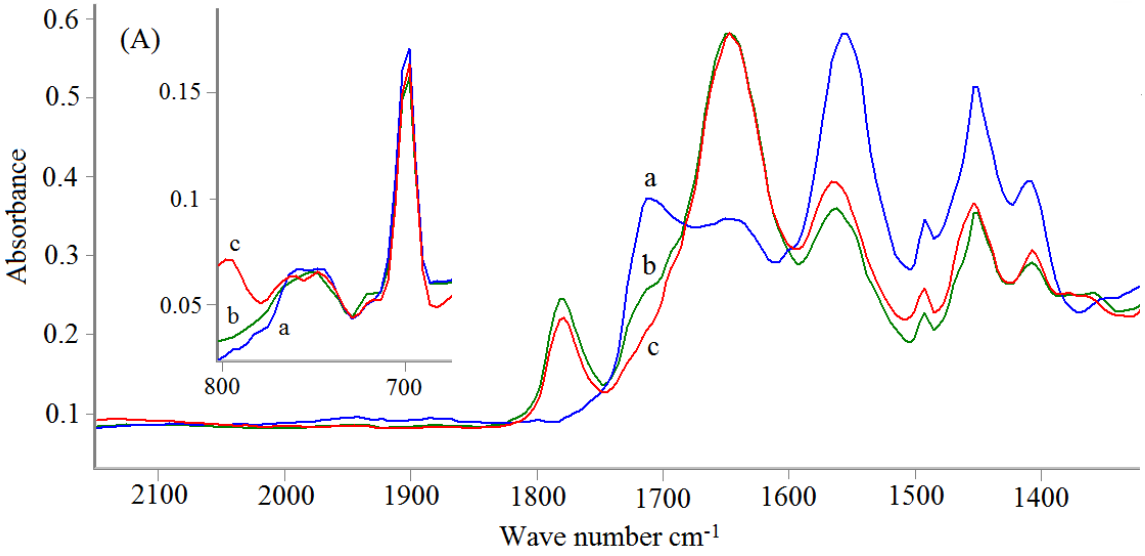

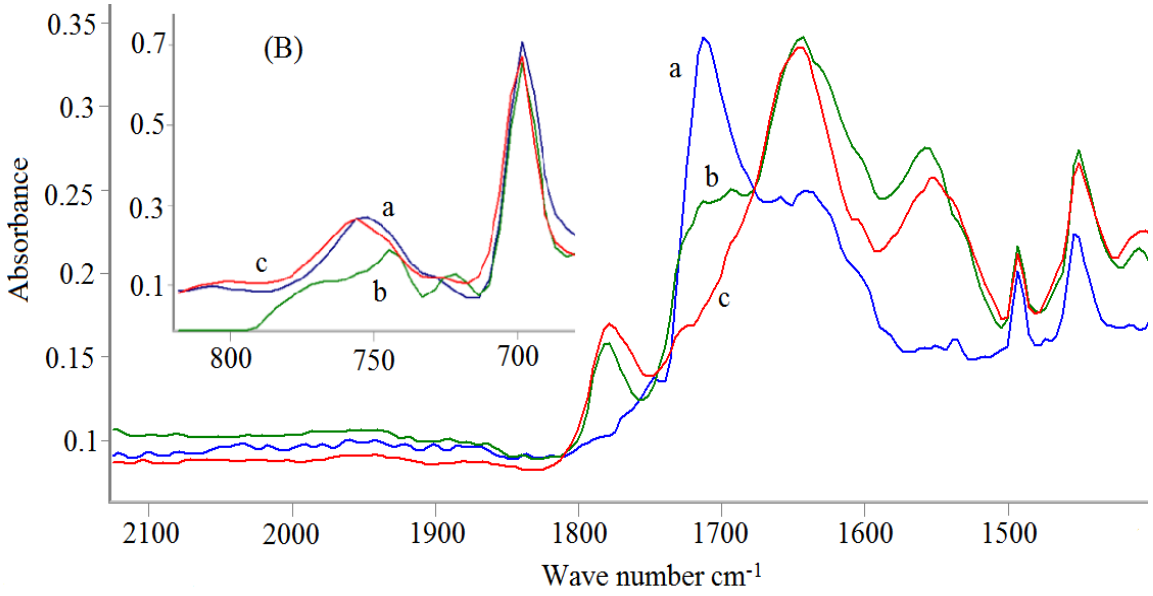

Figure 4.7 IR spectra of (A) block-89 and (B) block-47 (a) adsorbed on the membranes, (b) DFB 50 % and (c) DFB 100 % reacted with the block-89 and-47. Inset: spectral region between 900 and 700 cm^{-1}.

4.3.1.2 Fe^{3+} reaction with DFB treated membranes

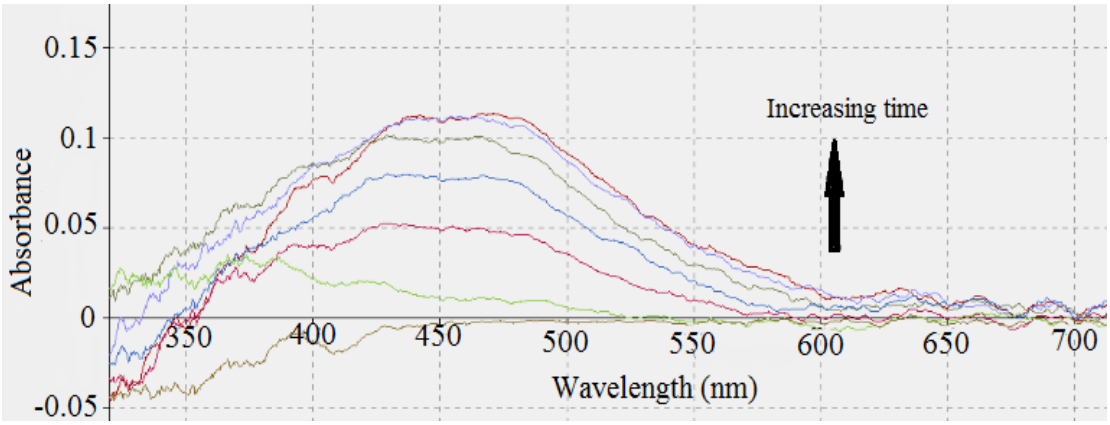

Figure 4.8 UV-Vis spectra recorded at 5 minute intervals while flowing a 10 ppm $FeCl_3$ solution through a 100 % DFB/block-180/membrane at 2 ml/min. The solution pH was 2.7

Figure 4.8 shows a representative set of spectra recorded while flowing a Fe^{3+} solution through 100 % DFB/block-180/membrane at 2 ml/min. The reaction of Fe^{3+} with the DFB anchored on the membrane leads to a broad band with a λ_{max} between 430 - 470 nm. The average absorbance for the values at 600 and 650 nm were used to establish the baseline value for the peak at 470 nm. The absorbance value for the band at 470 nm was determined by subtracting the average absorbance value recorded at 600 and 650 nm from the value at 470 nm. Figure 4.9 contains plots of the intensity of the band at 470 nm as a function of time for all three blocks at both 50 % and 100 % DFB loadings. Each point is the average value for three consecutive runs of passing 10 ppm Fe^{3+} solution followed by removal of the Fe^{3+} by passing the oxalate solution.

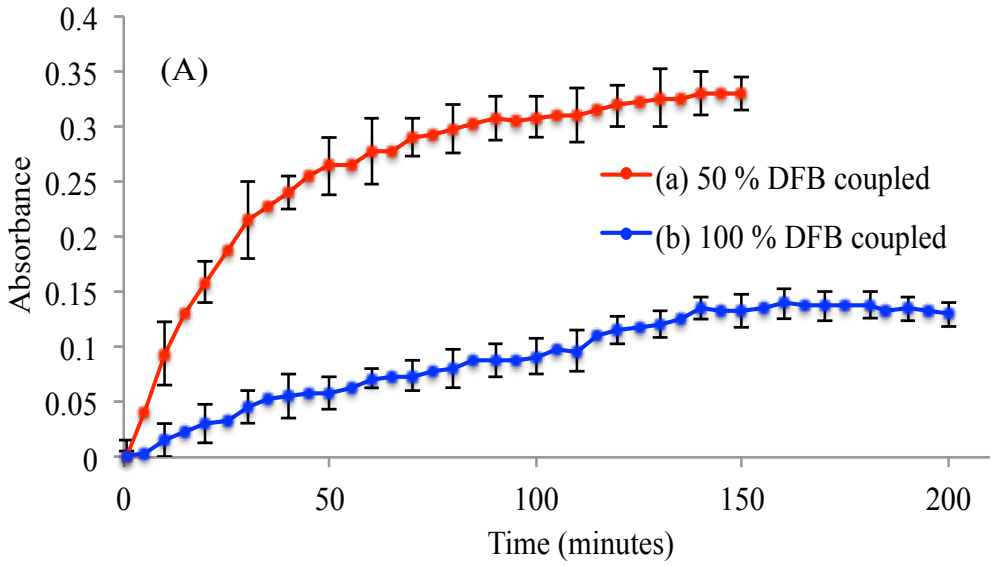

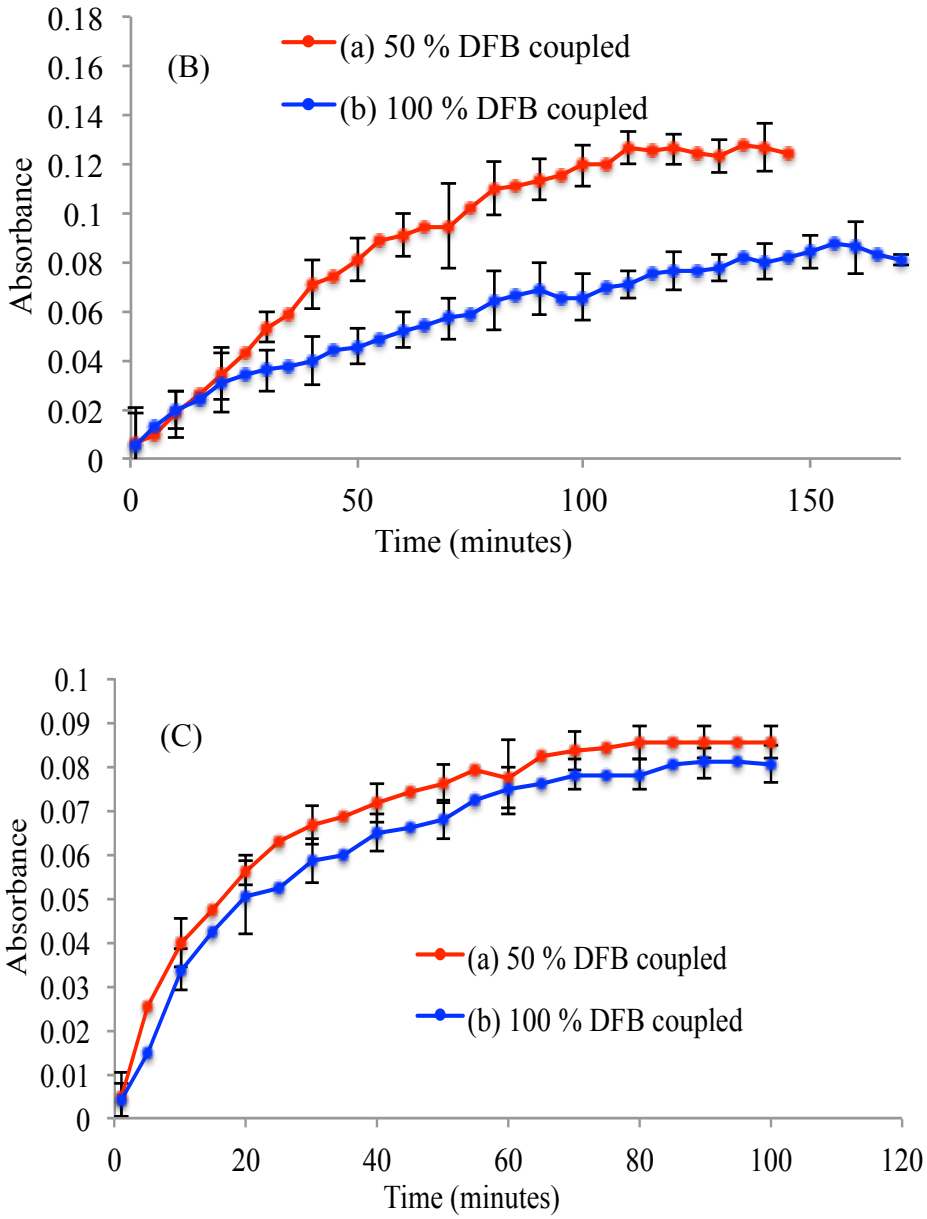

Figure 4.9 Absorbance *vs.* time for the peak at 470 nm while flowing a 10 ppm $FeCl_3$ solution at pH 2.7 at 50 and 100 % DFB coverage with (A) block-180/membrane, (B) block-89/membrane, and (C) block-47/membrane. The flow rate was 2 ml/min. The error bars are the 95 % confidence values based upon three replicates.

All curves in Figure 4.9 show an initial rapid rise that plateau. This is expected given that the amount of Fe^{3+} is in excess and eventually all available sites become occupied. In all three figures, the final amount of Fe^{3+} adsorbed is a higher value for the 50 % DFB sample than the corresponding 100 % DFB sample. In particular, the final value obtained for the ratio of the amount of Fe^{3+} on the 50 %/100 % samples are 2.2, 1.5 and 1.1 for block-180, block-89 and block-47, respectively. This shows that increasing the density of DFB is not desirable and in fact, can result in a decrease in the number of DFB that are active to bind Fe^{3+}. For example, a membrane with 100 % DFB (See Figure 4.9A (b)) captures 47 % percent less Fe^{3+} even though there is twice the number of anchored DFB. This is because more DFB are sterically hindered from binding to Fe^{3+} at the higher DFB loading. When DFB wraps around the Fe^{3+} ion it undergoes a significant conformational change, which requires a three-dimensional space that is constrained by the presence of neighboring DFB molecules. In addition, the close proximity of DFB due to the packing density means that the Fe^{+3} could possibly bind between multiple adjacent DFB molecules and leading to the formation of DFB-Fe matrices with limit permeability. At the lower DFB coverage, a higher fraction of the DFB molecules are less restricted by neighboring DFB molecules to undergo the necessary conformational change to bind Fe^{3+}.

This steric argument also explains the difference in the ratio of adsorbed Fe^{3+} on 50 %/100 % DFB membranes for the three relative block sizes. In essence, the density of the DFB is not only dependent on the percent reaction with the COOH groups on PAA but also the initial packing density of the PAA itself. As I have stated earlier, the initial

packing density of the PAA depends on the adsorbed amount and the relative block size. The block 180 would have a brush configuration in which a high PAA density results in extension of the PAA units away from the surface (see Figure 4.10). In contrast, the block-47 would have less steric interactions with adjacent block copolymers because it exists as a less dense coiled blob on the surface. Hence, the effect of DFB loading is much larger on the more densely packed PAA units of block-180 compared to block-47.

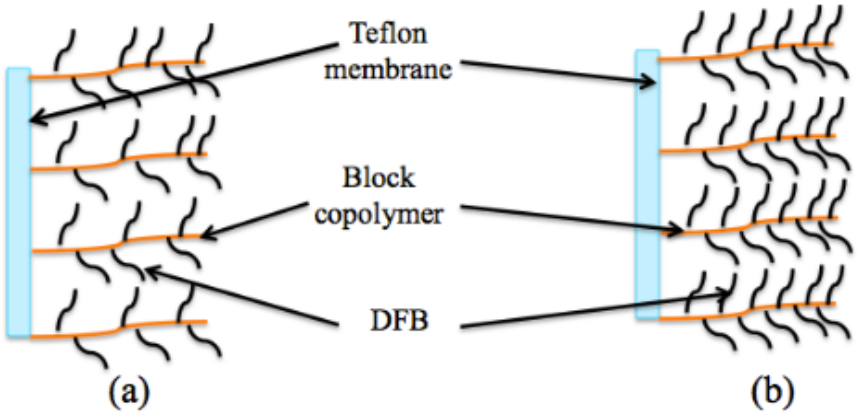

Figure 4.10 Schematic representation (a) 50 % and (b) 100 % DFB on block copolymer/membranes.

The curves in Figure 4.9 show that the total amount of Fe^{3+} bound does not scale with the absolute amount of DFB attached to the membrane. This is because the number of active DFB molecules increases as the surface density of DFB decreases. The increase in number of active DFB molecules will impact the % Fe uptake and may also increase the reaction rate.

Table 4.1 % of Fe^{+3} chelated with three block types for 50 % and 100 % DFB coupled membranes

Block copolymer	*No: of moles of PAA (moles)*	*Amount of Fe^{+3} captured (DFB 50%) (moles)* *(UV data)*	*Amount of Fe^{+3} captured (DFB 100%) (moles)* *(UV data)*	*% of DFB reacted with Fe^{+3} (DFB 50 %)*	*% of DFB reacted with Fe^{+3} (DFB 100 %)*
Block - 180	2.4×10^{-6}	5.7×10^{-8}	2.3×10^{-8}	4.7	1
Block - 89	9.3×10^{-7}	2.4×10^{-8}	1.5×10^{-8}	5.25	1.7
Block - 47	7.0×10^{-7}	2.2×10^{-8}	1.3×10^{-8}	5.26	1.8

From the mass of block copolymer deposited, the number of PAA monomers was calculated. I assumed that the amount of DFB bound is based on 1:1 DFB per –COOH binding site on the block copolymer for 100 % DFB coupled membranes and 0.5:1 DFB per –COOH binding site for 50% DFB coupled membranes. From Table 4.1, block 47/ 50 % DFB membrane has the highest % of DFB reacted with Fe^{+3}. Block 180/ 100 % DFB membrane has the lowest amount of DFB. According to steric arguments, the efficacy of Fe^{+3} loading with block copolymer increased with the size of buoy block of block copolymer decrease. The active number of DFB is very low in all these six cases. I assumed all the COOH react with DFB to form an amide linkage on the membrane surface. However, amide formation is not the only reaction that could occur in this membrane surface with EDC as a catalyst. Anhydride formation is a known side reaction

that could occur when two COOH react with each other and EDC used as a catalyst. I observe a band near 1800 cm^{-1} (Figure 4.6, 4.7A and B) because of the formation of anhydride and anhydride band suggest that not all COOH react with DFB. Thus, the number of DFB measured by IR are overestimated. In addition to anhydride formation, the low amount of active DFB could occur because of the close proximity of DFB packed on the membrane since Fe^{+3} could bind between multiple DFB molecules.

In Figure 4.11, I plot the % Fe^{3+} uptake as a function of time at a flow rate of 2 ml/min. The % Fe^{3+} uptake is defined as the amount of Fe^{3+} bound ratioed to the amount of Fe^{3+} passed through the membrane as a function of time. All curves show a higher % Fe^{3+} uptake at the beginning that slowly decreases as the percentage of free DFB decreases. As expected from the curves shown in Figure 4.11C, there is little difference in the % Fe^{3+} uptake on block-47 with DFB coverage. However, on the block-180 (Figure 4.11A) the % Fe^{3+} uptake for DFB 50 % membrane is 7 times higher than the % Fe^{3+} uptake for DFB 100 % membrane.

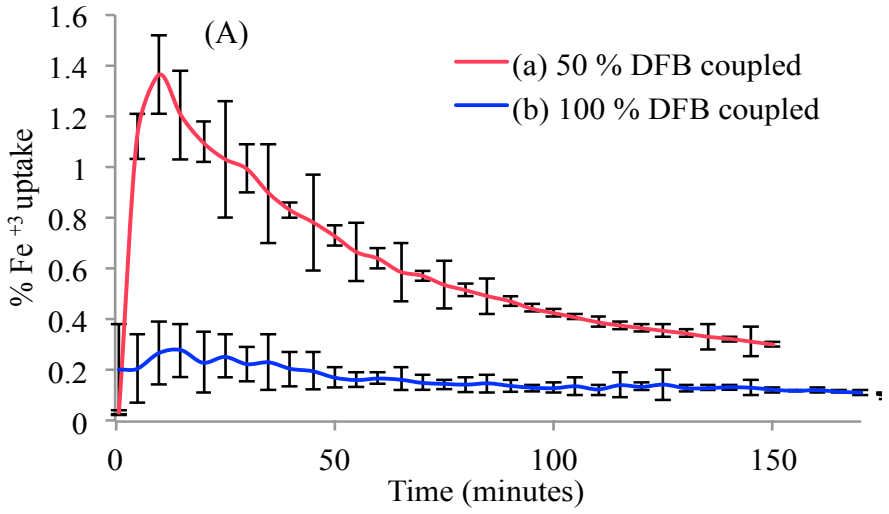

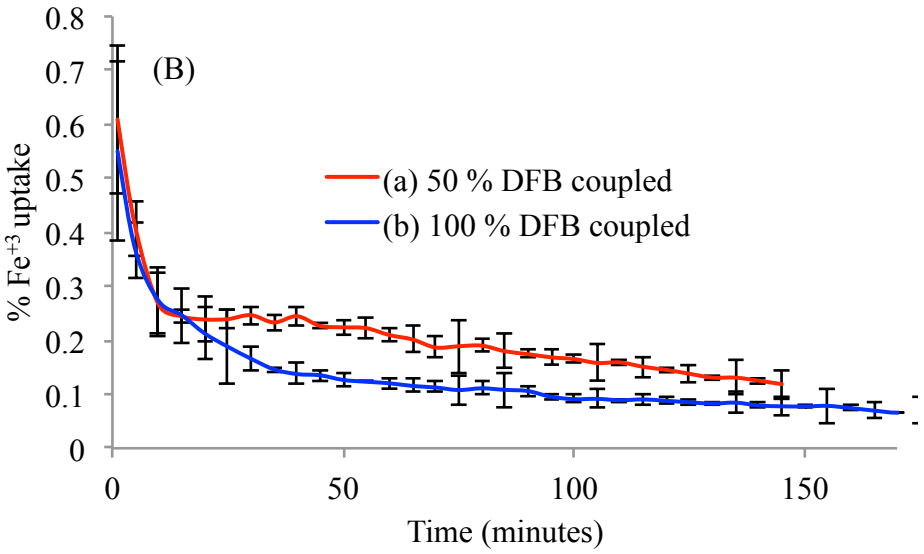

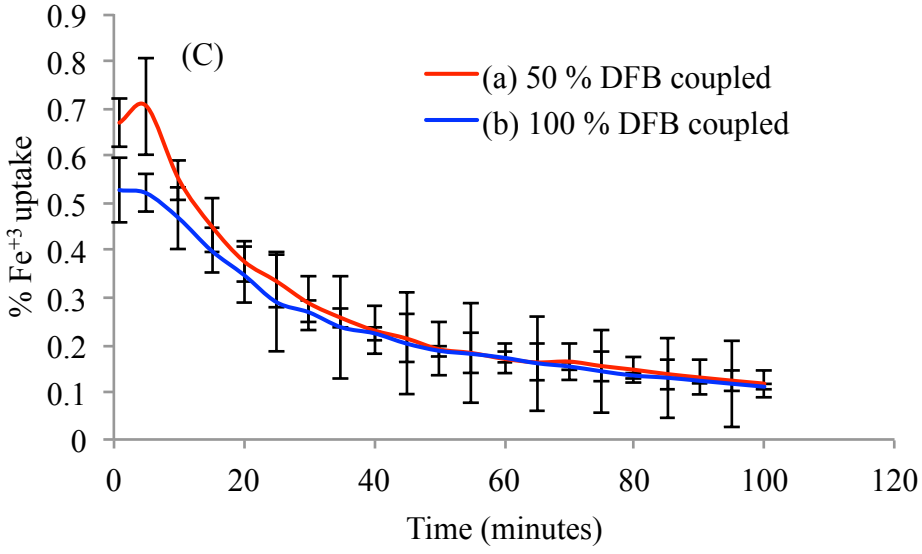

Figure 4.11 The % Fe^{3+} uptake as a function of time for the data shown in Figure 4.9.

While the uptake of Fe^{3+} is 7 times higher, it does not necessarily mean the DFB-normalized dynamics of Fe^{3+} capture is seven times higher. It is clear that reducing to 50

% DFB loading increases the number of DFB molecules that are active in terms of their ability to capture Fe^{3+}. Overall, there is 2.2 times more Fe^{3+} captured on the 50 % DFB loaded membrane than the 100 % DFB loaded membrane. Thus, an increase, by a factor of seven in uptake of Fe^{3+} in the same time span on the 50 % DFB loaded membrane, could be attributed, or at least partially attributed, to a higher number of active DFB.

The % Fe uptake on the block-89 based membranes (Figure 4.11B) show two regions; one similar to the trends observed for block-180 and a second region where the trends are similar to block-47. During the first 20 minutes, the uptake of Fe^{3+} with DFB is the same for 50 % and 100 % DFB loading levels. This shows that the first DFB to bind Fe^{3+} in both loading levels are in similar unrestricted local environments. This is similar to that found for block-47 at the two DFB loadings. After the 20 minute point, the Fe^{3+} uptake with the 50 % DFB is higher than the 100 % DFB coupled block-89 membranes. It is concluded that the remaining active DFB in the 100 % DFB membrane is more sterically hindered to chelate Fe^{3+} than the DFB on the 50 % DFB membranes. This second region follows the same trend observed for the block-180. Overall, the trends in the uptake of Fe^{3+} on the three blocks are consistent with the picture of the density of the PAA groups depicted in Figure 4.5. Nevertheless, in absolute terms, the highest % Fe^{3+} capture rate is only 3.5 % at 2 ml/min which is too low a capture rate for use in a detection system.

4.3.1.3 Flow rate dependency of Fe^{3+} uptake

The question remains as to whether these steric effects alter the kinetics of adsorption and thus, the flow rate dependence in percent Fe^{3+} coverage. In other words, does a lower DFB density also lead to a higher rate of capture of the Fe^{3+}. In the next set of experiments, the effect of flow rate on the uptake of Fe^{3+} by DFB was measured by passing 10 ppm aqueous solutions of $FeCl_3$ at pH 2.7 through 50 % and 100 % DFB loaded on block-180 based membranes at flow rates of 2, 1, and 0.1 ml/min. Of the three block copolymers, block-180 showed the highest % uptake at 2 ml/min and hence, was the best candidate material for further investigation with flow rates. The change of intensity in the band at 470 nm with time for the three different flow rates is shown in Figure 4.12.

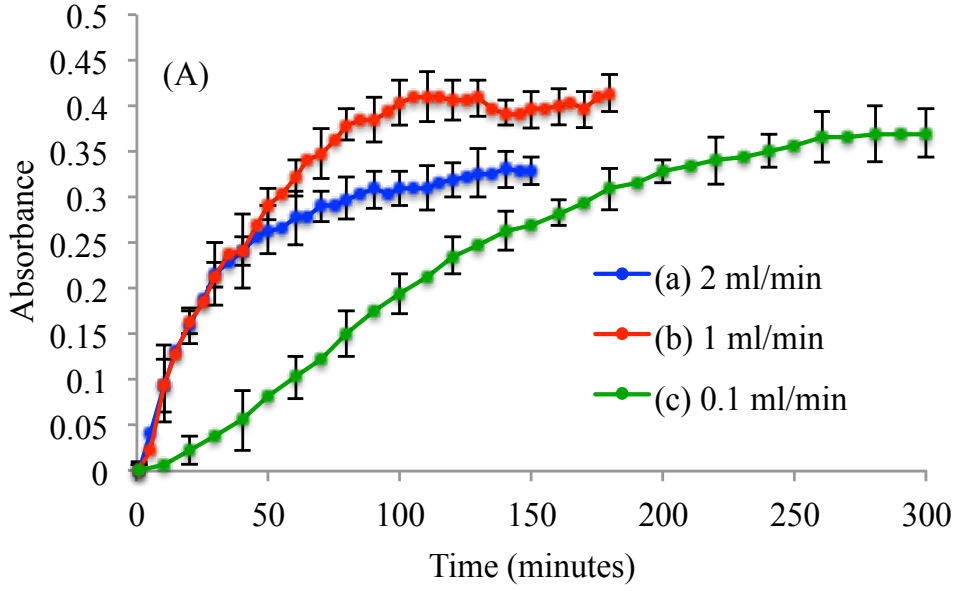

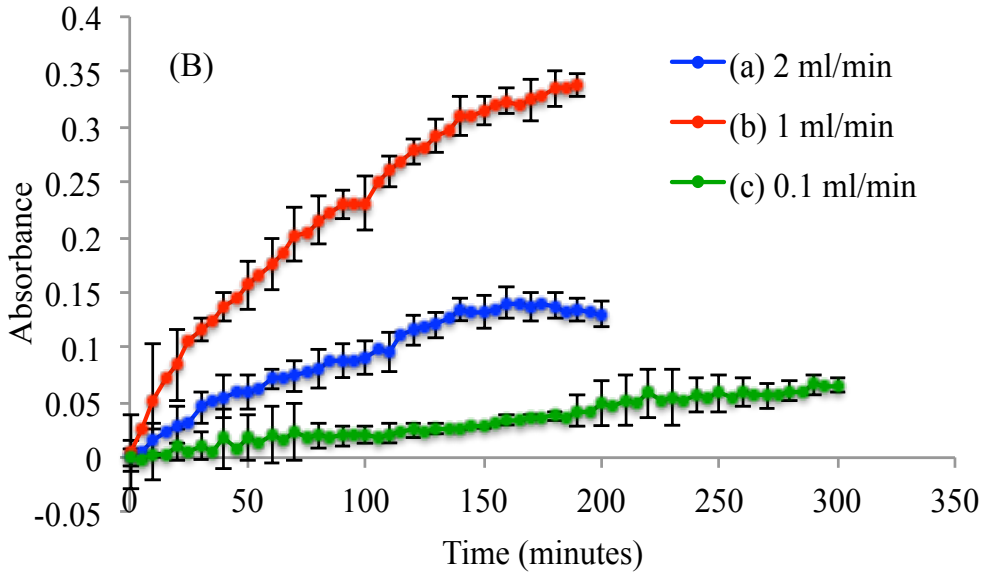

Figure 4.12 DFB (A) 50 % and (B) 100 % coupled block-180/membrane exposed to 10 ppm $FeCl_3$ solution at pH 2.7 at flow rates of (a) 2 ml/min, (b) 1 ml/min, and (c) 0.1 ml/min.

Figure 4.12 uses time for the abscissa scale and as a result, the plots do not convey the capture rate simply because the total number of moles of Fe^{3+} passed through the membrane depends on flow rate. For example, at 0.1 ml/min rate, the amount of Fe^{3+} transported through the membrane in a given period of time is 20 times less compared to 2 ml/min flow rate. A more informative plot is the % Fe^{3+} uptake verses the number of moles of Fe^{3+} passed through the membrane. This is shown in Figure 4.13.

Now if the rate of Fe^{3+} uptake was 100 % at all flow rates, the highest flow rate is unarguably the best from a mass transport limited perspective. The curves in Figure 4.13 show that this is not the case and that there is flow rate dependence in Fe^{3+} uptake. The highest amount of Fe^{3+} is recovered by the 50 % DFB and 100 % DFB membranes at the

0.1 ml/min flow rate. Moreover, at 0.1 ml/min, the % Fe^{3+} capture on the 50 % DFB loaded in the initial stages has a value of 30 %, 30 times higher than the approximate 1 % capture measured in the corresponding initial stages on the 100 % DFB loaded membrane. Comparing flow rate dependence on each membrane, I find that the initial % Fe^{3+} uptake on the 50 % DFB membrane to be 30 times higher at 0.1 ml/min compared to 2 ml/min flow rates. On the 100 % DFB membrane, the same comparison is 5 times higher at 0.1 ml/min. Hence, the steric hindrance is more pronounced in the 100 % DFB loaded membrane, which contributes to increasing the time for the DFB to chelate an Fe^{3+} ion.

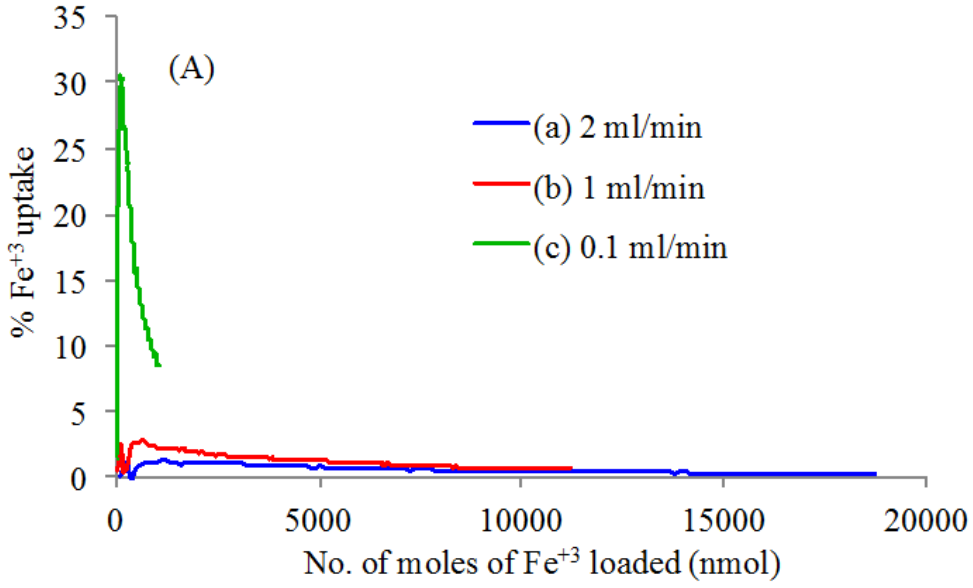

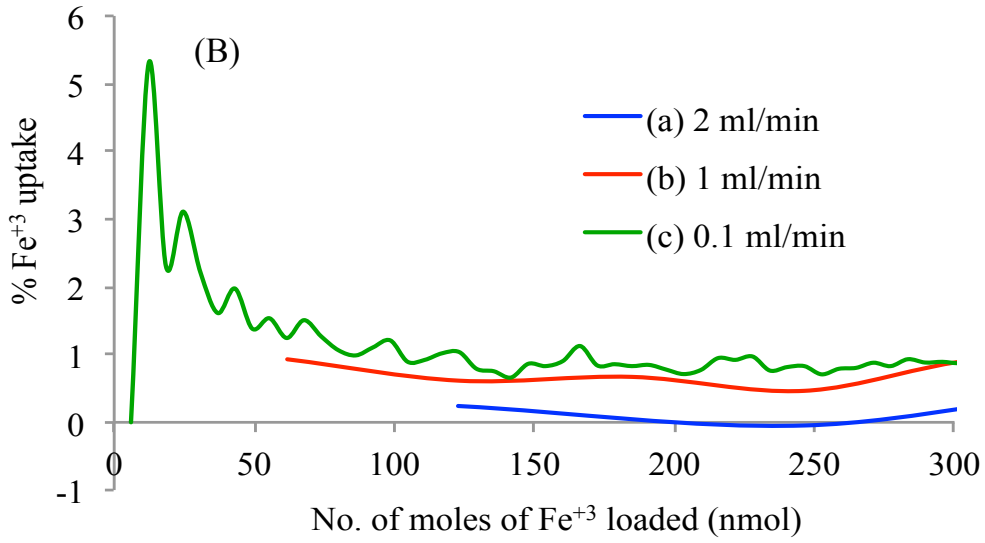

Figure 4.13 % Fe^{3+} uptake *vs.* number of nmols of Fe^{3+} for (A) 50 % DFB and (B) 100 % DFB-block-180 membranes at flow rates of (a) 2 ml/min, (b) 1 ml/min, and (c) 0.1 ml/min.

The kinetics for the chelation of Fe^{3+} with DFB is second order in both the concentration of DFB and Fe^{3+}.[160] Thus, as the number of active DFB is reduced due to chelation with Fe^{3+}, there is less active DFB remaining and hence the % Fe^{3+} uptake decreases. It is noted that at the parts per trillion level of Fe^{3+}, the DFB on the surface would be in large excess. Furthermore, the pre-concentration step would decrease the volume from the starting liter to approximately 1-5 ml, which will provide a practical scenario for operating at flow rates of 0.1 ml/min.

4.3.2 Section II: Modification of Transparent Beads (DFB coupled block copolymer/Teflon® beads)

As shown in Section I of this chapter, the low parts per trillion concentrations of Fe^{3+} will require liter quantities of sample in order to collect 30-100 ng of Fe^{3+} on the membrane which is not practical when flow rates of 0.1 ml/min are required. A pre-concentration step will be required in which the Fe^{3+} is passed through a toyopearl resin derivatized with DFB to capture Fe^{3+} and elute this into a volume of 1 ml for passage through the membrane.[160] The elution into a smaller volume could potentially be avoided by substitution of the toyopearl beads with a material that is transparent in the visible region of the spectrum. UV spectral analysis would then be performed directly on the beads.

The beads would require a similar refractive index to water to be transparent and are also required to be a minimum of 30-40 μm in diameter to enable flow rates in the 10 ml/min range. High DFB coverage on these relatively large beads would be achieved by self-assembly of block-180 on the beads. Here, I provide some preliminary data on preparing beads with block copolymers. The first candidates were Teflon® and polyacrylimide hydrogels, as these have refractive indices near that of water.

4.3.2.1 Preparation of DFB coupled block copolymer/Teflon® beads

A sample containing 0.27 g of block-180 with Teflon® beads were mixed in a beaker with DI water. The beads initially aggregated on the surface of the water (Figure 4.14a). As the content in the beaker was vigorously stirred for about 2-3 days, the beads began to sink to the bottom of the beaker. This provided an indication of the adsorption

of the block-180 on the Teflon® beads. Essentially, the hydrophobic PS segment of the block copolymer adsorbs on to the Teflon® beads while the hydrophilic PAA segment of the block copolymer extends from the surface. As the particles became hydrophilic due to adsorption of the block copolymer, they began to sink to the bottom of the beaker (see Figure 4.14b).

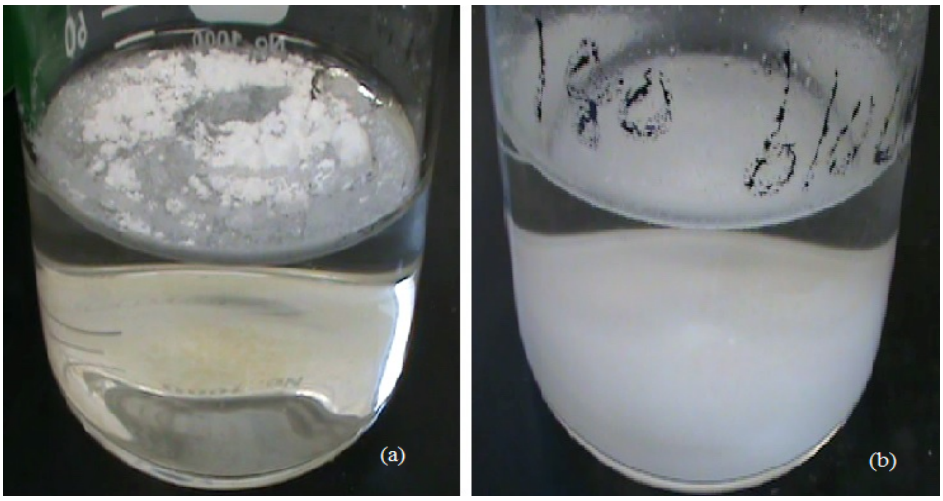

Figure 4.14 Teflon® beads mixed with block-180 copolymer in DI water (a) at the beginning of mixing and (b) after 4 days of vigorous stirring.

IR spectra were recorded to determine the level of coating of the block-180 on the Teflon® beads. The beads were captured on the transparent membrane and air dried. Figure 4.15a is an IR spectrum of a dry membrane. A strong band at 1713 cm^{-1} is due to the C=O stretching mode of the coating on the membrane. Figure 4.15b is the spectrum of the beads treated with the block-180. The inset of Figure 4.15b shows a band at 700 cm^{-1} due to a bending mode of CH groups in PS. This provides direct evidence of the adsorption of the block-180 on the beads.

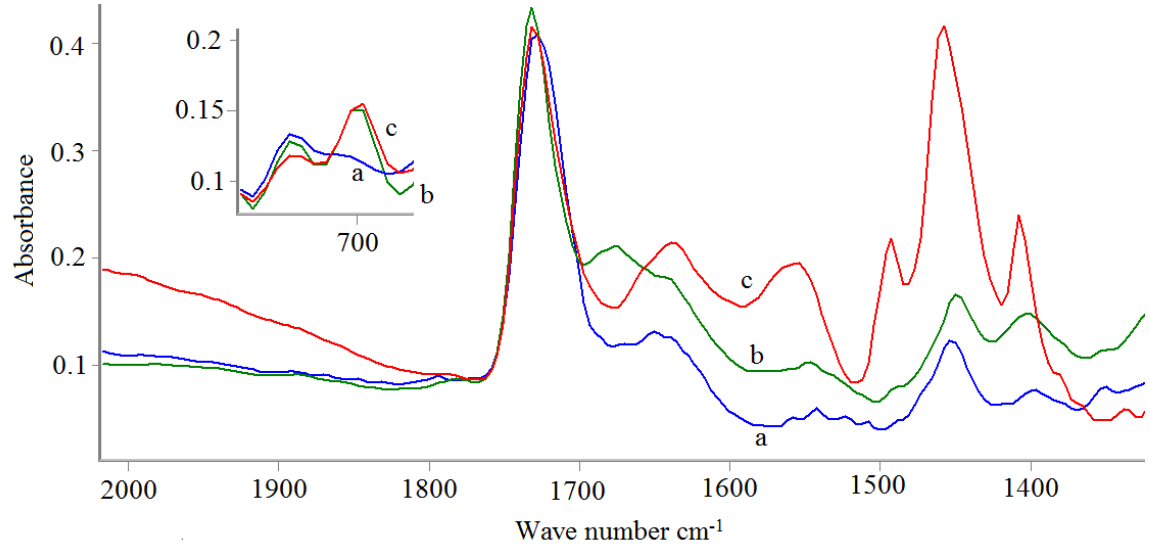

Figure 4.15 IR spectrum of (a) membrane, (b) block-180 copolymer bound to Teflon® beads, and (c) reacted with DFB. Inset: 600-700 cm^{-1} spectral region of (a) membrane (b) block-180/beads and (c) DFB coupled block-180/beads.

A portion of block copolymer/beads was reacted with DFB in the presence of EDC catalyst in water. The coupling reaction between the primary amine group of DFB and the COOH groups of the polyacrylate resulted in formation of an amide bond. An IR spectrum of the DFB reacted with block-180/Teflon® beads was recorded by capturing the beads on a membrane, as shown in Figure 4.15c. Two new bands appear at 1635 and 1554 cm^{-1} regions corresponding to the amide I and amide II stretching modes of the amide bond.

4.3.2.2 Pre-concentrating aqueous Fe^{3+} solutions by using DFB coupled block copolymer/Teflon® beads

The total dissolved Fe^{3+} concentration in seawater typically ranges from 50 pmol l^{-1} to 5 nmol l^{-1}.[1] Such small quantities present real challenges in detection for using the

membrane approach due to the large volumes that would need to be processed at low flow rates. Here, I tested the potential of using the DFB modified beads in a pre-concentration step. First, a column was prepared by packing wet DFB coupled block/beads in a glass pipette and then a solution containing 100 ppm $FeCl_3$ (about 100 ml) was passed through the column. The elutant was clear and a reddish-brown ring appeared on the top portion of the column. This showed that the beads did concentrate the Fe^{3+} from the solution. In order to elute the Fe^{3+} in to a smaller volume of aqueous solution, an oxalate solution (10 ml) of 0.1 M concentration at pH 1.5 (adjusted with Conc. HCl) passed through the column. The reddish-brown ring in the column disappeared. At pH 1.5, oxalate is a better chelating agent for Fe^{3+} then DFB, therefore, removed Fe^{3+} from the DFB coupled block/Teflon® beads.

While the above showed some key elements of the approach, the Teflon® beads were not transparent in the UV-vis spectral region, due to excessive scattering, which prevented a direct measurement on the DFB coupled block/beads. As a next step, Teflon® beads were replaced by a polyacrylamide hydrogel.

4.3.2.3 Preparation of DFB coupled block copolymer/hydrogels

Polyacrylamide hydrogels in the dry form are solid particles and are highly scattering. However, upon adding DI water, hydrophilic polymer networks become a swollen gel in water and more importantly become transparent as shown in Figure 4.16a. Hydrogels can typically absorb 10 to 1000 times of water compared to their dry volume.

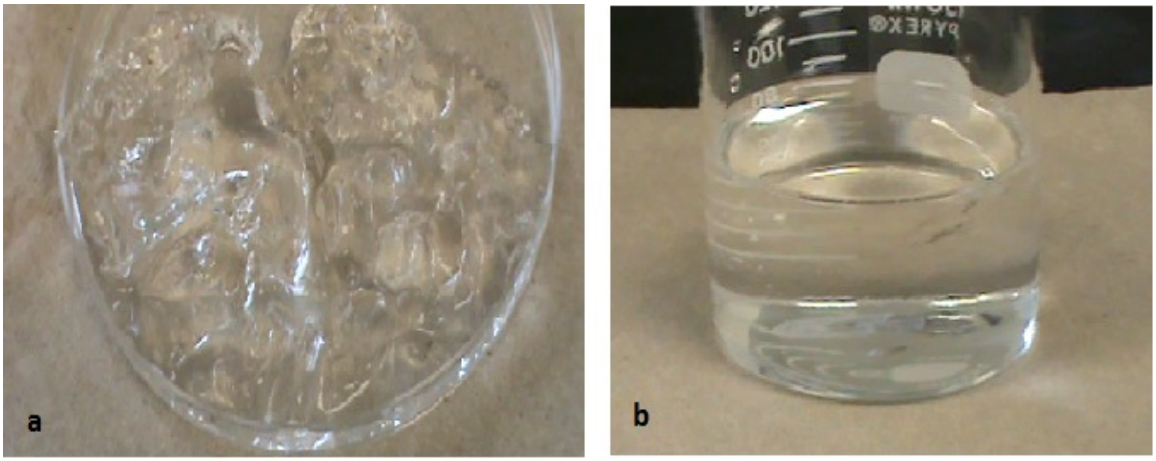

Figure 4.16 Polyacrylamide hydrogel (a) after soaking with water for 12h, (b) coupled with block-180 copolymer in water after 4 days of vigorous stirring.

An IR spectrum of dry polyacrylamide hydrogel film on a ZnSe window is shown in Figure 4.17a. The bands at 1560 and 1450 cm^{-1} are due to carboxylate stretching of acrylate. The appearance of the hydrogel after deposition of block copolymers is transparent (see Figure 4.16b) and the evidence of the binding of block copolymers to the hydrogel is presented in Figure 4.17b. When the block copolymers adsorbs on the hydrogel, bands at 1713 and 1547 cm^{-1} due to carbonyl asymmetric stretching of carboxylic acid and carboxylate of the PAA segments, respectively are observed. While the hydrogel also has bands in these regions, the intensity of the 1713 and 1547 cm^{-1} in Figure 4.17b are much greater than the ratio of these bands to other hydrogel bands in Figure 4.17. Furthermore, the new two bands appearing at 2950 and 700 cm^{-1} are due to a CH stretching and bending mode of the polystyrene segment of the block copolymer. These bands do not disappear upon multiple washings of the block copolymer/hydrogel with DI water, indicating a stable amount of block-180 on the hydrogel.

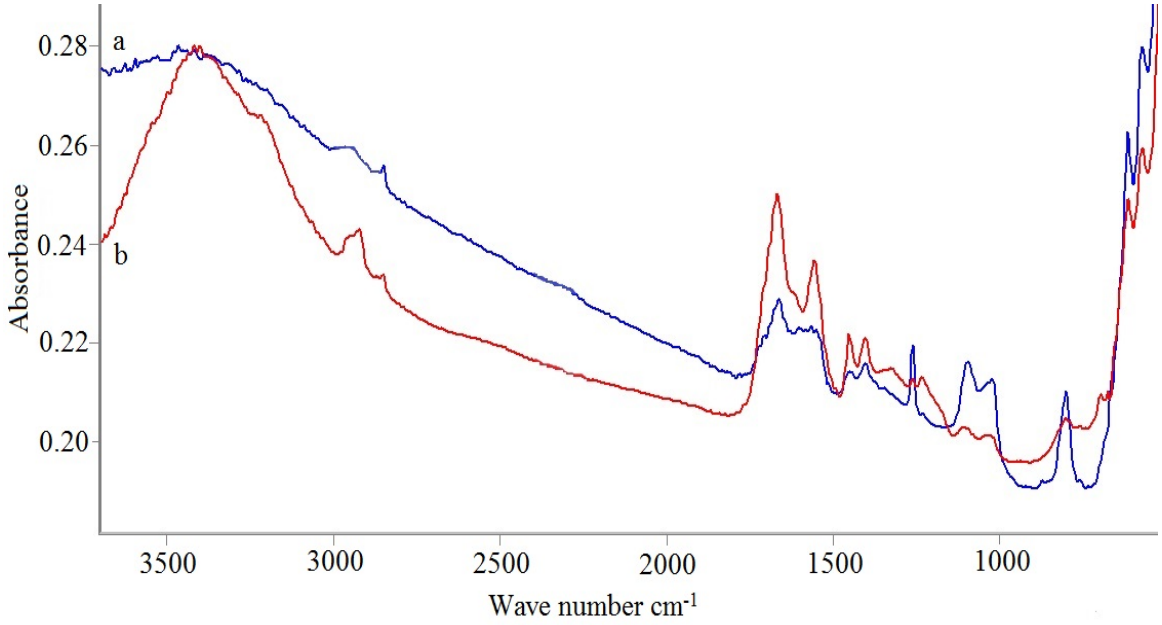

Figure 4.17 Polyacrylamide hydrogel (a) before and (b) after coupling with block-180.

Next, the block bound hydrogel was mixed with DFB and EDC catalyst to couple DFB with acrylate segments of the block copolymer. A white precipitate formed (see Figure 4.18). The white solid was opaque which prevented further development for use in detecting Fe^{3+} in seawater.

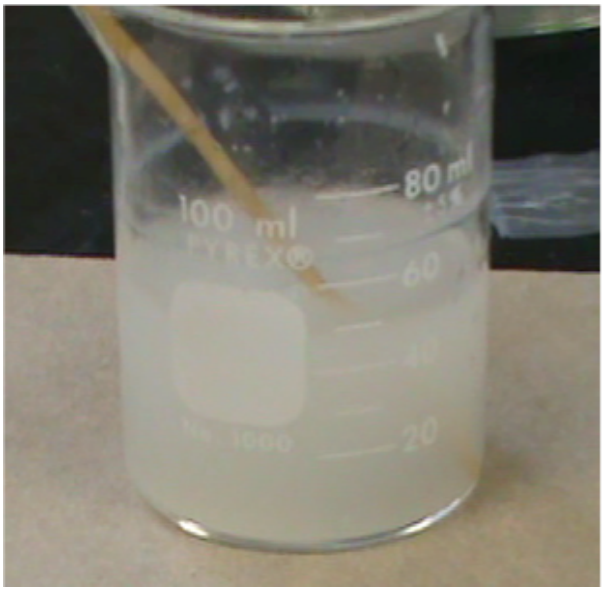

Figure 4.18 White precipitate of DFB coupled block/hydrogel in DI water.

In order to determine whether the precipitation was dictated by the choice of block copolymer, I repeated the reaction with two other block copolymers, block-47 and block-89. In both cases, a precipitate formed during reaction with DFB. Next, the order of the reaction was changed. The DFB and block copolymers were first reacted forming an amide linkage using EDC catalyst. This modified block copolymer was added to the hydrogel suspension. A white precipitate formed. Then EDC and DFB were mixed independently with the hydrogel. Mixing the hydrogels with the DFB or EDC alone did not lead to a precipitate. It was concluded that the precipitate forms because of flocculation when the DFB coupled to the block copolymer adsorbing on the hydrogel. The IR spectrum of the precipitate is shown in Figure 4.19. While two bands at 1650 and 1550 cm^{-1} are due to the amide modes and could arise from the reaction between

carboxylic acid group of polyacrylate and amine group of DFB, there are numerous other bands that clearly show the reaction is more complex.

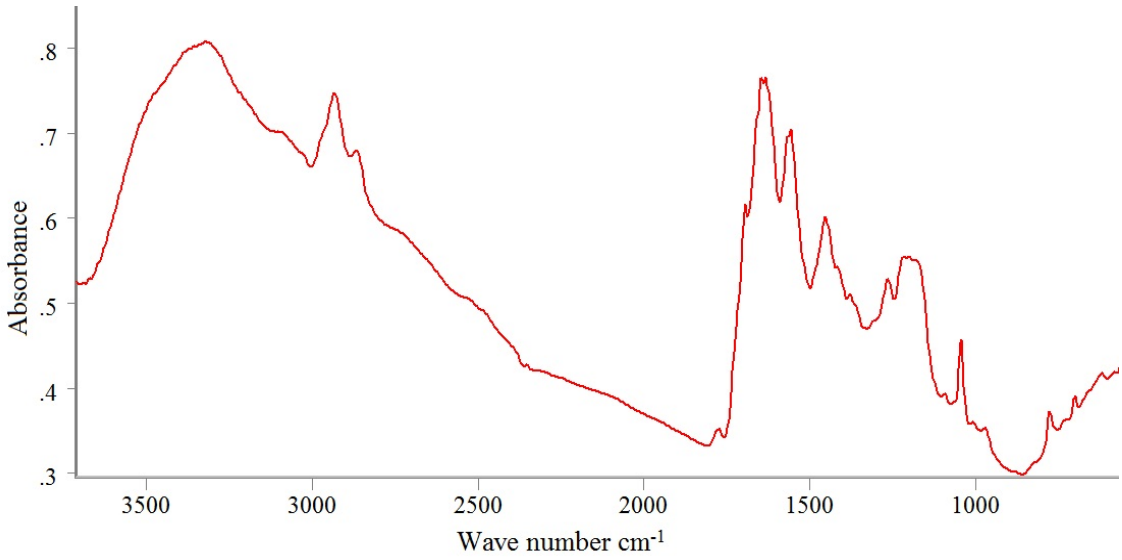

Figure 4.19 IR spectrum of DFB coupled block-180 copolymer/hydrogel.

Next, a third candidate material for this approach was examined. In this case, agarose particles were treated with block-copolymers and then reacted with DFB. It was shown that these particles were partially transparent in the visible region of the spectrum and that Fe^{3+} could be adsorbed on the particles and subsequently eluted using an oxalate wash at pH 2. This work is currently under investigation and forms the basis of the undergraduate thesis work of Kaiya Hansen.

4.4 Conclusion

The concept of vertical amplification though the use of PS-PAA block copolymers to increase the density of DFB on the surface of membranes was studied as a function of the relative size of the blocks and the degree of reaction of the blocks with DFB. It was shown that the amount of Fe^{3+} uptake depended on both the relative size of the PS-PAA block copolymer and the degree of reaction of the COOH groups on the adsorbed block copolymer with DFB. Block copolymers with a larger PAA block have a higher packing density of the PAA on the surface than obtained for block copolymers with a smaller PAA block. The result is a much larger difference in the effect of DFB loading on the amount and rate of % Fe^{3+} uptake on the denser block copolymer layer compared to the smaller buoy blocks.

Higher amounts of Fe^{3+} adsorbed are obtained at 50 % DFB loadings compared to 100 % loadings on the same block. This is because the numbers of DFB that can bind with the Fe^{3+} are dependent on the spatial packing of the DFB on the surface. The spatial packing of the DFB also has an effect on the rate of capture of the Fe^{3+}. For example, a 50 % DFB membrane provided 30 times higher % Fe^{3+} capture rate at 0.1 ml/min compared to the 100 % DFB membrane which reflects a greater number of free and active DFB on the surface at the lower DFB coverage. Since the DFB/Fe^{3+} chelation requires movement of the DFB around the Fe^{3+}, the kinetics are highly dependent on the packing density.

CHAPTER 5: RECOMMENDATIONS FOR FUTURE WORK

5.1 LbL

I demonstrated for the first time an ATR-IR spectroscopic method that simultaneously measures the dynamics of the mass adsorbed and polyelectrolyte conformation during the formation of PEM's. In particular, I followed the sequential adsorption of NaPA and PDADMAC from DI water and as a function of ionic strength. It is recommended to use this method to elucidate the molecular processes occurring in LbL deposition under other experimental conditions. For the current system of alternating layers of NaPA and PDADMAC, these include studying the dynamics as a function of molecular weight of the polyelectrolytes[166], concentration of the polyelectrolyte solution[112], solvent quality[112], temperature[167] and pH.[56,57] Extending these studies to these areas will lead to a clearer picture of the mechanism leading to linear and exponential film growth.

Expanding the method to study alternative polyelectrolyte systems would also be an area to explore. The first systems would maintain the use of NaPA because of the ability to determine the bound fraction from changes in the C=O stretching mode of the COOH group. The current system uses PDADMAC, which is a strong electrolyte. Substituting the PDADMAC for a weak cationic polyelectrolyte such as poly (allylamine) hydrochloride would be of interest. PAM's formed with alternating layers of weak polyelectrolytes often show huge changes in the adsorbed amount per layer over narrow pH ranges. My ATR method may provide some insight to the molecular processes leading to this pH dependence in layer growth in weak/weak electrolyte systems.

One of the principle features of IR spectroscopy is its ability to identify and monitor chemical reactions between molecules. I have shown in this thesis that electrostatic interactions with the COO^- groups on NaPA can be monitored indirectly through changes in the IR bands due to COOH groups. It is thus recommended to use my approach to measure dynamical processes between other modes of adsorption such as LbL films formed through hydrogen bonding between layers and those that involve other types of bond formation.

5.2 Fe^{3+} detection

In Chapter 4, I showed that the packing density of DFB on the PS-PAA block copolymers controlled the amount and rate of Fe^{3+} uptake on the membrane. I had worked at 50 % and 100 % loading levels only so; a natural extension to this work would be to determine the optimal loading level leading the highest amount and uptake rate of Fe^{3+}.

These include:

1. Varying the amount of DFB coupled on the block/membranes and measure the amount and rate of % Fe^{3+} uptake at various flow rates.

2. Investigation of a molecular imprinting approach. In essence, the Fe^{3+} would be reacted with the DFB first and then, the Fe-DFB would be reacted with the block copolymer/membrane. In this case, the DFB would already exist in a conformation conducive to binding Fe^{3+}. The maximum loading of DFB on the

block would be determined as well as the amount and % Fe^{3+} uptake as a function of flow rate.

As shown in section 4.3.1, the low parts per trillion concentrations of Fe^{3+} in the sea water would require a liter quantity of sample flow through the membrane in flow rate of 0.1 ml/min which is not practical. The pre-concentration step was proposed to overcome this problem. This pre-concentration step could potentially be avoided by substitution of transparent beads. In section 4.3.2, I described developing a detection method with DFB coupled teflon beads. Teflon beads have a refractive index of 1.35-1.38 and were not transparent in the visible region. Agarose particles or Nafion beads have a refractive index closer to the refractive index of water and, as a result these two particles are partially transparent in the visible region of the spectrum. Development of a transparent column based on Agarose or Nafion particulates coupled with DFB as a method for detection of iron in seawater is recommended.

REFERENCES

(1) Iler, R. K.: Multilayers of colloidal particles. *Journal of Colloid and Interface Science* **(1966)**, *21*, 569-&.

(2) Niesen, T. P.; De Guire, M. R.: Review: Deposition of ceramic thin films at low temperatures from aqueous solutions. *Journal of Electroceramics* **(2001)**, *6*, 169-207.

(3) Niesen, T. P.; De Guire, M. R.: Review: deposition of ceramic thin films at low temperatures from aqueous solutions. *Solid State Ionics* **(2002)**, *151*, 61-68.

(4) X. Zhang, J. C. S.: Self-Assembled ultrathin films: from layered nanoarchitectures to functional assemblies. *Advanced Materials* **(1999)**, *11*, 1139 - 1143.

(5) Decher, G.; Hong, J. D.; Schmitt, J.: Buildup of ultrathin multilayer films by a self-assembly process .3. Consecutively alternating adsorption of anionic and cationic polyelectrolytes on charged surfaces. *Thin Solid Films* **(1992)**, *210*, 831-835.

(6) Ladam, G.; Schaad, P.; Voegel, J. C.; Schaaf, P.; Decher, G.; Cuisinier, F.: In situ determination of the structural properties of initially deposited polyelectrolyte multilayers. *Langmuir* **(2000)**, *16*, 1249-1255.

(7) Decher, G.: Fuzzy nanoassemblies: Toward layered polymeric multicomposites. *Science* **(1997)**, *277*, 1232-1237.

(8) Decher, G.; Lvov, Y.; Schmitt, J.: Proof of multilayer structural organization in self-assembled polycation polyanion molecular films. *Thin Solid Films* **(1994)**, *244*, 772-777.

(9) Losche, M.; Schmitt, J.; Decher, G.; Bouwman, W. G.; Kjaer, K.: Detailed structure of molecularly thin polyelectrolyte multilayer films on solid substrates as revealed by neutron reflectometry. *Macromolecules* **(1998)**, *31*, 8893-8906.

(10) Hammond, P. T.: Form and function in multilayer assembly: New applications at the nanoscale. *Advanced Materials* **(2004)**, *16*, 1271-1293.

(11) Prevo, B. G.; Hwang, Y.; Velev, O. D.: Convective assembly of antireflective silica coatings with controlled thickness and refractive index. *Chemistry of Materials* **(2005)**, *17*, 3642-3651.

(12) Kommireddy, D. S.; Patel, A. A.; Shutava, T. G.; Mills, D. K.; Lvov, Y. M.: Layer-by-layer assembly of TiO2 nanoparticles for stable hydrophilic biocompatible coatings. *Journal of Nanoscience and Nanotechnology* **(2005)**, *5*, 1081-1087.

(13) McDonald, B. T.; Cui, T.: Superhydrophilic surface modification of copper surfaces by Layer-by-Layer self-assembly and Liquid Phase Deposition of TiO2 thin film. *Journal of Colloid and Interface Science* **(2011)**, *354*, 1-6.

(14) Liao, K.-S.; Wan, A.; Batteas, J. D.; Bergbreiter, D. E.: Superhydrophobic surfaces formed using layer-by-layer self-assembly with aminated multiwall carbon nanotubes. *Langmuir* **(2008)**, *24*, 4245-4253.

(15) Buck, M. E.; Schwartz, S. C.; Lynn, D. M.: Superhydrophobic Thin Films Fabricated by Reactive Layer-by-Layer Assembly of Azlactone-Functionalized Polymers. *Chemistry of Materials* **(2010)**, *22*, 6319-6327.

(16) Shutava, T. G.; Pattekari, P. P.; Arapov, K. A.; Torchilin, V. P.; Lvov, Y. M.: Architectural layer-by-layer assembly of drug nanocapsules with PEGylated polyelectrolytes. *Soft Matter* **(2012)**, *8*, 9418-9427.

(17) Ariga, K.; McShane, M.; Lvov, Y. M.; Ji, Q. M.; Hill, J. P.: Layer-by-layer assembly for drug delivery and related applications. *Expert Opinion on Drug Delivery* **(2011)**, *8*, 633-644.

(18) Chang-Yen, D. A.; Gale, B. K.: An integrated optical oxygen sensor fabricated using rapid-prototyping techniques. *Lab on a Chip* **(2003)**, *3*, 297-301.

(19) Kleinfeld, E. R.; Ferguson, G. S.: Stepwise formation of multilayered nanostructural films from macromolecular precursors. *Science* **(1994)**, *265*, 370-373.

(20) Gao, M. Y.; Gao, M. L.; Zhang, X.; Yang, Y.; Yang, B.; Shen, J. C.: Constructing PbI2 nanoparticles into a multilayer structure using the molecular deposition (md) method. *Journal of the Chemical Society-Chemical Communications* **(1994)**, 2777-2778.

(21) Rogach, A. L.; Koktysh, D. S.; Harrison, M.; Kotov, N. A.: Layer-by-layer assembled films of HgTe nanocrystals with strong infrared emission. *Chemistry of Materials* **(2000)**, *12*, 1526-+.

(22) Fu, Y.; Xu, H.; Bai, S. L.; Qiu, D. L.; Sun, J. Q.; Wang, Z. Q.; Zhang, X.: Fabrication of a stable polyelectrolyte/Au nanoparticles multilayer film. *Macromolecular Rapid Communications* **(2002)**, *23*, 256-259.

(23) Zhang, X.; Gao, M. L.; Kong, X. X.; Sun, Y. P.; Shen, J. C.: Buildup of a new-type of ultrathin-film of porphyrin and phthalocyanine based on cationic and anionic electrostatic attraction. *Journal of the Chemical Society-Chemical Communications* **(1994)**, 1055-1056.

(24) Sun, Y. P.; Zhang, X.; Sun, C. Q.; Wang, Z. Q.; Shen, J. C.; Wang, D. J.; Li, T. J.: Supramolecular assembly of alternating porphyrin and phthalocyanine layers based on electrostatic interactions. *Chemical Communications* **(1996)**, 2379-2380.

(25) Zhang, H. Y.; Fu, Y.; Wang, D.; Wang, L. Y.; Wang, Z. Q.; Zhang, X.: Hydrogen-bonding-directed layer-by-layer assembly of dendrimer and poly(4-vinylpyridine) and micropore formation by post-base treatment. *Langmuir* **(2003)**, *19*, 8497-8502.

(26) Huo, F. W.; Xu, H. P.; Zhang, L.; Fu, Y.; Wang, Z. Q.; Zhang, X.: Hydrogen-bonding based multilayer assemblies by self-deposition of dendrimer. *Chemical Communications* **(2003)**, 874-875.

(27) Wei, H.; Ma, N.; Shi, F.; Wang, Z. Q.; Zhang, X.: Artificial nacre by alternating preparation of layer-by-layer polymer films and CaCO3 strata. *Chemistry of Materials* **(2007)**, *19*, 1974-1978.

(28) Olek, M.; Ostrander, J.; Jurga, S.; Mohwald, H.; Kotov, N.; Kempa, K.; Giersig, M.: Layer-by-layer assembled composites from multiwall carbon nanotubes with different morphologies. *Nano Letters* **(2004)**, *4*, 1889-1895.

(29) Correa-Duarte, M. A.; Kosiorek, A.; Kandulski, W.; Giersig, M.; Liz-Marzan, L. M.: Layer-by-layer assembly of multiwall carbon nanotubes on spherical colloids. *Chemistry of Materials* **(2005)**, *17*, 3268-3272.

(30) Hong, J. D.; Lowack, K.; Schmitt, J.; Decher, G.: Layer-by-layer deposited multilayer assemblies of polyelectrolytes and proteins - from ultrathin films to protein arrays. In *Trends in Colloid and Interface Science Vii*; Laggner, P., Glatter, O., Eds., **(1993)**; Vol. 93; pp 98-102.

(31) Kong, W.; Zhang, X.; Gao, M. L.; Zhou, H.; Li, W.; Shen, J. C.: A new kind of immobilized enzyme multilayer based on cationic and anionic interaction. *Macromolecular Rapid Communications* **(1994)**, *15*, 405-409.

(32) Sun, J. Q.; Sun, Y. P.; Wang, Z. Q.; Sun, C. Q.; Wang, Y.; Zhang, X.; Shen, J. C.: Ionic self-assembly of glucose oxidase with polycation bearing Os complex. *Macromolecular Chemistry and Physics* **(2001)**, *202*, 111-116.

(33) Lvov, Y.; Decher, G.; Sukhorukov, G.: Assembly of thin-films by means of successive deposition of alternate layers of dna and poly(allylamine). *Macromolecules* **(1993)**, *26*, 5396-5399.

(34) Shchukin, D. G.; Patel, A. A.; Sukhorukov, G. B.; Lvov, Y. M.: Nanoassembly of biodegradable microcapsules for DNA encasing. *Journal of the American Chemical Society* **(2004)**, *126*, 3374-3375.

(35) Lvov, Y.; Haas, H.; Decher, G.; Mohwald, H.; Mikhailov, A.; Mtchedlishvily, B.; Morgunova, E.; Vainshtein, B.: Successive deposition of alternate layers of polyelectrolytes and a charged virus. *Langmuir* **(1994)**, *10*, 4232-4236.

(36) Wang, L. Y.; Wang, Z. Q.; Zhang, X.; Shen, J. C.; Chi, L. F.; Fuchs, H.: A new approach for the fabrication of an alternating multilayer film of poly(4-vinylpyridine) and poly(acrylic acid) based on hydrogen bonding. *Macromolecular Rapid Communications* **(1997)**, *18*, 509-514.

(37) Shimazaki, Y. M., M.; Ito, S.: Preparation of the Layer-by-Layer deposited ultrathin film based on the charge-transfer interaction. *LANGMUIR* **(1997)**, *13*, 1385-1387.

(38) Shimazaki, Y.; Mitsuishi, M.; Ito, S.; Yamamoto, M.: Preparation and characterization of the layer-by-layer deposited ultrathin film based on the charge-transfer interaction in organic solvents. *Langmuir* **(1998)**, *14*, 2768-2773.

(39) Decher, G.; Lehr, B.; Lowack, K.; Lvov, Y.; Schmitt, J.: New nanocomposite films for biosensors - layer-by-layer adsorbed films of polyelectrolytes, proteins or dna. *Biosensors & Bioelectronics* **(1994)**, *9*, 677-684.

(40) Bourdillon, C.; Demaille, C.; Moiroux, J.; Saveant, J. M.: Step-by-step immunological construction of a fully active multilayer enzyme electrode. *Journal of the American Chemical Society* **(1994)**, *116*, 10328-10329.

(41) Lvov, Y.; Ariga, K.; Ichinose, I.; Kunitake, T.: Layer-by-layer architectures of concanavalin a by means of electrostatic and biospecific interactions. *Journal of the Chemical Society-Chemical Communications* **(1995)**, 2313-2314.

(42) Anzai, J.; Kobayashi, Y.; Nakamura, N.; Nishimura, M.; Hoshi, T.: Layer-by-layer construction of multilayer thin films composed of avidin and biotin-labeled poly(amine)s. *Langmuir* **(1999)**, *15*, 221-226.

(43) Xiong, H. M.; Zhou, Z.; Wang, Z. Q.; Zhang, X.; Shen, J. C.: A new approach to fabrication of a self-organizing film of heterostructured polymer/CdS nanoparticles. *Supramolecular Science* **(1998)**, *5*, 623-626.

(44) Priya, D. N.; Modak, J. M.; Raichur, A. M.: LbL fabricated poly(styrene sulfonate)/TiO(2) multilayer thin films for environmental applications. *ACS Appl Mater Interfaces* **(2009)**, *1*, 2684-93.

(45) Guzman, E.; Ritacco, H. A.; Ortega, F.; Rubio, R. G.: Growth of Polyelectrolyte Layers Formed by Poly(4-styrenesulfonate sodium salt) and Two Different Polycations: New Insights from Study of Adsorption Kinetics. *J. Phys. Chem. C* **(2012)**, *116*, 15474-15483.

(46) Porcel, C.; Lavalle, P.; Ball, V.; Decher, G.; Senger, B.; Voegel, J.-C.; Schaaf, P.: From Exponential to Linear Growth in Polyelectrolyte Multilayers. *Langmuir* **(2006)**, *22*, 4376-4383.

(47) Chen, H.; Zeng, G. H.; Wang, Z. Q.; Zhang, X.; Peng, M. L.; Wu, L. Z.; Tung, C. H.: To combine precursor assembly and layer-by-layer deposition for incorporation of single-charged species: Nanocontainers with charge-selectivity and nanoreactors. *Chemistry of Materials* **(2005)**, *17*, 6679-6685.

(48) Fabianowski, W.; Roszko, M.; Brodzinska, W.: Optical sensor with active matrix built from polyelectrolytes smart molecules mixture. *Thin Solid Films* **(1998)**, *327*, 743-747.

(49) Chang-Yen, D. A.; Lvov, Y.; McShane, M. J.; Gale, B. K.: Electrostatic self-assembly of a ruthenium-based oxygen sensitive dye using polyion-dye interpolyelectrolyte formation. *Sensors and Actuators B-Chemical* **(2002)**, *87*, 336-345.

(50) Das, S.; Pal, A. J.: Layer-by-layer self-assembling of a low molecular weight organic material by different electrostatic adsorption processes. *Langmuir* **(2002)**, *18*, 458-461.

(51) Nicol, E.; Habib-Jiwan, J. L.; Jonas, A. M.: Polyelectrolyte multilayers as nanocontainers for functional hydrophilic molecules. *Langmuir* **(2003)**, *19*, 6178-6186.

(52) Takahashi, A.: Conformational states of polymers adsorbed on interfaces. *Polym. J. (Tokyo)* **(1991)**, *23*, 715-24.

(53) Haynie, D. T.; Cho, E.; Waduge, P.: "In and Out Diffusion" Hypothesis of Exponential Multilayer Film Buildup Revisited. *Langmuir* **(2011)**, *27*, 5700-5704.

(54) Lavalle, P.; Picart, C.; Mutterer, J.; Gergely, C.; Reiss, H.; Voegel, J.-C.; Senger, B.; Schaaf, P.: Modeling the Buildup of Polyelectrolyte Multilayer Films Having Exponential Growth✗. *The Journal of Physical Chemistry B* **(2003)**, *108*, 635-648.

(55) Guzman, E.; Ritacco, H.; Ortega, F.; Rubio, R. G.: Evidence of the influence of adsorption kinetics on the internal reorganization of polyelectrolyte multilayers. *Colloids Surf., A* **(2011)**, *384*, 274-281.

(56) Hoffmann, K.; Friedrich, T.; Tieke, B.: Layer-by-Layer Assembled Polyelectrolyte Blend Membranes and Their Use for Ion Separation and Rejection. *Polymer Engineering and Science* **(2011)**, *51*, 1497-1506.

(57) Shiratori, S. S.; Rubner, M. F.: pH-Dependent Thickness Behavior of Sequentially Adsorbed Layers of Weak Polyelectrolytes. *Macromolecules* **(2000)**, *33*, 4213-4219.

(58) Dubas, S. T.; Schlenoff, J. B.: Factors Controlling the Growth of Polyelectrolyte Multilayers. *Macromolecules* **(1999)**, *32*, 8153-8160.

(59) Von, K. R.: Internal structure of polyelectrolyte multilayer assemblies. *Phys. Chem. Chem. Phys.* **(2006)**, *8*, 5012-5033.

(60) Wang, B.; Vyas, R. N.; Shaik, S.: Preparation Parameter Development for Layer-by-Layer Assembly of Keggin-type Polyoxometalates. *Langmuir* **(2007)**, *23*, 11120-11126.

(61) Stockton, W. B.; Rubner, M. F.: Molecular-level processing of conjugated polymers .4. Layer-by-layer manipulation of polyaniline via hydrogen-bonding interactions. *Macromolecules* **(1997)**, *30*, 2717-2725.

(62) Wang, L. Y.; Cui, S. X.; Wang, Z. Q.; Zhang, X.; Jiang, M.; Chi, L. F.; Fuchs, H.: Multilayer assemblies of copolymer PSOH and PVP on the basis of hydrogen bonding. *Langmuir* **(2000)**, *16*, 10490-10494.

(63) Fu, Y.; Chen, H.; Qiu, D. L.; Wang, Z. Q.; Zhang, X.: Multilayer assemblies of poly(4-vinylpyridine) and poly(acrylic acid) bearing photoisomeric spironaphthoxazine via hydrogen bonding. *Langmuir* **(2002)**, *18*, 4989-4995.

(64) Zhang, H. Y.; Wang, Z. Q.; Zhang, Y. Q.; Zhang, X.: Hydrogen-bonding-directed layer-by-layer assembly of poly(4-vinylpyridine) and poly(4-vinylphenol): Effect of solvent composition on multilayer buildup. *Langmuir* **(2004)**, *20*, 9366-9370.

(65) Zhang, X.; Chen, H.; Zhang, H. Y.: Layer-by-layer assembly: from conventional to unconventional methods. *Chemical Communications* **(2007)**, 1395-1405.

(66) Huck, W.: Multilayer thin films-sequential assembly of nanocomposite materials by editors Gero Decher and Joseph Schlenoff. *ChemPhysChem* **(2003)**, *4*, 892-893.

(67) Wu, G. Z., X: *Polymer Thin Films*; In Tech, **(2010)**.

(68) Sukhishvili, S. A.; Granick, S.: Layered, Erasable, Ultrathin Polymer Films. *J. Am. Chem. Soc.* **(2000)**, *122*, 9550-9551.

(69) Kharlampieva, E.; Kozlovskaya, V.; Sukhishvili, S. A.: Layer-by-Layer Hydrogen-Bonded Polymer Films: From Fundamentals to Applications. *Advanced Materials* **(2009)**, *21*, 3053-3065.

(70) Quinn, J. F.; Caruso, F.: Facile tailoring of film morphology and release properties using layer-by-layer assembly of thermoresponsive materials. *Langmuir* **(2004)**, *20*, 20-22.

(71) Wang, X. Q.; Naka, K.; Itoh, H.; Uemura, T.; Chujo, Y.: Preparation of oriented ultrathin films via self-assembly based on charge transfer interaction between pi-conjugated poly(dithiafulvene) and acceptor polymer. *Macromolecules* **(2003)**, *36*, 533-535.

(72) Shimazaki, Y.; Ito, S.; Tsutsumi, N.: Adsorption-induced second harmonic generation from the layer-by-layer deposited ultrathin film based on the charge-transfer interaction. *Langmuir* **(2000)**, *16*, 9478-9482.

(73) Gao, C. F., Z; Wang, Z: Stepwise Assembly of the Same Polyelectrolytes Using Host-Guest Interaction To Obtain Microcapsules with Multiresponsive Properties. *Chemistry of Materials* **(2008)**, *20*, 4194 - 4199.

(74) Lehn, J. M.: Perspectives in supramolecular chemistry - from molecular recognition towards molecular information-processing and self-organization. *Angewandte Chemie-International Edition in English* **(1990)**, *29*, 1304-1319.

(75) Lehn, J. M.: Supramolecular chemistry. *Science* **(1993)**, *260*, 1762-1763.

(76) Anzai, J.; Kobayashi, Y.: Construction of multilayer thin films of enzymes by means of sugar-lectin interactions. *Langmuir* **(2000)**, *16*, 2851-2856.

(77) Li, H. Y.; Tripp, C. P.: Interaction of sodium polyacrylate adsorbed on TiO2 with cationic and anionic surfactants. *Langmuir* **(2004)**, *20*, 10526-10533.

(78) Liu, S. Q.; Kurth, D. G.; Mohwald, H.; Volkmer, D.: A thin-film electrochromic device based on a polyoxometalate cluster. *Advanced Materials* **(2002)**, *14*, 225-+.

(79) Kim, H. J.; Lee, K.; Kumar, S.; Kim, J.: Dynamic sequential layer-by-layer deposition method for fast and region-selective multilayer thin film fabrication. *Langmuir* **(2005)**, *21*, 8532-8538.

(80) Kim, J. Y.; DeRocher, J. P.; Mao, P.; Han, J.; Cohen, R. E.; Rubner, M. F.: Formation of Nanoparticle-Containing Multilayers in Nanochannels via Layer-by-Layer Assembly. *Chemistry of Materials* **(2010)**, *22*, 6409-6415.

(81) Jia, Y.; Han, W.; Xiong, G.; Yang, W.: Layer-by-layer assembly of TiO2 colloids onto diatomite to build hierarchical porous materials. *Journal of Colloid and Interface Science* **(2008)**, *323*, 326-331.

(82) Ninness, B. J.; Bousfield, D. W.; Tripp, C. P.: The importance of adsorbed cationic surfactant structure in dictating the subsequent interaction of anionic

surfactants and polyelectrolytes with pigment surfaces. *Colloids and Surfaces a-Physicochemical and Engineering Aspects* **(2002)**, *203*, 21-36.

(83) Decher, G.; Lvov, Y.; Schmitt, J.: Proof of multilayer structural organization in self-assembled polycation-polyanion molecular films. *Thin Solid Films* **(1994)**, *244*, 772-777.

(84) Hoogeveen, N. G.; Stuart, M. A. C.; Fleer, G. J.; Bohmer, M. R.: Formation and stability of multilayers of polyelectrolytes. *Langmuir* **(1996)**, *12*, 3675-3681.

(85) Gittleson, F. S.; Kohn, D. J.; Li, X. K.; Taylor, A. D.: Improving the Assembly Speed, Quality, and Tunability of Thin Conductive Multilayers. *Acs Nano* **(2012)**, *6*, 3703-3711.

(86) Ramsden, J. J.; Lvov, Y. M.; Decher, G.: Determination of optical-constants of molecular films assembled via alternate polyion adsorption. *Thin Solid Films* **(1995)**, *254*, 246-251.

(87) Freeman, R. G.; Grabar, K. C.; Allison, K. J.; Bright, R. M.; Davis, J. A.; Guthrie, A. P.; Hommer, M. B.; Jackson, M. A.; Smith, P. C.; Walter, D. G.; Natan, M. J.: Self-assembled metal colloid monolayers - an approach to sers substrates. *Science* **(1995)**, *267*, 1629-1632.

(88) Schmitt, J.; Decher, G.; Dressick, W. J.; Brandow, S. L.; Geer, R. E.; Shashidhar, R.; Calvert, J. M.: Metal nanoparticle/polymer superlattice films: Fabrication and control of layer structure. *Advanced Materials* **(1997)**, *9*, 61-&.

(89) Vozar, S.; Poh, Y.-C.; Serbowicz, T.; Bachner, M.; Podsiadlo, P.; Qin, M.; Verploegen, E.; Kotov, N.; Hart, A. J.: Automated spin-assisted layer-by-layer assembly of nanocomposites. *Review of Scientific Instruments* **(2009)**, *80*.

(90) Ariga, K.; Hill, J. P.; Ji, Q. M.: Layer-by-layer assembly as a versatile bottom-up nanofabrication technique for exploratory research and realistic application. *Physical Chemistry Chemical Physics* **(2007)**, *9*, 2319-2340.

(91) Cho, J.; Char, K.; Hong, J. D.; Lee, K. B.: Fabrication of highly ordered multilayer films using a spin self-assembly method. *Advanced Materials* **(2001)**, *13*, 1076-+.

(92) Trick, C. G.; Bill, B. D.; Cochlan, W. P.; Wells, M. L.; Trainer, V. L.; Pickell, L. D.: Iron enrichment stimulates toxic diatom production in high-nitrate, low chlorophyll areas. *Proc. Natl. Acad. Sci. U. S. A.* **(2010)**, *107*, 5887-5892.

(93) Wells, M. L.; Price, N. M.; Bruland, K. W.: Iron chemistry in seawater and its relationship to phytoplankton: a workshop report. *Mar. Chem.* **(1995)**, *48*, 157-82.

(94) Lohan, M. C.; Aguilar-Islas, A. M.; Bruland, K. W.: Direct determination of iron in acidified (pH 1.7) seawater samples by flow injection analysis with catalytic spectrophotometric detection: Application and intercomparison. *Limnology and Oceanography-Methods* **(2006)**, *4*, 164-171.

(95) Izquierdo, A.; Ono, S. S.; Voegel, J. C.; Schaaf, P.; Decher, G.: Dipping versus spraying: Exploring the deposition conditions for speeding up layer-by-layer assembly. *Langmuir* **(2005)**, *21*, 7558-7567.

(96) Porcel, C. H.; Izquierdo, A.; Ball, V.; Decher, G.; Voegel, J. C.; Schaaf, P.: Ultrathin coatings and (poly(glutamic acid)/polyallylamine) films deposited by continuous and simultaneous spraying. *Langmuir* **(2005)**, *21*, 800-802.

(97) Michel, A.; Izquierdo, A.; Decher, G.; Voegel, J. C.; Schaaf, P.; Ball, V.: Layer by layer self-assembled polyelectrolyte multilayers with embedded phospholipid vesicles obtained by spraying: Integrity of the vesicles. *Langmuir* **(2005)**, *21*, 7854-7859.

(98) Lu, C. H.; Donch, I.; Nolte, M.; Fery, A.: Au nanoparticle-based multilayer ultrathin films with covalently linked nanostructures: Spraying layer-by-layer assembly and mechanical property characterization. *Chemistry of Materials* **(2006)**, *18*, 6204-6210.

(99) Krogman, K. C.; Lyon, K. F.; Hammond, P. T.: Metal Ion Reactive Thin Films Using Spray Electrostatic LbL Assembly. *Journal of Physical Chemistry B* **(2008)**, *112*, 14453-14460.

(100) Schlenoff, J. B.; Dubas, S. T.; Farhat, T.: Sprayed polyelectrolyte multilayers. *Langmuir* **(2000)**, *16*, 9968-9969.

(101) Merrill, M. H.; Sun, C. T.: Fast, simple and efficient assembly of nanolayered materials and devices. *Nanotechnology* **(2009)**, *20*.

(102) Chen, Y. Y.; Zeng, G. H.; Pan, F.; Wang, J. B.; Chi, L. F.: Controlled Assembly and Release of Retinoic Acid Based on the Layer-by-Layer Method. *Langmuir* **(2013)**, *29*, 2708-2712.

(103) Tripp, C. P.; Hair, M. L.: Kinetics of the Adsorption of a Polystyrene-Poly(ethylene oxide) Block Copolymer on Silica: A Study of the Time Dependence in Surface/Segment Interactions. *Langmuir* **(1996)**, *12*, 3952-3956.

(104) Guzman, E.; Ritacco, H. A.; Ortega, F.; Rubio, R. G.: Growth of Polyelectrolyte Layers Formed by Poly(4-styrenesulfonate sodium salt) and Two Different Polycations: New insights from Study of Adsorption Kinetics. *Journal of Physical Chemistry C* **(2012)**, *116*, 15474-15483.

(105) Guzman, E.; Ritacco, H.; Ortega, F.; Rubio, R. G.: Evidence of the influence of adsorption kinetics on the internal reorganization of polyelectrolyte multilayers. *Colloids and Surfaces a-Physicochemical and Engineering Aspects* **(2011)**, *384*, 274-281.

(106) Jiang, C.; Li, H.; Tripp, C. P.: Infrared method for in situ studies of polymer/surfactant adsorption on silica powders from aqueous solution. *Appl. Spectrosc.* **(2003)**, *57*, 1419-1424.

(107) Lefort, M.; Popa, G.; Seyrek, E.; Szamocki, R.; Felix, O.; Hemmerle, J.; Vidal, L.; Voegel, J.-C.; Boulmedais, F.; Decher, G.; Schaaf, P.: Spray-On Organic/Inorganic Films: A General Method for the Formation of Functional Nano- to Microscale Coatings. *Angew. Chem., Int. Ed.* **(2010)**, *49*, 10110-10113, S10110/1-S10110/21.

(108) Sohn, B.-H.; Kim, T.-H.; Char, K.: Process-Dependent Photocatalytic Properties of Polymer Thin Films Containing TiO2 Nanoparticles: Dip vs Spin Self-Assembly Methods. *Langmuir* **(2002)**, *18*, 7770-7772.

(109) McDonald, B. T.; Cui, T.: Superhydrophilic surface modification of copper surfaces by Layer-by-Layer self-assembly and Liquid Phase Deposition of TiO2 thin film. *J. Colloid Interface Sci.* **(2011)**, *354*, 1-6.

(110) Stuart, M. A. C.; Hoogendam, C. W.; De, K. A.: Kinetics of polyelectrolyte adsorption. *J. Phys.: Condens. Matter* **(1997)**, *9*, 7767-7783.

(111) Kawaguchi, M.; Takahashi, A.: Polymer adsorption at solid-liquid interfaces. *Adv. Colloid Interface Sci.* **(1992)**, *37*, 219-317.

(112) Dobrynin, A.; Rubinstein, M.: Theory of polyelectrolytes in solutions and at surfaces. *Progress in Polymer Science* **(2005)**, *30*, 1049-1118.

(113) Chibowski, S.; Patkowski, J.; Grzadka, E.: Adsorption of polyethyleneimine and polymethacrylic acid onto synthesized hematite. *J. Colloid Interface Sci.* **(2008)**, *329*, 1-10.

(114) Berndt, P.; Kurihara, K.; Kunitake, T.: Adsorption of poly(styrenesulfonate) onto an ammonium monolayer on mica: a surface forces study. *Langmuir* **(1992)**, *8*, 2486-90.

(115) Steitz, R.; Jaeger, W.; von, K. R.: Influence of Charge Density and Ionic Strength on the Multilayer Formation of Strong Polyelectrolytes. *Langmuir* **(2001)**, *17*, 4471-4474.

(116) Lavalle, P.; Picart, C.; Mutterer, J.; Gergely, C.; Reiss, H.; Voegel, J. C.; Senger, B.; Schaaf, P.: Modeling the buildup of polyelectrolyte multilayer films having exponential growth. *Journal of Physical Chemistry B* **(2004)**, *108*, 635-648.

(117) Salomaki, M.; Vinokurov, I. A.; Kankare, J.: Effect of temperature on the buildup of polyelectrolyte multilayers. *Langmuir* **(2005)**, *21*, 11232-11240.

(118) Haynie, D. T.; Cho, E. H.; Waduge, P.: "In and Out Diffusion" Hypothesis of Exponential Multilayer Film Buildup Revisited. *Langmuir* **(2011)**, *27*, 5700-5704.

(119) Liufu, S.; Xiao, H.; Li, Y.: Adsorption of poly(acrylic acid) onto the surface of titanium dioxide and the colloidal stability of aqueous suspension. *J. Colloid Interface Sci.* **(2005)**, *281*, 155-163.

(120) Dobrynin, A. V.; Colby, R. H.; Rubinstein, M.: Scaling Theory of Polyelectrolyte Solutions. *Macromolecules* **(1995)**, *28*, 1859-71.

(121) De, G. P. G.: Scaling theory of polymer adsorption. *J. Phys. (Paris)* **(1976)**, *37*, 1445-52.

(122) Bragaru, A.; Kusko, M.; Radoi, A.; Danila, M.; Simion, M.; Craciunoiu, F.; Pascu, R.; Mihalache, I.; Ignat, T.: Microstructures and growth characteristics of polyelectrolytes on silicon using layer-by-layer assembly. *Cent. Eur. J. Chem.* **(2013)**, *11*, 205-214.

(123) Barrantes, A.; Santos, O.; Sotres, J.; Arnebrant, T.: Influence of pH on the build-up of poly-L-lysine/heparin multilayers. *J. Colloid Interface Sci.* **(2012)**, *388*, 191-200.

(124) Porcel, C.; Lavalle, P.; Decher, G.; Senger, B.; Voegel, J. C.; Schaaf, P.: Influence of the polyelectrolyte molecular weight on exponentially growing multilayer films in the linear regime. *Langmuir* **(2007)**, *23*, 1898-1904.

(125) Sun, Y.-x.; Ren, K.-f.; Zhao, Y.-x.; Liu, X.-s.; Chang, G.-x.; Ji, J.: Construction of Redox-Active Multilayer Film for Electrochemically Controlled Release. *Langmuir* **(2013)**, *29*, 11163-11168.

(126) McAloney, R. A.; Sinyor, M.; Dudnik, V.; Goh, M. C.: Atomic Force Microscopy Studies of Salt Effects on Polyelectrolyte Multilayer Film Morphology. *Langmuir* **(2001)**, *17*, 6655-6663.

(127) El Haitami, A. E.; Martel, D.; Ball, V.; Nguyen, H. C.; Gonthier, E.; Labbe, P.; Voegel, J.-C.; Schaaf, P.; Senger, B.; Boulmedais, F.: Effect of the Supporting Electrolyte Anion on the Thickness of PSS/PAH Multilayer Films and on Their Permeability to an Electroactive Probe. *Langmuir* **(2009)**, *25*, 2282-2289.

(128) Ruths, J.; Essler, F.; Decher, G.; Riegler, H.: Polyelectrolytes I: Polyanion/polycation multilayers at the air/monolayer/water interface as elements for quantitative polymer adsorption studies and preparation of hetero-superlattices on solid surfaces. *Langmuir* **(2000)**, *16*, 8871-8878.

(129) Paloniemi, H.; Lukkarinen, M.; Aaritalo, T.; Areva, S.; Leiro, J.; Heinonen, M.; Haapakka, K.; Lukkari, J.: Layer-by-layer electrostatic self-assembly of single-wall carbon nanotube polyelectrolytes. *Langmuir* **(2006)**, *22*, 74-83.

(130) Jones, F.; Farrow, J. B.; Van Bronswijk, W.: An Infrared Study of a Polyacrylate Flocculant Adsorbed on Hematite. *Langmuir* **(1998)**, *14*, 6512-6517.

(131) Guzman, E.; Ritacco, H.; Rubio, J. E. F.; Rubio, R. G.; Ortega, F.: Salt-induced changes in the growth of polyelectrolyte layers of poly(diallyl-dimethylammonium chloride) and poly(4-styrene sulfonate of sodium). *Soft Matter* **(2009)**, *5*, 2130-2142.

(132) Baur, J. W.; Rubner, M. F.; Reynolds, J. R.; Kim, S.: Foerster energy transfer studies of polyelectrolyte heterostructures containing conjugated polymers: A means to estimate layer interpenetration. *Langmuir* **(1999)**, *15*, 6460-6469.

(133) Arys, X.; Laschewsky, A.; Jonas, A. M.: Ordered Polyelectrolyte "Multilayers". 1. Mechanisms of Growth and Structure Formation: A Comparison with Classical Fuzzy "Multilayers". *Macromolecules* **(2001)**, *34*, 3318-3330.

(134) Clark, S. L.; Montague, M.; Hammond, P. T.: Selective deposition in multilayer assembly: SAMs as molecular templates. *Supramol. Sci.* **(1997)**, *4*, 141-146.

(135) Bohmer, M. R.; Evers, O. A.; Scheutjens, J. M. H. M.: Weak polyelectrolytes between two surfaces: adsorption and stabilization. *Macromolecules* **(1990)**, *23*, 2288-301.

(136) Muthukumar, M.: Theory of counter-ion condensation on flexible polyelectrolytes: Adsorption mechanism. *J. Chem. Phys.* **(2004)**, *120*, 9343-9350.

(137) Oosawa, F.: *Polyelectrolytes*; Dekker, **(1971)**.

(138) Manning, G. S.: Limiting laws and counterion condensation in polyelectrolyte solutions .I. Colligative properties. *Journal of Chemical Physics* **(1969)**, *51*, 924-&.

(139) Beer, M.; Schmidt, M.; Muthukumar, M.: The electrostatic expansion of linear polyelectrolytes: effects of gegenions, co-ions, and hydrophobicity. *Macromolecules* **(1997)**, *30*, 8375-8385.

(140) Ikeda, Y.; Beer, M.; Schmidt, M.; Huber, K.: Ca2+ and Cu2+ induced conformational changes of sodium polymethacrylate in dilute aqueous solution. *Macromolecules* **(1998)**, *31*, 728-733.

(141) Liu, S.; Ghosh, K.; Muthukumar, M.: Polyelectrolyte solutions with added salt: A simulation study. *Journal of Chemical Physics* **(2003)**, *119*, 1813-1823.

(142) Jeon, J.; Dobrynin, A. V.: Necklace Globule and Counterion Condensation. *Macromolecules (Washington, DC, U. S.)* **(2007)**, *40*, 7695-7706.

(143) Han, L.; Mao, Z.; He, W.; Wu, J.; Gong, X.; Yang, Y.; Gao, C.: Modulating the Structure and Properties of Poly(sodium 4-styrenesulfonate)/Poly(diallyldimethylammonium chloride) Multilayers with Concentrated Salt Solutions. *Langmuir* **(2012)**, *28*, 193-199.

(144) Nolte, A. J.; Takane, N.; Hindman, E.; Gaynor, W.; Rubner, M. F.; Cohen, R. E.: Thin Film Thickness Gradients and Spatial Patterning via Salt Etching of Polyelectrolyte Multilayers. *Macromolecules (Washington, DC, U. S.)* **(2007)**, *40*, 5479-5486.

(145) Sabine, C. L.; Tanhua, T.: Estimation of anthropogenic CO2 inventories in the ocean. *Ann Rev Mar Sci* **(2010)**, *2*, 175-98.

(146) Mahowald, N. M.; Engelstaedter, S.; Luo, C.; Sealy, A.; Artaxo, P.; Benitez-Nelson, C.; Bonnet, S.; Chen, Y.; Chuang, P. Y.; Cohen, D. D.; Dulac, F.; Herut, B.; Johansen, A. M.; Kubilay, N.; Losno, R.; Maenhaut, W.; Paytan, A.; Prospero, J. M.; Shank, L. M.; Siefert, R. L.: Atmospheric iron deposition: global distribution, variability, and human perturbations. *Ann Rev Mar Sci* **(2009)**, *1*, 245 78.

(147) Martin, J. H.; Coale, K. H.; Johnson, K. S.; Fitzwater, S. E.; Gordon, R. M.; Tanner, S. J.; Hunter, C. N.; Elrod, V. A.; Nowicki, J. L.; et, a.: Testing the iron hypothesis in ecosystems of the equatorial Pacific Ocean. *Nature (London)* **(1994)**, *371*, 123-9.

(148) Martin, J. H.; Fitzwater, S. E.: Iron deficiency limits phytoplankton growth in the north-east Pacific subarctic. *Nature (London)* **(1988)**, *331*, 341-3.

(149) Lam, C. K. S. C. C.; Jickells, T. D.; Richardson, D. J.; Russell, D. A.: Fluorescence-Based Siderophore Biosensor for the Determination of Bioavailable Iron in Oceanic Waters. *Anal. Chem.* **(2006)**, *78*, 5040-5045.

(150) Lawrence, M. G.: Side effects of oceanic iron fertilization. *Science (Washington, DC, U. S.)* 2002, *297*, **(1993)**.

(151) Roy, E. G.; Jiang, C.; Wells, M. L.; Tripp, C.: Determining Subnanomolar Iron Concentrations in Oceanic Seawater Using a Siderophore-Modified Film Analyzed by Infrared Spectroscopy. *Anal. Chem. (Washington, DC, U. S.)* **(2008)**, *80*, 4689-4695.

(152) Blain, S.; Treguer, P.: Iron(II) and iron(III) determination in sea water at the nanomolar level with selective online preconcentration and spectrophotometric determination. *Anal. Chim. Acta* **(1995)**, *308*, 425-32.

(153) Huang, Y.; Yuan, D.; Ma, J.; Zhang, M.; Chen, G.: Rapid speciation of trace iron in rainwater by reverse flow injection analysis coupled to a long path length liquid waveguide capillary cell and spectrophotometric detection. *Microchim. Acta* **(2009)**, *166*, 221-228.

(154) Gledhill, M.; van den Berg, C. M. G.: Measurement of the redox speciation of iron in seawater by catalytic cathodic stripping voltammetry. *Mar. Chem.* **(1995)**, *50*, 51-61.

(155) Aydin, F. A.; Soylak, M.: Separation, preconcentration and inductively coupled plasma-mass spectrometric (ICP-MS) determination of thorium(IV), titanium(IV), iron(III), lead(II) and chromium(III) on 2-nitroso-1-naphthol impregnated MCI GEL CHP20P resin. *J. Hazard. Mater.* **(2010)**, *173*, 669-674.

(156) Hirata, S.; Yoshihara, H.; Aihara, M.: Determination of iron(II) and total iron in environmental water samples by flow injection analysis with column preconcentration of chelating resin functionalized with N-hydroxyethylethylenediamine ligands and chemiluminescence detection. *Talanta* **(1999)**, *49*, 1059-67.

(157) Neilands, J. B.: Siderophores - structure and function of microbial iron transport compounds. *Journal of Biological Chemistry* **(1995)**, *270*, 26723-26726.

(158) Jiang, C.: Development of techniques for detection of biological available Fe(III) in seawater. University of Maine, **(2005)**.

(159) Chandrasoma, A.; Hamid, A. A. A.; Bruce, A. E.; Bruce, M. R. M.; Tripp, C. P.: An infrared spectroscopic based method for mercury(II) detection in aqueous solutions. *Anal. Chim. Acta* **(2012)**, *728*, 57-63.

(160) Helm, Z.: Determining oceanic iron concentrations using a siderophore based sensor. Thesis, The University of Maine, **(2013)**.

(161) Chandrasoma, A.; Hamid, A. A. A.; Bruce, A. E.; Bruce, M. R. M.; Tripp, C. P.: An infrared spectroscopic based method for mercury(II) detection in aqueous solutions. *Analytica Chimica Acta* **(2012)**, *728*, 57-63.

(162) Roy, E. G.; Jiang, C.; Wells, M. L.; Tripp, C.: Determining Subnanomolar Iron Concentrations in Oceanic Seawater Using a Siderophore-Modified Film Analyzed by Infrared Spectroscopy. *Analytical Chemistry* **(2008)**, *80*, 4689-4695.

(163) Hair, M. L.; Tripp, C. P.: Adsorption of block polymers on well-defined silica surfaces. *Prog. Colloid Polym. Sci.* **(1996)**, *101*, 51-57.

(164) Marques, C.; Joanny, J. F.; Leibler, L.: Adsorption of block copolymers in selective solvents. *Macromolecules* **(1988)**, *21*, 1051-9.

(165) Belder, G. F.; ten Brinke, G.; Hadziioannou, G.: Influence of Anchor Block Size on the Thickness of Adsorbed Block Copolymer Layers. *Langmuir* **(1997)**, *13*, 4102-4105.

(166) Milkova, V.; Radeva, T.: Effect of ionic strength and molecular weight on electrical properties and thickness of polyelectrolyte bi-layers. *Colloids Surf., A* **(2013)**, *424*, 52-58.

(167) Salomaeki, M.; Vinokurov, I. A.; Kankare, J.: Effect of Temperature on the Buildup of Polyelectrolyte Multilayers. *Langmuir* **(2005)**, *21*, 11232-11240.

BIOGRAPHY OF THE AUTHOR

Madhira Nishadi Gammana was born and raised in Kalutara, Sri Lanka on April 21, 1975. She graduated from St. Paul's girl's school, Milagiriya, Colombo Sri lanka in 1994. Madhira worked as a teacher during 1996 to 1998, teaching science in middle school. She then attended the University of Kalaniya Sri Lanka, and the Open University of Sri Lanka and graduated in 2003 and 2004 with Bachelor of science degree in Microbiology and Bachelor of science degree in Chemistry respectively. She also completed the diploma course in Medical Laboratory Technologist at National Institute of Health Sciences, Kalutara, Sri Lanka. In May 2009 she enrolled in the graduate program at the University of Maine. Madhira is a candidate for the Doctor of Philosophy degree in Chemistry from the University of Maine in August 2014.